UNIVERSITÀ
DEGLI STUDI
DEL MOLISE

# Ph.D. program in Ecology and Territory

Curriculum: Bioscience and Territory

Cycle XXXV

Coordinator Prof. Bruno Lasserre

# New sensors and methods for forest monitoring through remote sensing



ACADEMIC DISCIPLINE

AGR/05 - Forest management and silviculture

Doctoral Candidate                    Supervisor
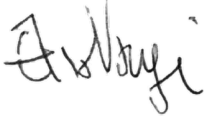Elia Vangi                             Prof. Marco Marchetti

Coordinator
Prof. Bruno Lasserre
Years 2019/2023
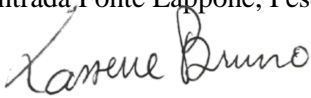
**Ph.D. Candidate**
**Elia Vangi**
elia.vangi@stud.unimol.it
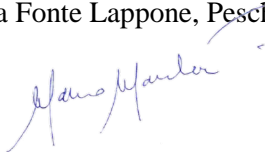
**Ph.D. coordinator**
**Prof. Bruno Lasserre**
Dep. of Bioscience and Territory,
University of Molise,
Contrada Fonte Lappone, Pesche, Italy.

**Ph.D. supervisor**
**Prof. Marco Marchetti**
Dep. of Bioscience and Territory,
University of Molise,
Contrada Fonte Lappone, Pesche, Italy.

**Reviewers**

**Prof. Giorgio Vacchiano**
Department of Agricultural and Environmental Sciences,
University of  Milano,
Via Celoria 2, Milano, 20132, Italy.

**Prof. Davide Ascoli**
Department of Agriculture, Forest and Food Sciences (DISAFA), Università degli Studi di   Torino,   Largo   Paolo   Braccini,   2,   Grugliasco,   (TO),   Italy.

# Contents

7

# New sensors and methods for forest monitoring through remote sensing

## Abstract

Forests are sources of multifunctional services capable of meeting environmental, social, cultural, and economic demands. Therefore, climate research and international reporting activity need accurate data about forests. Remote sensing technologies nowadays provide data useful for such aim. In particular, satellite remote sensing technologies generate a constantly updated stream of data from different platforms with different characteristics, able to satisfy different purposes. New sensors and platforms sprout every year with improved capacity to meet research and operational goals and needs. In 2022, NASA alone launched four earth observation missions and planned over 10 to launch by 2030. ESA also planned to launch 9 satellite missions within the same year. Planned missions will provide new insights into the carbon and water cycle, vegetation, radiation budget, atmospheric and oceanic circulation, and much more. In parallel with the rapid advance in sensor technologies and available platforms, the capabilities for processing raw remotely sensed data into useful information also advanced thanks to the use of cloud computing technologies and Artificial Intelligence approaches.

This thesis aims to explore the benefits and drawbacks of new remote sensing data and develop new tools and procedures for fully exploiting these emerging technologies. Four central studies are here presented.

Study I was motivated by the very first release of data from the hyperspectral sensor carried on board the new PRISMA satellite the first mission for Earth Observation (EO) completely developed by the Italian Space Agency (ASI). So due to the very innovative type of data it was interesting to investigate their potential contribution for mapping forest areas in Italy. We analysed the band separability in two study areas, for two types of nomenclature systems and we compared the results against the well-known Sentinel-2's Multi-Spectral Instrument (MSI). We found that PRISMA sensor, allowed for a better discrimination in all forest types, increasing the performance when the

complexity of the nomenclature system also increased. PRISMA achieved an average improvement of 40% for the discrimination between two forest categories (coniferous vs. broadleaves) and of 102% in the discrimination between five forest types based on main tree species groups.

In the second part of my PhD I concentrated my effort on studying the use of remotely sensed data for monitoring forests on larger areas, and especially how to integrate this data with existing field-based systems such as the National Forest Inventory.

In study II we investigated on how to optimise the wall-to-wall national growing stock volume estimation in Italy based on the lastly available national forest inventory (NFI) data (INFC2005). For such a purpose we compared several forest masks (FMs), and for each test we calculated model assisted estimations that were compared against the official national forest inventory estimates finding a negative correlation between the accuracies of the FMs and the differences between the model-assisted growning stock volume (GSV) estimates and the NFI estimate, demonstrating that the choice of the FM plays an important role in GSV estimation when using the model-assisted estimator. At the national and regional levels, the model-assisted GSV estimates based on the FM constructed as a mosaic of local forest maps were closest to the official NFI estimates with $r^2 = 0.986$ and $r^2 = 0.972$, for total and mean GSV, respectively.

In Study III presents we were interested in integrating GEDI (Global Ecosystem Dynamics Investigation) data into such wall-to-wall spatial estimation of forest variables. GEDI is a cutting-edge spaceborne full waveform LiDAR specifically conceived to study vegetation dynamics and retrieve vertical vegetation structure. But since the elaboration of raw GEDI data is time consuming we presented the development of a new open-source R package (GEDI4R) that provides efficient methods for downloading, reading, clipping, visualizing, and exporting the new GEDI level 4A data.

Finally, in the last study (IV) we presented a new methodology where the different elements developed in the previous studies were used to produce yearly high-resolution forest above-ground carbon pools and growing stock volume maps. The idea is to provide small-area estimations based on integrating several EO-based products with NFI data in a modeling environment. These new products allow the spatial analysis of

the annual forest carbon stock changes for Italy to fit better the international reporting requirements, consistent with the IPCC guidelines.

Additionally, during my Ph.D., I participated as a co-author inine otherne papers and in 21 conference contributions (5 of them as first author).

# List of papers

**Paper I**

Vangi, E.; D'Amico, G.; Francini, S.; Giannetti, F.; Lasserre, B.; Marchetti, M.; Chirici, G. (2021). The New Hyperspectral Satellite PRISMA: Imagery for Forest Types Discrimination. Sensors 21, 1182, 2021. https://doi.org/10.3390/s21041182

**Paper II**

Vangi E., D'Amico G., Francini S., Giannetti F., Lasserre B., Marchetti M., McRoberts RE., Chirici G. (2021). The Effect of Forest Mask Quality in the Wall-to-Wall Estimation of Growing Stock Volume. Remote Sensing. 13(5):1038. https://doi.org/10.3390/rs13051038

**Paper III**

Vangi E., D'Amico G., Francini S., Chirici G. (2023) GEDI4R: An R package for NASA's GEDI level 4A data downloading, processing and visualization. Earth Science Informatics, https://doi.org/10.1007/s12145-022-00915-3

**Paper IV**

Vangi E., D'Amico G., Francini S., Borghi C., Giannetti F., Coron P., Marchetti M., Travaglini D., Pellis G., Vitullo M., Chirici G. (2023). Large-scale high-resolution yearly modeling of forest growing stock volume and above-ground carbon pool. Environmental Modelling and Software, 159, 2023, 105580 https://doi.org/10.1016/j.envsoft.2022.105580

## Abbreviations

| | |
|---|---|
| 3D | Three dimensional |
| ABA | Area-based approach |
| ALOS | Advanced Land Observing Satellite |
| ALS | Airborne laser scanning |
| CC | Climate Change |
| CHM | Canopy height model |
| CLMS | Copernicus Land Monitoring Service |
| CO2 | Carbon Dioxide |
| EEA | European environment agency |
| ESA | European Space Agency |
| FAO | Food and Agriculture Organization of the United Nations |

| | |
|---|---|
| FRA | Forest resource assessment |
| GMES | Global Monitoring for Environment and Security programme |
| GSV | Growing stock volume |
| HRL | High-resolution layer |
| IPCC | International Panel on Climate Change |
| JAXA | Japanese Aerospace Exploration Agency |
| LiDAR | Light detection and ranging |
| NFI | National forest inventory |
| NFN | National forest mask |
| ANN | Artificial neural network |
| PALSAR | Phased Array type L-band Synthetic Aperture Radar |
| REDD+ | Reducing emissions from deforestation and forest degradation projects |
| RS | Remote Sensing |
| S2 | Sentinel-2 |
| SAR | Synthetic Aperture Radars |

# 1. Introduction

Forest ecosystems have the capability to slow anthropogenic climate change (CC) by reducing the rate of atmospheric carbon dioxide ($CO_2$) increase through increased photosynthetic $CO_2$ assimilation, tree growth, and carbon (C) storage in plants and soil (Pugh et al., 2019; Friedlingstein et al., 2020; Dalmonech et al., 2022). Each ton (t) of C stored as wood corresponds to 3.67 t of $CO_2$ removed from the atmosphere. Approximately half of the weight of dry wood is C, so each t of wood (dry weight) stores 1.83 t of $CO_2$ out of the atmosphere (Oliver et al., 2014). Forests are estimated to sequester 7.6 Gt $CO_2$ $y^{-1}$, corresponding to 30% of the total global $CO_2$ released into the atmosphere annually (Houghton & Nassikas, 2017), reflecting a balance between gross carbon removals and gross emissions from deforestation and other disturbances. Increasing the carbon stored in above and below-ground forest biomass is a generally accepted mitigation mechanism to fight CC and offset anthropogenic emissions worldwide (Di Cosmo et al., 2016; Lippke et al., 2021). A recent initiative considered an essential first step to achieve this goal is to increase the photosynthetically active area by planting trees (Trillion Trees Act, 2020), increasing the C stored and the wood availability.

Consequently, using wood to substitute for and displace fossil fuel-intensive product ensures long-term storage of C. Beyond the undoubted value in the fight against CC, forests are also a source of multifunctional services capable of meeting social, cultural, environmental, and economic demands (FOREST EUROPE, 2020). In this context, forest management practices can be crucial in enhancing the carbon storage potential and other ecosystem benefits. In Europe, *circa* 165 Mha of forests are managed in a way that drives a net uptake of $CO_2$, maximizing biomass production rather than the yield of timber products (Grassi et al., 2021). The concrete and cost-effective toolset aimed at maintaining and preserving the capacity to generate ecosystem services for future generations is called sustainable forest management (SFM). SFM aims to promote better practices over time and foster the development of healthier and more productive forests, taking into account the environmental, economic, social, cultural, and spiritual needs of the full range of stakeholder groups in the countries involved. The multi-faceted nature of SFM calls for increasingly complex and wide-ranging

information at different local and temporal scales, posing new challenges in monitoring and evaluating national trends in forest conditions (White et al., 2016). As such, forest information must be accurate, spatially detailed, and up to date, and should characterize forest composition, structure, and wood supply attributes.

In this framework, the concept "If you cannot measure it, you cannot improve it" is especially true and a key principle for forest ecosystems. Measuring, reporting and verification requirements are needed by the international climate policy such as the enhanced transparency framework of the Paris Agreement, the Sustainable Development Goals, the Glasgow Climate Pact (UNFCCC, 2015; UNDC, 2022; UNFCCC, 2021) or in the context of restoration programs (e.g., Reducing emissions from deforestation and forest degradation projects, REDD and REDD+). Achieving these objectives depends on the international community's ability to measure greenhouse gas (GHG) stocks and fluxes accurately and, consequently, to alter their emission trends (Perugini et al., 2021). For these reasons, such pivotal ecosystems are the target of extensive ad repeated monitoring activity. Tools devoted to quantifying and monitoring forest resources that double as primary data sources under national and international policies are national forest inventories (NFIs). NFIs use probability-based approaches to infer the estimates for large areas such as countries and regions within countries (McRoberts et al., 2007, 2013). The most common forest variables needed to assess the composition, structure, and distribution of forest vegetation that, in turn, can be used as base information for reporting activity and management decisions are forest area, growing stock volume (GSV), biomass, and increments (Brosofske et al., 2014; Kangas et al., 2018). However, many NFIs are not designed for continuous yearly monitoring and cannot cope with the UNFCCC required reporting frequency due to longer update cycles (McRoberts et al., 2018). Estimating forest parameters such as GSV and carbon stock changes between consecutive NFIs is a critical step in accomplishing the international reporting requirements and filling the information gaps left by the long updating cycle of periodic NFIs. For this reason, in several countries with long NFI histories such as Sweden, Finland, Denmark (Næsset et al., 2004; Nord-Larsen and Schumacher, 2012; Tomppo et al., 2008), Canada (Boudreau et al., 2008; Matasci et al., 2018), Austria (Hollaus et al., 2009) and Switzerland (Waser et al., 2017, 2015), the typical NFI ground survey is enhanced by spatially continuous and updated

predictions of forest variables, characterized as wall-to-wall (WW) maps, which rely on models and auxiliary data such as remotely sensed (RS) data.

## 1.1. Remote sensing technologies in forestry

The inference from ground measurements, such as those made in NFIs, requires spatial extrapolation to provide meaningful and sound statistics through design-based methods (the traditional approach) or with a vast array of statistical techniques where RS data can be used for model based, model-assisted or hybrid inference systems (Ståhl et al., 2016). Even the traditional design-based methods benefit from using RS data (Goetz & Dubayah, 2011); for example, for land cover or land use classification via visual interpretation or sampling stratification. RS technologies, which nowadays provide high-quality geospatial information, are considered crucial for improving repeatable measurements, actions, and processes in forestry (Holopainen et al., 2014; Kovácsová & Antalová, 2010). Many authors have already pointed out that RS technologies are essential for monitoring, quantifying, and mapping forest variables (Hansen et al., 2013; Waser et al., 2017; Kangas et al., 2018; Chirici et al., 2020). There are several ways in which airborne or satellite observations can be used in forestry applications and to support national and international emission reporting (Lechner et al., 2020; Goetz & Dubayah, 2011). This is reflected in the steadily increasing use of these technologies in the forestry field, also thanks to the increasing availability of such data in the new open access and open data era.

Spectral data are collected in many forms and scales by satellite, aircraft, and drones, with a spatial resolution ranging from tens of meters to a few centimeters. Some data are collected daily or at regular intervals across the globe, while others may be collected on demand. Optical sensors are then divided into multispectral and hyperspectral according to the number of spectral bands in which they measure the reflected radiation; for each measurement band, an image is acquired, representing reflectance at a precise wavelength, usually in the visible and infrared spectrum. The former is able to capture the reflectance from three to the order of tens of bands, while the latter can sample hundreds or even thousands of narrower and contiguous bands. Optical sensors are usually not designed for specific applications, and today we are witnessing the rapid

development of multispectral and hyperspectral image processing technology. For this reason, these data are increasingly used in several remote sensing fields such as ecology, atmosphere, ocean, agriculture, and forestry (Liu et al., 2020). These sensors provide a synoptic view of the forest canopy in a map-like format that provides a complete survey of the sensor's field of view (Lechner et al., 2020). Spaceborne optical data are often available everywhere in various temporal scales providing a constantly updateable stream of imagery of the entire planet, making them particularly suitable to change detection tasks and cloud-free compositions.

In addition to spectral data, structural or three-dimensional (3D) information can be gathered using laser, radar, and also optical data, allowing forests to be measured in ways that were not previously possible. Among these technologies, Light Detection And Ranging (LiDAR) data collected by airplane or helicopter platforms (Airborne Laser Scanning, ALS) and, more recently, by satellite and other spatial platforms (i.e., the Geoscience Laser Altimeter System [GLAS] carried by the Ice, Cloud, and land Elevation Satellite [ICESat] and the Global Ecosystem Dynamics Investigation [GEDI] carried by the International Space Station [ISS]) is considered the most helpful technology for forest characterization (Figure 1).
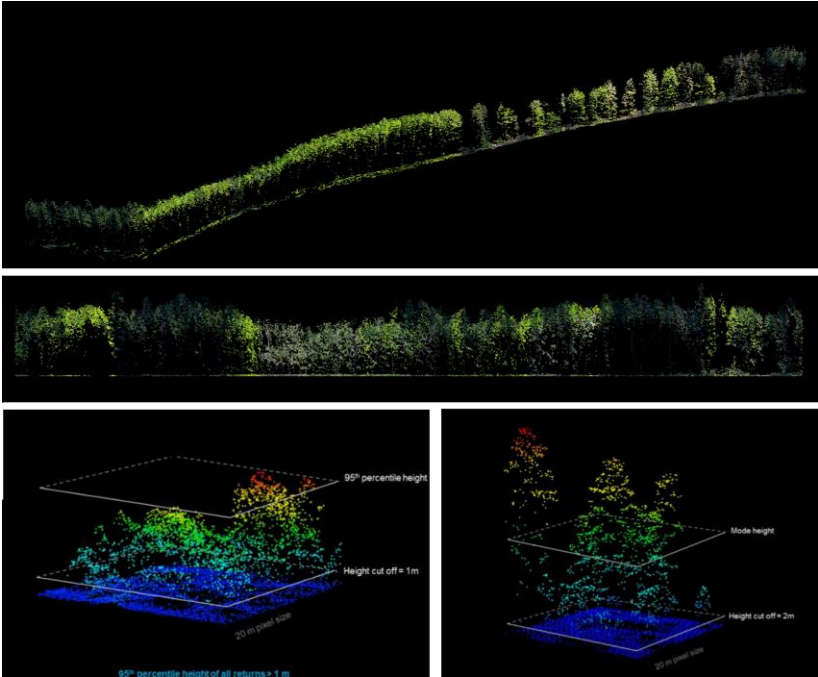


Figure 1. Airborne laser scanning dataset of a mixed forest. From the top:

front view of the point-cloud; DTM-normalized point-cloud; a close-up view of individual trees ( figure courtesy of Francesca Giannetti).

LiDAR systems are categorized by the mode with which they record the energy returning to the sensor. Discrete return systems record single or few returns (Lim et al., 2003), while a full-waveform system record the returning energy as one continuous return or waveform (Lefsky et al., 2002).

LiDAR sensors have the ability to penetrate the canopy providing a full 3D rendering of forest structure (Holopainen et al., 2014, Hyyppa et al., 2008), making it possible to estimate biophysical variables easily (e.g., tree heights, vertical structure, GSV, carbon stock) (Dubayah & Drake, 2000; Goetz & Dubayah, 2011; Babcock et al., 2015). In the last decades, many studies demonstrated the utility of LiDAR data in monitoring forest resources (Nelson, 2013; Kangas et al., 2018), biodiversity (Corona et al., 2011; Lim et al., 2003; Mura et al., 2015; Valbuena et al., 2016, 2013; Wulder et al., 2008) and in the context of NFIs (Chirici et al., 2020; McRoberts et al., 2013; Næsset, 2007; Næsset et al., 2004). Given its proven capabilities in mapping forest variables, the use of ALS data is increasing rapidly worldwide (Zolkos et al., 2013). LiDAR data are acquired explicitly in many countries to enhance forest inventory programs. Operationally, LiDAR data are exploited as predictors through the statistical relationship with ground-based measurements in a two-stage procedure called the area-based approach (ABA, Næsset, 2002). ABA has become the standard for supplementing NFI with WW spatial prediction of forest variables. Its application in a wide variety of environments and management contexts makes it a proven concept (Wulder et al., 2013).

Regardless of the approach, spatial knowledge of the area covered by forest land is an essential prerequisite in WW estimation tasks, both to restrict the establishment of field plots and the application of the models. A forest mask (FM) indicates the location of forest land and is often in a raster or a spatial polygon database format. Such information is crucial to integrate ALS data with other data, such as field surveys conducted by the NFI, or to plan future LiDAR acquisitions. The big data availability led to an exponential increase in the number of forest maps made available at different spatial scales, produced independently by different agencies, each with individual weaknesses and strengths. For instance, Italian information about forest area, as defined by the FAO Forest Resource Assessment (FRA) (FAO, 2020), can be estimated from

any of several FM, including i. the CORINE Land Cover project (Büttner et al., 2004), started in 1990 and updated in 2000, 2006, 2012, and 2018 to monitor land-use changes; ii. the forest type maps available among the High-Resolution Layers (HRL) covering entire Europe for the years 2012 and 2015 (Langanke, 2017), in the framework of ESA Copernicus Land Monitoring Service (CLMS); iii. the global forest mask produced by the International Institute for Applied Systems Analysis (IIASA) for the reference year 2000 by combining multiple data sets calibrated with FAO FRA country statistics (Schepaschenko, 2015), and iv. the Japanese Aerospace Exploration Agency (JAXA) provided an FM with a 25 m resolution for the entire globe for the years 2007, 2008, 2009, 2010, and 2015 by automatic processing of multi-polarization backscatter signals acquired by two Synthetic Aperture Radars missions (JAXA, 2016). Spatial differences among these products are relevant at the national scale. They can lead to substantial variations when used to infer forest statistics in NFIs (Di Biase et al., 2018) or to assess forest variables at the national scale. However, few studies have examined the effects of using different forest masks on the uncertainty of estimates of forest variables. Furthermore, these studies have yet to be done in the Mediterranean.

## 1.2. New remote sensing platforms and sensors

Over the past few decades, increasing attention has been focused on improving remote sensing Earth Observation (EO) technologies. Since the 1970s, when the Landsat mission, the world's most extended remote sensing program for EO, has been launched, new missions and sensors have undergone significant improvements to meet the new challenges posed by a rapidly changing world. The main changes concern: i. new satellite mission, ii. more satellites in orbit per mission; iii. the increased spectral, spatial, and temporal resolution of satellites, and iv. the free-and-open data policy of EO programs.

Some of the most crucial sensors and platforms that joined the ongoing EO programs are the Sentinel-2 (S2) mission, in the framework of the Copernicus program, an initiative led by the European Commission (EC) in collaboration with the European Space Agency (ESA), launched on June 23rd, 2015. S2 comprises a constellation of two twin polar-orbiting satellites (Sentinel-2A and 2B) placed in the same sun-synchronous

orbit, phased at 180° to each other, ensuring a high revisit time (10 days at the equator with one satellite, and five days with two satellites under cloud-free conditions which result in 2-3 days at mid-latitudes) with a wide swath of 290 km. S2 Multi-Spectral Instrument (MSI) payload acquires high-resolution multispectral imagery in 13 spectral bands: four bands at 10 m, six bands at 20 m, and three bands at 60 m spatial resolution. The mission will be joined in 2024 and 2025 by two other twin satellites, Sentinel-2C, and 2D, to further decrease the revisit time; The Landsat 9 satellite, launched on September 27th, 2021, intends to pursue the longest EO mission still active. The instruments onboard Landsat 9 are improved replicas of those currently collecting data onboard Landsat 8, which already provide radiometrically and geometrically superior data than the previous generation Landsat satellites. The platform carries two scientific instruments, the Operational Land Imager 2 (OLI-2) and the Thermal Infrared Sensor 2 (TIRS-2). The OLI–2 captures observations of the Earth's surface in visible, near-infrared (VNIR), and shortwave-infrared (SWIR) bands, and TIRS-2 measures thermal infrared radiation emitted from the Earth's surface. OLI-2 will provide data for nine spectral bands with 30 m spatial resolution and higher radiometric resolution of 14-bit quantization. In the late-2030, Landsat Next will continue the legacy of the Landsat mission with a new constellation of three smaller satellites with an enhanced spatial and temporal resolution, each able to detect 26 wavelengths of light and thermal energy; The new PRISMA (Precursore IperSpettrale della Missione Applicativa) satellite launched on March 22nd, 2019. PRISMA is a national EO cutting-edge hyperspectral mission fully funded by the Italian Space Agency (ASI).

The instruments onboard the platform include a Hyperspectral Imager, able to capture images in a continuum of 240 spectral bands ranging between 400 and 2500 nm, 66 in the VNIR and 173 in the SWIR spectrum, with a spectral resolution smaller than 12 nm, and a spatial resolution of 30 m. Nine bands are acquired in a wavelength overlapping region between the VNIR and the SWIR cube. The spacecraft also carries a 5 m resolution Panchromatic Camera (ASI, PRISMA product specification, 2019). PRISMA acquires images on demand, in specific individual locations requested by the users, in a "standard" mode, resulting in a 30x30 km scene and a "strip" mode, generating an image 30 km wide and having a maximum length of 1800 km. The mission can potentially provide major contributions to forest analysis, precision agriculture, water

quality assessment, and climate change research. A second-generation satellite, PRISMA2G, will continue the mission with an increased spatial resolution of 10 m; The GEDI sensor launched on December 5th, 2018, on the ISS. This is the first space mission conceived explicitly for retrieving vertical vegetation structures. The sensor consists of a geodetic-class full-waveform LiDAR comprised of three lasers emitting 242 pulses per second at 1064 nm wavelength. Two of the lasers are full power, and one is split into two beams, producing a total of four beams. A Beam Dithering Units change the deflection of the outgoing laser beams shifting them by 600 m on the ground. This produces eight ground tracks, four power, and four cover tracks of 25 m footprints separated by 60 m along the track and 600 m across the track, providing measurements of forest height in temperate and tropical forests (between 51.6° N and 51.6° S Latitude). The science of GEDI is centered on quantifying the distribution of above-ground carbon stored in forests, assessing vegetation disturbance and recovery effects on carbon stock, and quantifying the spatial and temporal distribution of habitat structure and its influence on habitat quality and biodiversity. To address these scientific goals, GEDI products are supplied at different processing levels that allow the derivation of a variety of forest variables, such as foliar canopy profiles, leaf area index (LAI), sub-canopy topography, and canopy height.

The advent of new EO missions and sensors offers unprecedented detailed data through higher revisit times and finer spectral and spatial resolution, paving the way for the era of big data in forest monitoring. Remote sensing big data computing is challenging due to the extensive nature of the analysis, combined with the large amount of data handled (Ma et al., 2015). Big data analytics in the EO field relies on processing, analyzing, and merging multiple images with other data sources to create previously unavailable information that requires heavy computing power. In the meantime, supercomputers, high-performance computing systems, frequently provided by cloud platforms universally available, as well as classification and processing of remote-sensing imagery are advancing in leaps and bounds (Gorelik et al., 2017; Lechner et al., 2020). Computer vision, machine learning, and time-series analysis are the next step in leveraging the data generated by modern sensors. In this sense, the freely available Google Earth Engine (GEE) platform has had enormous uptake in the RS community

and beyond. GEE is a combination of an image repository (it includes nearly all freely available remote-sensing imagery and products, such as surface reflectance and vegetation indices), high-performance computing, and a web-based mapping application. GEE reduced the remote RS workflows and opened the possibility of processing data at a much larger and even global scale on a simple desktop with an internet connection by a single operator (Lechner et al., 2020).

To keep pace with the unprecedented proliferation of new sensors, it is essential to develop new processing techniques and methods able to thoroughly scrape all available information from massive datasets, such as those generated by new RS sensors and instruments.

## 2. Background motivation and aims

The availability of new RS data from multiple sources and the possibility offered by cloud computing platforms and machine learning techniques inspired the research work of this thesis. This research explores the potential of new sources of remote sensing data to support national and international reporting activity and forest monitoring. New tools and procedures were developed to reduce the gap in research between advances in RS technologies and forestry applications. In particular, the focus was on exploring the benefits and drawbacks of new RS data and proposing solutions to scientific questions and operational needs. The specific objectives of the papers are:

- to investigate the capabilities of the new PRISMA satellite hyperspectral sensor for the recognition of forest categories through a pairwise separability analysis in two study areas in Italy, on a band-by-band basis (Paper I);

- to assess the impacts of the accuracies of different national forest masks on the estimation of GSV based on the integration of field information and remotely sensed data (Paper II);

- to develop a specific software and dedicated functions for downloading and processing GEDI level 4A data. An R package for downloading and processing level 4A data was presented; and applied over the whole of Italy as illustrative example (Paper III);

- to present a new spatial approach for the WW estimation of GSV and carbon stock, filling the information gaps left by the long updating cycle of the periodic Italian NFI (Paper IV).

# 3. Reference

Babcock C., Finley A.O., Bradford J.B., Kolka R., Birdsey R., Ryan M.G., 2015. LiDAR based prediction of forest biomass using hierarchical models with spatially varying coefficients. Remote Sensing of Environment 169, 113-127. doi:10.1016/j.rse.2015.07.028.

Boudreau J., Nelson R.F., Margolis H.A., Beaudoin A., Guindon L., Kimes D.S., 2008. Regional aboveground forest biomass using airborne and spaceborne LiDAR in Québec. Remote Sensing of Environment 112, 3876–3890. doi: 10.1016/j.rse.2008.06.003.

Brosofske K.D., Froese R.E., Falkowski M.J., Banskota A., 2014. A review of methods for mapping and prediction of inventory attributes for operational forest management. Forest Science 60, 733–756. doi: 10.5849/forsci.12-134.

Büttner, G.; Feranec, J.; Jaffrain, G.; Mari, L.; Maucha, G.; Soukup, T. The CORINE Land Cover project 2000. EARSeLeProceedings 3, 3/2004 331. 2004. Available online: https://citeseerx.ist.psu.edu/viewdoc/download?doi=10.1.1.618.9940&rep=rep1&type=pdf (accessed on September 2021).

Chirici G., Giannetti F., McRoberts R.E., Travaglini D., Pecchi M., Maselli F., Chiesi M., Corona P., 2020. Wall-to-wall spatial prediction of growing stock volume based on Italian National Forest Inventory plots and remotely sensed data. International Journal of Applied Earth Observation and Geoinformatics 84, 101959. doi: 10.1016/j.jag.2019.101959.

Corona P., Chirici G., McRoberts R.E., Winter S., Barbati A., 2011. Contribution of large-scale forest inventories to biodiversity assessment and monitoring. Forest Ecology and Management 262, 2061–2069. doi:10.1016/j.foreco.2011.08.044.

Dalmonech D., Marano G., Amthor J.S., Cescatti A., Lindner M., Trotta C., Collalti, A. 2022. Feasibility of enhancing carbon sequestration and stock capacity in temperate and boreal European forests via changes to management regimes, Agricultural and Forest Meteorology, Volume 327, 109203, ISSN 0168-1923, https://doi.org/10.1016/j.agrformet.2022.109203.

Di Biase R.M., Fattorini L., Marchi M., 2018. Statistical inferential techniques for approaching forest mapping. A review of methods. Annals of Silvicultural Research 42: 46-58. - doi: 10.12899/asr-1738.

Di Cosmo, L., Gasparini, P., Tabacchi, G., 2016. A national-scale, stand-level model to predict total above-ground tree biomass from growing stock volume. For. Ecol. Manag. 361, 269–276. https://doi.org/10.1016/j.foreco.2015.11.008, 0378–1127.

Dubayah R.O., Drake J.B., 2000. Lidar remote sensing for forestry. Journal of forestry 98.6: 44-46. doi: 10.1093/jof/98.6.44.

European Enviromental Agency, EEA, 2007. Enviromental Statement; Office for Official Publications of the European Communities: Luxembourg; ISBN 978-92-9167-936-2.

FAO, UNCCD. Sustainable Financing for Forest and Landscape Restoration: The Role of Public Policy Makers; FAO: Rome, Italy, 2015.

FAO, 2020. Global Forest Resources Assessment 2020: Main report. Rome. https://doi.org/10.4060/ca9825en.

FOREST EUROPE, 2020. State of Europe's Forests 2020., Ministerial Conference on the Protection of Forests in Europe, FOREST EUROPE Liaison Unit Bratislava.

Friedlingstein, P., O'Sullivan, M., Jones, M.W., Andrew, R.M., Hauck, J., Olsen, A., Peters, G.P., Peters, W., Pongratz, J., Sitch, S., Le Qu´er´e, C., Canadell, J.G., Ciais, P., Jackson, R.B., Alin, S., Arag˜ao, L.E.O.C., Arneth, A., Arora, V., Bates, N.R., Zaehle, S., 2020. Global Carbon Budget 2020. Earth Syst. Sci. Data 12 (4), 3269–3340. https://doi.org/10.5194/essd-12-3269-2020.

Goetz S., Dubayah R., 2011. Advances in remote sensing technology and implications for measuring and monitoring forest carbon stocks and change, Carbon Management, 2:3, 231-244, DOI: 10.4155/cmt.11.18

Gorelick N., Hancher M., Dixon M., Ilyushchenko S., Thau D., Moore R., 2017. Google Earth Engine: Planetary-scale geospatial analysis for everyone. Remote sensing of Environment 202, 18-27. doi: 10.1016/j.rse.2017.06.031.

Grassi, G., Stehfest, E., Rogelj, J., van Vuuren, D., Cescatti, A., House, J., Nabuurs, G.J., Rossi, S., Alkama, R., Vi˜nas, R.A., Calvin, K., Ceccherini, G., Federici, S., Fujimori, S., Gusti, M., Hasegawa, T., Havlik, P., Humpen¨oder, F., Korosuo, A., Popp, A., 2021. Critical adjustment of land mitigation pathways for assessing countries' climate progress. Nat. Clim. Change 11 (5), 425–434. https://doi.org/10.1038/s41558-021- 01033-6.

Hansen M.C., Potapov P.V., Moore R., Hancher M., Turubanova S.A., Tyukavina A., 2013. High-resolution global maps of 21st-century forest cover change. Science 342 (6160): 850-853. - doi: 10.1126/science.1244693.

Hollaus M., Dorigo W., Wagner W., Schadauer K., Höfle B., Maier B., 2009. Operational wide-area stem volume estimation based on airborne laser scanning and national forest inventory data. International Journal Remote Sens. 30, 5159–5175. doi: 10.1080/01431160903022894.

Holopainen M., Vastaranta M., Hyyppa J., 2014. Outlook for the next generation's precision forestry in Finland. Forests 5: 1682-1694. - doi: 10.3390/f5071682.

Houghton, R.A., Nassikas, A.A., 2017. Global and regional fluxes of carbon from land use and land cover change 1850–2015. Global Biogeochem. Cycles 31 (3), 456–472.

H.R.5859 - 116th Congress (2019-2020): Trillion Trees Act. (2020, February 26). https://www.congress.gov/bill/116th-congress/house-bill/5859/text

Hyyppa J., Hyyppa H., Leckie D., Gougeon F., Yu X., Maltamo M., 2008. Review of methods of small-footprint airborne laser scanning for extracting forest inventory data in boreal forests. International Journal of Remote Sensing 29 (5): 1339-1366. - doi: 10.1080/01431160701736489.

ITTO/FAO, 1995. Report on Harmonization of Criteria and Indicators for Sustainable Forest Management, FAO/ITTO Expert Consultation, 13 - 16 February 1995. Rome, Italy.

JAXA. Global 25m Resolution PALSAR-2/PALSAR Mosaic and Forest/Non-Forest Map (FNF) Dataset Description; Japan Aerospace Exploration Agency (JAXA), Earth Observation Research Center (EORC), 2016. Available online: https://www.eorc.jaxa.jp/ALOS/en/palsar_fnf/DatasetDescription_PALSAR2_Mosaic_FNF_revE.pdf (accessed on September 2021).

Kangas A., Astrup R., Breidenbach J., Fridman J., Gobakken T., Korhonen K.T., Maltamo M., Nilsson M., Nord-Larsen T., Olsson H., 2018. Remote sensing and forest inventories in Nordic countries - Roadmap for the future. Scandinavian Journal of Forest Research 33: 397-412. - doi: 10.1080/02827581.2017.1416666.

Kovácsová P., Antalová M., 2010. Precision Forestry – Definition and Technologies. Šumarski List 143, 603–611.

Langanke T 2017. Copernicus Land Monitoring Service–High Resolution Layer Forest: Product Specifications Document 38; Copernicus team at EEA, 2017. Available online: https://www.eea.europa.eu/data-and-maps/data/copernicus-land-monitoring-servic ehigh (accessed on September 2021).

Lechner, A.M., Foody, G.M., & Boyd, D.S. (2020). Applications in Remote Sensing to Forest Ecology and Management. One Earth, 2, 405-412

Lefsky M., Cohen W.B., Parker G.G., Harding D.J., 2002. Lidar Remote Sensing for Ecosystem Studies. Bioscience 52, 19–30. doi:10.1641/0006-3568(2002)052[0019:LRSFES]2.0.CO;2.

Lim K.P., Treitz P., Wulder M.A., St-Onge B.A., Flood M., 2003. LiDAR remote sensing of forest structure. Progress in Physical Geography 27, 88–106. doi: 10.1191/0309133303pp360ra.

Lippke B., Puettmann M., Oneil E., OliverC. D., 2021. The Plant a Trillion Trees Campaign to Reduce Global Warming – Fleshing Out the Concept, Journal of Sustainable Forestry, 40:1, 1-31, DOI: 10.1080/10549811.2021.189495

Liu, H.; Zhang, F.; Zhang, L.; Lin, Y.; Wang, S.; Xie, Y. UNVI-Based Time Series for Vegetation Discrimination Using Separability Analysis and Random Forest Classification. Remote Sens. 2020, 12, 529.

Ma Y., Wu H., Wang L., Huang B., Ranjan R., Zomaya A., Jie W., 2015. Remote sensing big data computing: Challenges and opportunities. Future Generation Computer Systems, 51, 47-60. doi: 10.1016/j.future.2014.10.029.

Matasci G., Hermosilla T., Wulder M.A., White J.C., Coops N.C., Hobart G.W., Zald H.S.J., 2018. Large-area mapping of Canadian boreal forest cover, height, biomass and other structural attributes using Landsat composites and lidar plots. Remote Sensing of Environmet 209, 90–106. doi: 10.1016/j.rse.2017.12.020.

McRoberts, R.E., Tomppo, E.O., 2007. Remote sensing support for national forest inventories. Remote Sens. Environ. 110, 412–419. https://doi.org/10.1016/j.rse.2006. 09.034.

McRoberts R.E., Næsset E., Gobakken T., 2013. Inference for lidar-assisted estimation of forest growing stock volume. Remote Sensing of Environment 128, 268–275. doi:10.1016/j.rse.2012.10.007..

McRoberts, R.E., Næsset, E., Gobakken, T., Chirici, G., Condes, S., Hou, Z., Saarela, S., Chen, Q., Stahl, G., Walters, B.F., 2018. Assessing components of the model-based mean square error estimator for remote sensing assisted forest applications. Can. J. For. Res. 48, 642–649. https://doi.org/10.1139/cjfr-2017-0396.

Mura M., McRoberts R.E., Chirici G., Marchetti M., 2015. Estimating and mapping forest structural diversity using airborne laser scanning data. Remote Sensing of Environment 170, 133–142. doi: 10.1016/j.rse.2015.09.016.

Naesset E., 2002. Predicting forest stand characteristics with airborne scanning laser using a practical two-stage procedure and field data. Remote Sensing of Environment 80: 88-99. - doi: 10.1016/S0034-4257(01)00290-5.

Næsset E., 2007. Airborne laser scanning as a method in operational forest inventory: Status of accuracy assessments accomplished in Scandinavia. Scandinavian Journal of Forest Research 22, 433–422.

Næsset E., Bollandsås O.M., Gobakken T., Gregoire T.G., Ståhl G., 2013. Model-assisted estimation of change in forest biomass over an 11year period in a sample survey supported by airborne LiDAR: a case study with post-stratification to provide "activity data.". Remote Sensing of Environment 128, 299–314. doi: 10.1016/j.rse. 2012.10.008.

Nilsson M., Nordkvist K., Jonzén J., Lindgren N., Axensten P., Wallerman J., Egberth M., Larsson S., Nilsson L., Eriksson J., Olsson H., 2017. A nationwide forest attribute map of Sweden predicted using airborne laser scanning data and field data from the National Forest Inventory. Remote Sensing of Environment 194, 447–454. doi: 10.1016/j.rse.2016.10.022.

Nord-Larsen T., Schumacher J., 2012. Estimation of forest resources from a country wide laser scanning survey and national forest inventory data. Remote Sensing of Environment 119, 148–157. doi: 10.1016/j.rse.2011.12.022.

Oliver, C., Nassar, N. T., Lippke, B., & McCarter, J. B. (2014). Carbon, fossil fuel, and biodiversity mitigation with wood and forests. Journal of Sustainable Forestry, 33(3), 248–271. https://doi.org/10.1080/10549811.2013.839386.

Schepaschenko D., See L., Lesiv M., McCallum I., Fritz, S.; Salk, C.; Moltchanova, E.; Perger, C.; Shchepashchenko, M.; Shvidenko, A.; et al. Development of a global hybrid forest mask through the synergy of remote sensing, crowdsourcing and European Enviromental Agency. Enviromental Statement; Office for Official Publications of the European Communities: Luxembourg, 2007; ISBN 978-92-9167-936-2.

Seebach L., McCallum I., Fritz S., Kindermann G., LeDuc S., Böttcher H., Fuss S., 2012. Choice of forest map has implications for policy analysis: A case study on the EU biofuel target. Environmental Science & Policy 2012, 22, 13–24, doi:10.1016/j.envsci.2012.04.010.

Ståhl, G., Saarela, S., Schnell, S., Holm, S., Breidenbach, J., Healey, S.P., Patterson, P.L., Magnussen, S., Næsset, E., McRoberts, R.E., & Gregoire, T.G. (2016). Use of models in large-area forest surveys: comparing model-assisted, model-based and hybrid estimation. Forest Ecosystems, 3, 5

Tomppo E., Olsson H., Ståhl G., Nilsson M., Hagner O., Katila M., 2008. Combining national forest inventory field plots and remote sensing data for forest databases. Remote Sensing of Environment 112, 1982–1999. doi: 10.1016/j.rse.2007.03.032.

UNDP, 2022. The Sustainable Development Goals. https://unstats.un.org/sdgs/report/2022/The-Sustainable-Development-Goals-Report-2022.pdf. Accessed 07/01/2023

UNFCCC, 2015. The Paris Agreement. Report of the Conference of the Parties on its Twenty-First Session held in Paris from 30 November to 11 December 2015. http:// unfccc.int/files/meetings/paris_nov_2015/application/pdf/paris_agreement_english_.pdf. Accessed 05/10/2022

UNFCCC, 2021. Glasgow Climate Change Conference - October/November 2021. https://unfccc.int/event/cop-26. Accessed 03/01/2023

Valbuena R., Eerikäinen K., Packalen P., Maltamo M., 2016. Gini coefficient predictions from airborne lidar remote sensing display the effect of management intensity on forest structure. Ecological Indicators 60, 574–585. doi: 10.1016/j.ecolind.2015.08.001.

Valbuena R., Packalen P., Mehtätalo L., García-Abril A., Maltamo M., 2013. Characterizing forest structural types and shelterwood dynamics from Lorenz-based indicators predicted by airborne laser scanning. Canadian Journal of Forest Research 43(11): 1063-1074. doi: 10.1139/cjfr-2013-0147.

Vizzarri M., Sallustio L., Travaglini D., Bottalico F., Chirici G., Garfi V., Lafortezza R., Veca D.S.L.M., Lombardi F., Maetzke F., Marchetti M., 2017. The MIMOSE approach to support sustainable forest management planning at regional scale in Mediterranean contexts. Sustainability 9 (2): 316. doi: 10.3390/su9020316.

Waser L.T., Ginzler C., Rehush N., 2017. Wall-to-wall tree type mapping from countrywide airborne remote sensing surveys. Remote Sensing 9 (8): 766. doi: 10.3390/rs9080766

White J.C., Coops N.C., Wulder M.A., Vastaranta M., Hilker T., Tompalski P., 2016. Remote sensing technologies for enhancing forest inventories: a review. Canadian Journal of Remote Sensing 42: 619-641. doi: 10.1080/07038992.2016.12074 84.

Woodcock C.E., Allen R., Anderson M., Belward A., Bindschadler R., Cohen W., Gao F., Goward S.N., Helder D., Helmer E., Namani R., Oreopoilos L., Schott J., Thenkabail P.S., Vermote E.F., Vogelman J., Wulder M.A., Wynne R., 2008. Free access to Landsat imagery. Science 320: 1011. doi: 10.1126/science.320.5879.1011a.

Wulder M.A., Bater C.W., Coops N.C., Hilker T., White J., 2008. The role of LiDAR in sustainable forest management. The Forestry Chronicle 84, 807–826. doi: 10.5558/tfc84807-

Zolkos S., Goetz S., Dubayah R., 2013. A meta-analysis of terrestrial aboveground biomass estimation using lidar remote sensing. Remote Sensing of Environment 128, 289–298. doi: 10.1016/j.rse.2012.10.017.

# 4. Paper I

**The New Hyperspectral Satellite PRISMA: Imagery for Forest Types Discrimination**

*Vangi E.[1,2], D'Amico G.[2], Francini S.[1,2,3], Giannetti F.\*[2,4,5], Lasserre B.[1], Marchetti M.[1], Chirici G.[2,5]*

[1] Department of Bioscience and Territory (DiBT), University of Molise. Pesche 86090, (IS), Italy

[2] Department of Agriculture, Food, Environment and Forestry (DAGRI), University of Florence. Florence 50145, Italy

[3] Department of Innovation in Biological, Agro-Food and Forest System (DIBAF), University of Tuscia.Viterbo 01100, (VT), Italy

[4] Bluebiloba startup Innovativa S.R.L. Florence 50126, Italy

[5] ForTech, University of Florence joint laboratory, Florence, Italy

\* corresponding author francesca.giannetti@unifi.it

Sensors-

## Abstract

Different forest types based on different tree species composition may have similar spectral signatures if observed with traditional multispectral satellite sensors. Hyperspectral imagery, with a more continuous representation of their spectral behavior may instead be used for their classification. The new hyperspectral Precursore IperSpettrale della Missione Applicativa (PRISMA) sensor, developed by the Italian Space Agency, is able to capture images in a continuum of 240 spectral bands ranging between 400 and 2500 nm, with a spectral resolution smaller than 12 nm. The new sensor can be employed for a large number of remote sensing applications, including forest types discrimination.

In this study, we compared the capabilities of the new PRISMA sensor against the well-known Sentinel-2 Multi-Spectral Instrument (MSI) in recognition of different forest types through a pairwise separability analysis carried out in two study areas in Italy,

using two different nomenclature systems and four separability metrics. The PRISMA hyperspectral sensor, compared to Sentinel-2 MSI, allowed for a better discrimination in all forest types, increasing the performance when the complexity of the nomenclature system also increased. PRISMA achieved an average improvement of 40% for the discrimination between two forest categories (coniferous vs. broadleaves) and of 102% in the discrimination between five forest types based on main tree species groups.

# 1. Introduction

Hyperspectral sensors observe the earth's surface by simultaneously sampling hundreds of fine narrow contiguous spectral bands with a resolution of up to 0.01 _m in the visible and infrared spectrum. Each pixel in hyperspectral imagery (HSI) corresponds to a spectral vector, which reflects the characteristics of the land cover, making it possible to derive the reflectance behavior of the pixels in the image [1]. The rich spectral information helps to better discriminate surface features and objects than traditional multispectral imaging systems [2]. Hyperspectral sensors are not designed for specific applications,

and today we are witnessing the rapid development of hyperspectral image processing technology [3] and spaceborne hyperspectral missions [4]. For this reason, hyperspectral data are increasingly used in several remote sensing fields such as ecology, atmosphere,

ocean, agriculture and forestry [5].

The ongoing spaceborne hyperspectral missions were joined in March 2019 by PRISMA (Precursore IperSpettrale della Missione Applicativa), developed and operated by the Italian Space Agency (ASI). The purpose of the mission is to evaluate if the PRISMA sensor can be successfully used for monitoring natural resources and atmospheric characteristics and to evaluate possible new applications for environmental

risk management and land observation [6]. The new sensor can be employed for a large number of remote sensing applications. Land cover classification and target detection are some of the most common hyperspectral remote sensing applications [7] and are used to support biodiversity monitoring programs [8]. The underlying assumption in these tasks is that different materials of land cover have unique spectral characteristics [9]. For a "pure" material, these spectral characteristics are called endmembers [10]. Endmembers can be measured in the laboratory, in the field, or can be extracted from remotely sensed imagery. However, when manipulating real scenes, the spectral unicity assumption is difficult to meet because several factors produce noise in an imaging device, e.g., complex atmospheric transmission and interference conditions, as well as the aliasing between adjacent but different materials [9]. An unideal electromagnetic wave transmission environment means that some bands contain less discriminatory information than others [11], and some spectral intervals may not reveal important information for some applications [12]. For these reasons, the large number of hyperspectral bands may affect image classification due to the size, redundancy, and autocorrelation of the data cube.

A detailed description of hyperspectral sensors from various platforms can be already found in several publications [4,12–15], and here we recall their main characteristics in Table 1.

**Table 1**. Main characteristics of spaceborne hyperspectral sensors.

| Sensor | Spatial Resolution (m) | Number of Bands | Swath (km) | Spectral Range (nm) | Spectral Resolution | Launch |
|---|---|---|---|---|---|---|
| Hyperion, EO-1 (USA) | 30 | 196 | 7.5 | 427–2395 | 10 | 2000 |
| CHRIS, PROBA (ESA) | 25 | 19 | 17.5 | 200–1050 | 1.25–11 | 2001 |
| HyspIRI VSWIR (USA) | 60 | 210 | 145 | 380–2500 | 10 | 2020 |
| EnMAP HSI (Germany) | 30 | 200 | 30 | 420–1030 | 5–10 | Not launched yet |
| TianGong-1 (China) | 10 (VNIR) 20 (SWIR) | 128 | 10 | 400–2500 | 10 (VNIR) 23 (SWIR) | 2011 |

| | | | | | | |
|---|---|---|---|---|---|---|
| HISUI (Japan) | 30 | 185 | 30 | 400–2500 | 10 (VNIR) 12.5 (SWIR) | 2019 |
| SHALOM (Italy–Israel) | 10 | 275 | 30 | 400–2500 | 10 | 2021 |
| HypXIM (France) | 8 | 210 | 145–600 | 400–2500 | 10 | 2022 |
| PRISMA (Italy | 30 | 240 | 30 | 400–2500 | 10 | 2019 |

Legend: VNIR (Visible Near InfraRed); SWIR (Short Wave InfraRed); EO-1 (Earth observation-1); PROBA (Project for On Board Autonom); VSWIR (Visible Short Wave InfraRed); HIS (Hyperspectral Imager); HISUI (Hyperspectral Imager Suite); SHALOM (Spaceborne Hyperspectral Applicative Land and Ocean Mission); HypXIM (HYPperspectral-X Imagery); PRISMA (Precursore IperSpettrale della Missione Applicativa)

Several feature selection, spectral feature extraction, and classification methods were developed to cope with the challenging intrinsic nature of hyperspectral data. Some of the traditional approaches for classification include spectral mixture analysis (SMA), multiple endmember spectral mixture analysis (MESMA), and spectral angle mapper (SAM). These methods are based on the assumption that a mixed pixel can be resolved into a group of spectral endmembers, modeled as a linear or a nonlinear combination of these endmembers weighted by their sub-pixel fractional cover [9,16,17]. More recently, machine learning algorithms were used to classify HSI, such as supported vector machine (SVM), random forests (RF), and artificial neural network (ANN) [18]. The latest techniques rely on deep learning, mainly on various convolutional neural network (CNN) architectures [19].

Before starting with classification activities, it is essential to have a better comprehension of the spectral behavior of the different land covers through a discriminatory analysis based on spectral separability criteria. These criteria can be grouped into two categories: probabilistic distance and divergence. Some of the most common probabilistic distances are the Chernoff, Bhattacharyya, and Jeffreys–Matusita (JM) distances, based on the conditional density functions of two given land cover classes. The most common divergence measures are the Kullback–Leibler (KL) and the transformed divergence (TD). These are asymmetrical measures of difference between two probability distributions [11]. All these criteria are pairwise measures based on two-land cover

problems. Usually, it is possible to extend the validity of such criteria to the multi-class cases by averaging all pairwise measures [11].

In vegetation studies, and more specifically in forestry applications, several studies have used such criteria to discriminate different tree species or groups of species on a band-by-band basis. Roberts et al. [20] evaluated pairwise forest species separability at leaf to stand scale, by means of hyperspectral data. Vaiphasa et al. [21] were able to identify and distinguish 16 vegetation types in a mangrove wetland in Thailand, through the JM distance. In addition, Dalponte et al. [22, 23] adopted JM distance as a separability criterion in the hyperspectral band's selection task based on a sequential forward floating selection algorithm to classify boreal forest species, with different nomenclature systems. The JM distance was also adopted as a separability measure to reduce the redundancy of the spectral feature extracted from SPOT-5 images, retaining the class separability [24]. Aria et al. [25] evaluated the separability of three land cover classes in the USA, based on the JM and TD criteria, after applying a spectral region splitting method to three AVIRIS hyperspectral scenes. Attarchi and Gloaguen [26] used TD to identify the best combination of features, in an L-band Synthetic Aperture Radar (SAR) and Landsat classification problem, in the mountain environment of the Hyrcanian forest, Iran. TD was also used to assess Sentinel-2's capability to identify burnt areas in five study areas around the world [27]. More recently, the M-statistic was adopted to assess the capacity of seven spectral bands and 13 spectral indices to distinguish the burned area from four unburned land cover types, in three American states [28].

The degree of separability was also useful in feature selection problems. The bands-selection methods based on separability metrics have shown competitiveness with other methodologies, having the advantages of easy implementation and preservation of the physical interpretation [11,23,29].

This study was aimed at investigating the capabilities of the new PRISMA satellite hyperspectral sensor for the recognition of forest categories through a pairwise separability analysis in two study areas in Italy, on a band-by-band basis. This study was aimed at determining the separability based on two levels of the nomenclature system. First, we tried to separate coniferous vs. broadleaves because such wide forest categories are adopted in the official third level of the European Corine Land Cover

(CLC) [30] and are used in the framework of national and international reporting of forest statistics [31,32]. Then, we tried to separate the main groups of tree species (called forest types and representing a fourth level of the CLC nomenclature system) because this nomenclature is used in local forest management and mapping activities [33, 34].

In order to understand the improvement of the separability capability of the new PRISMA sensor, we compared the result against the spectral separability of the same classes with the Sentinel-2's Multi-Spectral Instrument (MSI) that can be considered for the moment a reference benchmark for forest mapping. To the best of our knowledge, this represents the first study aimed at investigating the potential of the new hyperspectral sensor PRISMA in forestry.

## 1.1. Overview of the PRIMSA mission and instruments

The PRISMA satellite, launched on the 22nd March 2019, has a relook time of approximately 29 days. The satellite is in the small size class (830 kg), with an operational lifetime of 5 years. The instruments onboard the platform include a Hyperspectral Imager, able to capture images in a continuum of 239 spectral bands ranging between 400 and 2500 nm, 66 in the Visible Near Infra Red (VNIR) and 173 in the Short Wave Infra Red (SWIR) spectrum, with a spectral resolution smaller than 12 nm, and a spatial resolution of 30 m. Nine bands are acquired in a wavelength overlapping region between the VNIR and the SWIR cube. The spacecraft also carries a 5 m resolution Panchromatic Camera [35]. The images can be acquired in an area of interest spanning from 180° W to 180° E longitude and 70° N to 70° S latitude. The PRISMA hyperspectral sensor is based on prisms as a dispersive element that projects the incoming radiation on a 2-D matrix detector, and the image scanning system is a "Pushbroom" type [36].

In addition, the platform carried a payload data handling and transmission subsystem (PDHT). This unit provides the memory for the temporary storage of the images and ancillary data and oversees the data transmission to the dedicated ground segment station.

The main characteristics of the sensor are listed in Table 2.

**Table 2.** Main characteristics of PRISMA mission.1

| | |
|---|---|
| Orbit altitude reference | 615 km |
| Swath/Field of view | 30 km/2.77° |
| Ground Sample Distance | Hyperspectral: 30 m<br>PAN: 5 m |
| Spatial pixels | Hyperspectral: 1000<br>PAN: 6000 |
| Pixel size | Hyperspectral: $30 \times 30$ μm<br>PAN: $6.5 \times 6.5$ μm |
| Spectral range | VNIR: 400–1010 nm (66 bands)<br>SWIR: 920–2500 nm (173 bands)<br>PAN: 400–700 nm |
| Spectral sampling interval (SSI) | ≤12 nm |
| Spectral width | ≤12 nm |
| Spectral calibration accuracy | ±0.1 nm |
| Radiometric quantization | 12 bit |
| VNIR Signal to noise ratio (SNR) | >200:1 |
| SWIR SNR | >100:1 |
| PAN SNR | >240:1 |
| Absolute radiometric accuracy | Better than 5% |

PRISMA acquires images on demand, in specific individual locations requested by the users, in a "standard" mode, resulting in a $30 \times 30$ km scene and a "strip" mode, generating an image 30 km width, and having a maximum length of 1800 km. The combination of hyperspectral and panchromatic products gives the ability to recognize the physical-chemical and geometric characteristics of the target of interest within a scene and can potentially provide major contributions in the field of forest analysis, precision agriculture, water quality assessment, and climate change research [6,37].

To date, the PRISMA mission has acquired 64,504 images around the globe, of which 58,479 were acquired in 2020 and the remaining in 2019. Searching for images with cloud cover lower than 10% and acquisition during the vegetative period (1st April–30th September) we resulted in only 23 images available in Italy, all acquired in 2019 in 15 different areas (Figure 1).

**Figure 1.** Spatial distribution of all the 23 PRISMA images from the portal prisma.asi.it available in Italy, all of them acquired in 2019 (with cloud cover lower than 10% and acquisition in the vegetative period).

### 1.2. Preprocessing levels of PRISMA cubes

PRISMA images can be freely downloaded after registration at http://prisma-i.it/index.php/en/ (Figure 1). They can be released with three levels of preprocessing [35]:

1. Level0: The L0 product contains raw data in binary files, including instrument and satellite ancillary data, like the cloud cover percentage.

2. Level1: The L1 product is a top-of-atmosphere radiance imagery organized as follows: two radiometrically calibrated hyperspectral and panchromatic radiance cubes and two co-registered HYPER and PAN radiance cubes.

3. Level2: The L2 product is divided in:

   - L2B: Atmospheric correction and geolocation of the L1 product (bottom-of-atmosphere radiance);

   - L2C: Atmospheric correction and geolocation of the L1 product (bottom-of-atmosphere reflectance, including aerosol optical thickness and water vapor map);

   - L2D: Geocoding (orthorectification) of L2C.

Levels 1 and 2 are generated on demand and released in the Hierarchical Data Format Release 5 (HDF5). The Level 2 products can be georeferenced with or without ground control points (GCP) according to user preference and GCP availability [6].

## 2. Materials and Methods

### 2.1. Study area

This study was conducted in two areas located in central Italy (42°53′ N, 11°6′ E and 43°17′ N, 12°13′ E) (Figure 2), each one covering 900 km$^2$, just as the PRISMA tiles do. The areas were selected based on the availability of reference data and PRISMA images with a cloud cover < 10% and an acquisition period during the leaf-on vegetation phase.

The first area is in the Province of Grosseto, Tuscany, in the Colline Metallifere, the main and most extensive hilly and mountainous system of the Tuscan Anti-Apennines which includes the city of Grosseto. The area is characterized by gentle slopes (mean slope = 8%) and large altitude differences (from sea level up to 1000 m a.s.l.). The area is dominated by Mediterranean evergreen oaks (*Quercus ilex L., Quercus suber L.*) and mesophilic deciduous forests (*Quercus cerris L., Quercus pubescens L., Ostrya carpinifolia Scop., Castanea sativa Mill.*). Other tree species include domestic pine (*Pinus pinea L.*), maritime pine (*Pinus pinaster Aito*), and Aleppo Pine (*Pinus halepensis Mill.*). The broadleaves part of the forest was actively managed with coppice clearcut for firewood production.

The second area is in the provinces of Arezzo and Perugia, between the regions of Tuscany and Umbria. The area includes the Trasimeno lake, the fourth largest lake in Italy, and the city of Perugia. The altitude ranges between 170 and 1100 m above sea level, with a steep slope, up to 140%. Broadleaves formations characterized the area, dominated by mesophilic deciduous oaks (*Quercus cerris L., Quercus pubescens L.*) and evergreen oaks (mainly *Quercus ilex L.*). Other tree species include Maritime pine (*Pinus pinaster Aito*) and Black pine (*Pinus nigra A.*). The management is less active than in Area 1, but still dominated by coppice for firewood production.
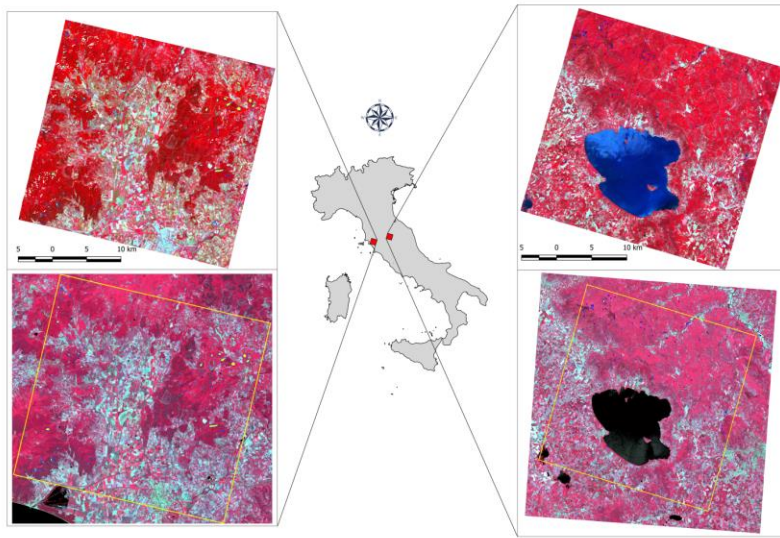
Figure 2. The two study areas. On top: PRISMA false color (RGB 66-35-17); on bottom: Sentinel-2A false color (RGB 8-4-3). In yellow: the boundaries of the PRISMA scene in the Sentinel one.

## 2.2. Reference data

Reference data consist of 161 polygons digitized from the 5 m resolution panchromatic images of the PRISMA satellite to assign the respective third and fourth CLC land cover classes, distributed evenly and proportionally to the abundance of forest types, to ensure that the spectral signatures are as pure as possible.

In the 161 polygons, the forest types were identified on the basis of a local land use and land cover databases of the Tuscan region based on a network of sampling points that are distributed on the basis of an unaligned systematic sampling design [38]. Sampling units are located randomly within $250 \times 250$ m grid cells for a total of 367.760 points. The nomenclature system we adopted refers to the third level of the Corine Land Cover [26], refined with a fourth level adapted locally (Table 3).

Table 3. Nomenclature system adopted in this study.

| Third Level | Description | Fourth Level | Description |
|---|---|---|---|
| 3.1.1 | Broadleaf | 3.1.1.1 | Deciduous evergreen |
| | | 3.1.1.2 | Deciduous broadleaf |

| | | 3.1.1.5 | Azonal formation |
|---|---|---|---|
| 3.1.2 | Coniferous | 3.1.2.1 | Mediterranean coniferous |
| | | 3.1.2.2 | Mountain coniferous |

A total of 250 ha (78 polygons) and 220 ha (83 polygons) were acquired in Area 1 and Area 2, respectively (Figure 3).
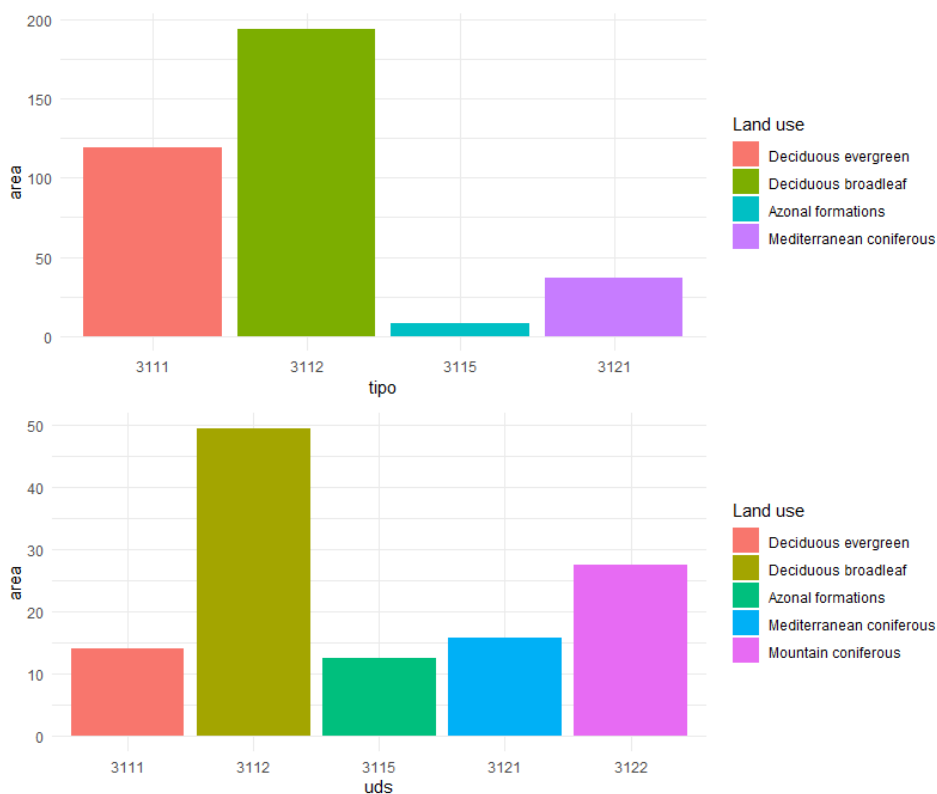


Figure 3. Distribution of forest types according to the reference dataset for the two study areas.

## 2.3. Remotely sensed data

To test the spectral separability of the forest types, we used two PRISMA L2D cloud free scenes acquired on 16th of June 2019 and the 4th of June 2019, respectively. Each image consists of 239 spectral bands at 30 m spatial resolution ranging between 402 and 2497 nm, with a footprint of 30 × 30 km, atmospherically corrected and orthorectified, provided in he5 format. From the overlapping wavelength region, we

retained only the bands from the VNIR cube, for a total of 230 considered spectral bands.

For comparison purposes, we also downloaded for the same areas the Sentinel-2A L2A scenes. The Sentinel-2 images were acquired on the 18th of June 2019 and on the 13th of June 2019, respectively. All the S2 scenes from the Multi-Spectral Instrument (MSI) have cloud cover <5% and are composed of 13 spectral bands with a spatial resolution of 10, 20, and 60 m depending on the wavelength, ranging between 440 and 2190 nm, with a footprint of 100 × 100 km. S2 images were atmospherically corrected and orthorectified. For this study, the bands b1, b9, and b10 were not used due to their coarse spatial resolution (60 m) and because they are specific to atmospheric characterization and not for land monitoring applications. The remaining bands were resampled to the PRISMA tiles resolution of 30 × 30 m with the nearest-neighbor algorithm.

All the remotely sensed images resulted cloud-free for the forest part of the study areas.

## 2.4. Methods

The PRISMA scenes were first converted in a suitable format by the R package *prismaread* [39], especially developed to import and convert the PRISMA hyperspectral cubes. After the conversion, from the resultant hyperspectral cube, we extracted the reflectance values for every pixel within the 161 reference polygons of the two study areas for each one of the 230 spectral bands. This procedure allows extracting an idealized, pure signature of the spectral classes [40]. These correspond to the full reflectance of pixels exclusively occupied by a single forest type.

The same procedure was repeated for the Sentinel-2A scenes.

A pairwise land cover spectral separability analysis was then carried out for each band of the two sensors. Four commonly used statistical measures were calculated to quantify the two-class separability of the different sensors at each one of the study areas [41–43]. The analysis was repeated for both the third and fourth levels of the nomenclature systems. The separability analysis was performed with the R package

*spatialEco* [44] for all the possible combinations of each forest type. The statistics were:

1. M-Statistic [45] (M): measures the difference of the distributional peaks of the reflectance values and is calculated as follows:

$$M = \frac{\mu_a - \mu_b}{\sigma_a + \sigma_b} \tag{1}$$

where $\mu_x$ is the mean value for class $x$ and $\sigma_x$ the standard deviation of class $x$. A high M-statistic indicates a good separation between the two classes as the within-class variance is minimized and the between-class variance maximized. The limitation of the M-statistic is that when the means of two classes are equal, the M-statistic will always be zero and cannot accurately reflect the separability.

2. Bhattacharyya distance [46] (B): measures the degree of dissimilarity between any two probability distributions, and is calculated as follows:

$$B = \frac{1}{8}(\mu_a - \mu_b)^T \left(\frac{\Sigma_a - \Sigma_b}{2}\right)^{-1} (\mu_a - \mu_b) + \frac{1}{2} ln \frac{\frac{\Sigma_a - \Sigma_b}{2}}{\sqrt{\Sigma_a - \Sigma_b}} \tag{2}$$

where $\mu_x$ is the mean value for class $x$ and $\Sigma_x$ are the covariances. The advantage with respect to the M-statistic is that the Bhattacharyya distance takes into account the class separability due to the covariance difference, expressed in the second term of the equation.

3. The Jeffries–Matusita distance [47] (JM distance): the JM distance is a function of separability that directly relates to the probability of how good a resultant classification will be. It is calculated as a function of the Bhattacharyya distance:

$$JM = \sqrt{2(1 - e^{-B})} \tag{3}$$

where $B$ is the Bhattacharyya distance.

The JM distance is asymptotic to √2, where values of √2 suggest complete separability. The JM distance can handle data that follow a multivariate normal distribution.

4. Transformed divergence [48,49] (TD): is a maximum likelihood approach that provides a covariance weighted distance between the class means to determine whether spectral signatures were separable:

$$TD = 2\left[1 - e^{-\frac{D}{8}}\right] \tag{4}$$

$$D = \frac{1}{2}tr[(C_a - C_b)(C^{-1}{}_a - C^{-1}{}_b)] + \frac{1}{2}tr[(C^{-1}{}_a - C^{-1}{}_b)(\mu_a - \mu_b)(\mu_a - \mu_b)^T] \tag{5}$$

where $C_x$ is the covariance matrix of class $x$, $\mu_x$ is the mean value for class $x$, $tr$ is the matrix trace function, and $T$ is the matrix transposition function. Transformed divergence ranges between 0 and 2 and gives an exponentially decreasing weight to increasing distances between the classes. As for the JM distance, the transformed divergence values are widely interpreted as being indicative of the probability of performing a correct classification [48].

Lastly, we calculated the percentage variation of the above four metrics obtained by PRISMA with respect to Sentinel-2, for both study areas and the two levels of the nomenclature system. The increment was calculated based on the maximum separability reached in each class pair by the two sensors with the formula:

$$I_m = \frac{Max_{P\,m} - Max_{S\,m}}{Max_{S\,m}}.100 \tag{6}$$

where $I_m$ is the percentage increment in separability for the metric $m$, $Max_{Pm}$ and $Max_{Sm}$ are, respectively, the maximum value of separability reached by PRISMA and Sentinel-2 for metric $m$.

## 3. Results

The spectral signatures derived from PRISMA and Sentinel-2A data are shown in Figure 4. These were calculated as the median reflectance value of every pixel fallen in the specific forest classes of the two levels of the nomenclature system. As expected,

the hyperspectral data allowed a more complete and continuous representation of the spectral behavior of the different forest types compared to the multispectral data.
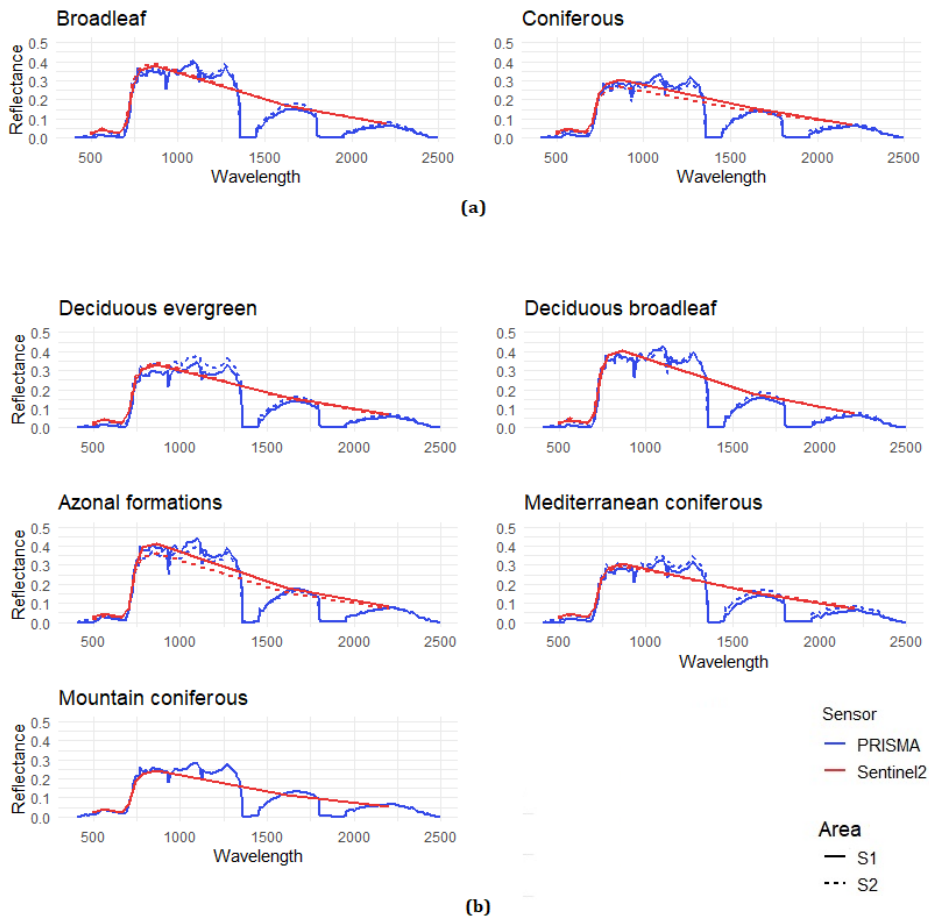


Figure 4. Spectral signatures of the considered forest classes based on PRISMA (blue line) and Sentinel-2 (red line). The solid line for Area 1, the dotted line for Area 2: (a) the third level nomenclature system; (b) the fourth level.

Based on the spectral signatures extracted within the 161 polygons, the four separability metrics between each pair of classes for each of the 230 bands were calculated for both levels of the nomenclature system, and for both the study areas. The results are shown in Figure 5 and the eight subgraphs represent the four statistical measurements for the two sensors on a band-by-band basis. For the third level, similar trends were observed between the two sensors, but with different results in the two study areas. In Area 1, the PRISMA data allow a better separability for the single class combination, in the visible

ranges. The coniferous–broadleaf combination was better distinguished from PRISMA, with a mean separability value of 0.64 occurred in the blue spectrum (between 450 and 503 nm), against a mean value of 0.13 obtained in the SWIR spectrum for Sentinel-2 (1613 nm, band 11). For both sensors, the best metrics for distinguishing the coniferous–broadleaf combination were the transformed divergence and the Jeffries–Matusita distance.
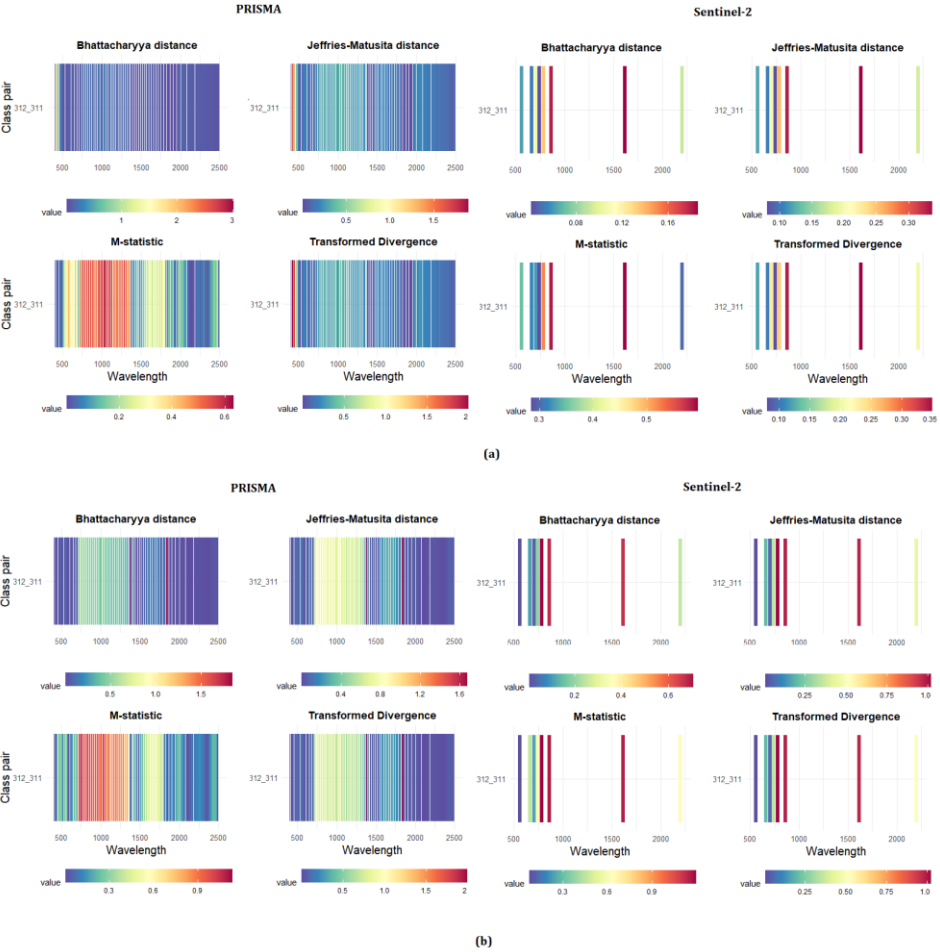


Figure 5. Results of the separability analysis for the third level nomenclature system, divided by statistical metrics and class pairs. The horizontal and vertical axes represent the wavelength and the pairwise vegetation combinations, respectively. The color of each grid cell represents the separability of the corresponding band and class pair, as reported by the legend bar at the bottom of the sub-panels. The higher the value is, the more separable the two classes become: (a) Area 1; and (b) Area 2.

In Area 2, the coniferous and broadleaf were distinguished only in two small portions of the spectrum, near 1380 and 1830 nm, that are not sensed by the Sentinel-2 MSI. In these wavelengths, the PRISMA sensor achieved a mean separability value of 0.75, against 0.43 of Sentinel-2, reached in bands 7, 8, and 11.

The results of the separability analysis on the fourth level of the nomenclature system are shown in Figure 6. In Area 1, the maximum separability value was reached by the PRISMA sensor between 428 and 443 nm, for the pair of Mediterranean coniferous–azonal formations (mean separability value = 0.69), followed by the pairs of azonal formation–evergreen broadleaf (mean separability = 0.68), azonal formation–evergreen broadleaf (mean separability = 0.58), and Mediterranean coniferous—evergreen broadleaf (mean separability = 0.45). The land cover pairs characterized by the least separability were those of Mediterranean coniferous–deciduous evergreen followed by the evergreen broadleaf–deciduous evergreen, with a mean separability value of 0.40 and 0.39, respectively. As for PRISMA, the class pairs better distinguished from Sentinel-2 were Mediterranean coniferous–azonal formation and the evergreen broadleaf–azonal formation, with a mean separability of 0.45 and 0.38, respectively. In Area 2, all the combinations were generally better distinguished by the PRISMA sensor in the NIR and SWIR wavelengths (1373 and 1822 nm), with the Mediterranean coniferous–evergreen broadleaf separability reached the maximum value of 0.74.
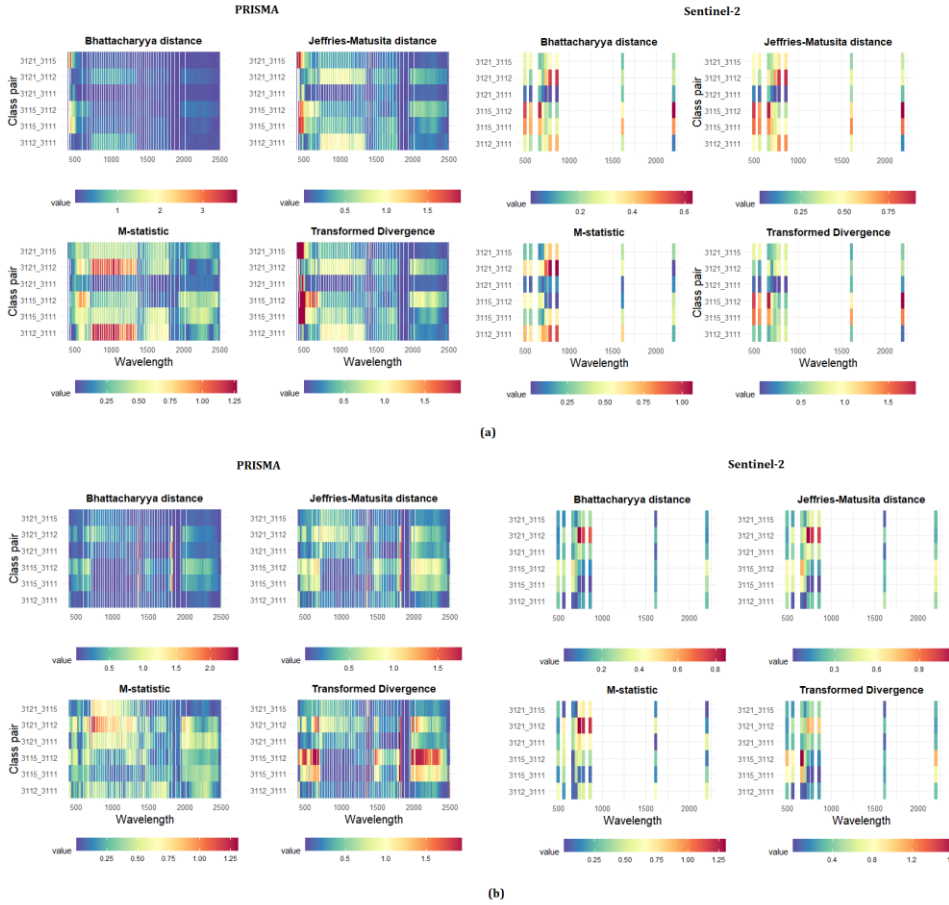
Figure 6. Results of the separability analysis on the fourth level of the nomenclature system, divided by statistical metrics and forest type pairs. Symbology as in Figure 6: (a) Area 1; (b) Area 2.

In both the study areas, the hyperspectral sensor outperformed Sentinel-2 in the differentiation of all the forest type combinations. Table 4 reports the maximum separability reached by each class pair in all considered metrics. The table also indicates the wavelength at which the maximum separability was reached. The best wavelength range for discrimination proved to be the blue and NIR spectrum in Areas 1 and 2, respectively.

Table 4. Best separability for each pairwise combination. In blue, the PRISMA sensor; and in red, the Sentinel-2 sensor. The number represents the wavelength where the highest separability was obtained. B for Bhattacharyya distance, JM for Jeffries–Matusita distance. M for M-Statistic, and TD for Transformed Divergence.

50

| Class Pair | PRISMA | | | | | Sentinel-2 | | | | |
|---|---|---|---|---|---|---|---|---|---|---|
| | Wavelength | B | JM | M | TD | Wavelength | B | JM | M | TD |
| **Area 1** 3112_3111 | 48 | 0.81 | 1.11 | 1.27 | 1.11 | 782 | 0.44 | 0.71 | 0.93 | 0.73 |
| 3115_3111 | 236 | 2.55 | 140 | 0.18 | 2.00 | 2202 | 0.47 | 0.75 | 0.43 | 1.47 |
| 3115_3112 | 464 | 2.11 | 1.36 | 0.22 | 2.00 | 2202 | 0.63 | 0.93 | 0.39 | 1.88 |
| 3121_3111 | 696 | 0.90 | 1.19 | 0.03 | 2.00 | 1613 | 0.15 | 0.27 | 0.05 | 0.37 |
| 3121_3112 | 989 | 0.77 | 1.07 | 1.24 | 1.07 | 864 | 0.57 | 0.87 | 1.07 | 0.90 |
| 3121_3115 | 1156 | 3.79 | 1.42 | 0.18 | 2.00 | 782 | 0.32 | 0.55 | 0.69 | 0.72 |
| **Area 2** 3112_3111 | 100 | 1.00 | 1.27 | 0.22 | 2.00 | 1613 | 0.20 | 0.36 | 0.63 | 0.36 |
| 3115_3111 | 375 | 2.07 | 1.35 | 0.24 | 2.00 | 664 | 0.36 | 0.60 | 0.05 | 1.09 |
| 3115_3112 | 561 | 1.71 | 1.224 | 0.10 | 2.00 | 664 | 0.51 | 0.80 | 0.03 | 1.62 |
| 3121_3111 | 791 | 2.41 | 1.40 | 0.20 | 2.00 | 740 | 0.31 | 0.54 | 0.79 | 0.54 |
| 3121_3112 | 1021 | 2.21 | 1.38 | 0.11 | 2.00 | 740 | 0.85 | 1.15 | 1.30 | 1.15 |
| 3121_3115 | 1190 | 0.41 | 0.67 | 0.89 | 0.68 | 782 | 0.27 | 0.47 | 0.73 | 0.48 |
| 3121_3122 | 1480 | 1.25 | 1.23 | 0.15 | 2.00 | 1613 | 0.30 | 0.52 | 0.77 | 0.53 |
| 3122_3111 | 1985 | 2.10 | 1.35 | 0.24 | 2.00 | 740 | 0.61 | 0.91 | 1.10 | 0.92 |
| 3122_3112 | 2171 | 1.75 | 1.25 | 0.09 | 2.00 | 740 | 1.35 | 1.28 | 1.64 | 1.48 |
| 3122_3115 | 2380 | 0.88 | 1.17 | 1.33 | 1.18 | 782 | 0.58 | 0.88 | 1.07 | 0.93 |

In Tables 5 and 6, we present the confusion matrix of two-class separability for PRISMA (in blue) and Sentinel-2 (in red), for the third and fourth levels of the nomenclature system, respectively. The cells of the matrix indicate the wavelengths at

which the separability for the two classes considered is maximum, according to the average of the four metrics M, JM, B, and TD.

In the third level, the two sensors reached the maximum separability at different wavelengths, in the red–NIR transition zone (called *red edge* for the vegetation spectrum) for Sentinel-2 MSI and in the blue for the SWIR for the PRISMA sensor.

Similar results were obtained for the fourth level. The red edge and NIR regions were best suited for separating the forest types only in Area 2, while in Area 1 the blue channel was particularly adapted to distinguish the azonal formations and deciduous broadleaf.

Table 5. Third level: best wavelength for two-class separability. In blue, the wavelength extracted from PRISMA; in red, from Sentinel-2.

| | | Class 2 | | | |
|---|---|---|---|---|---|
| | | Area 1 | | Area 2 | |
| | | 311 | 312 | 311 | 312 |
| Class 1 | 311 | / | 864 | / | 782 |
| | 312 | 450 | / | 1841 | / |

Table 6. Fourth level: best wavelength for two-class separability. In blue, the wavelength extracted from PRISMA; in red from Sentinel-2.

| | | Class 2 | | | | | | | |
|---|---|---|---|---|---|---|---|---|---|
| | | Area 1 | | | | Area 2 | | | |
| | | 3111 | 3112 | 3121 | 3122 | 3112 | 3115 | 3121 | 3122 |
| Class 1 | 3111 | / | 782 | 664 | / | 1613 | 703 | 740 | 740 |
| | 3112 | 814 | / | 864 | / | / | 740 | 740 | 740 |
| | 3115 | 443 | 428 | 782 | / | 1373 | / | 782 | 782 |
| | 3121 | 443 | 1029 | / | / | 1373 | 731 | / | 1613 |
| | 3122 | / | / | / | / | 1373 | 1142 | 1361 | / |

Based on the results of the separability analysis, we calculated the percentage variation of the four metrics obtained by PRISMA concerning Sentinel-2, for both the study areas and the two nomenclature levels (Figure 7).
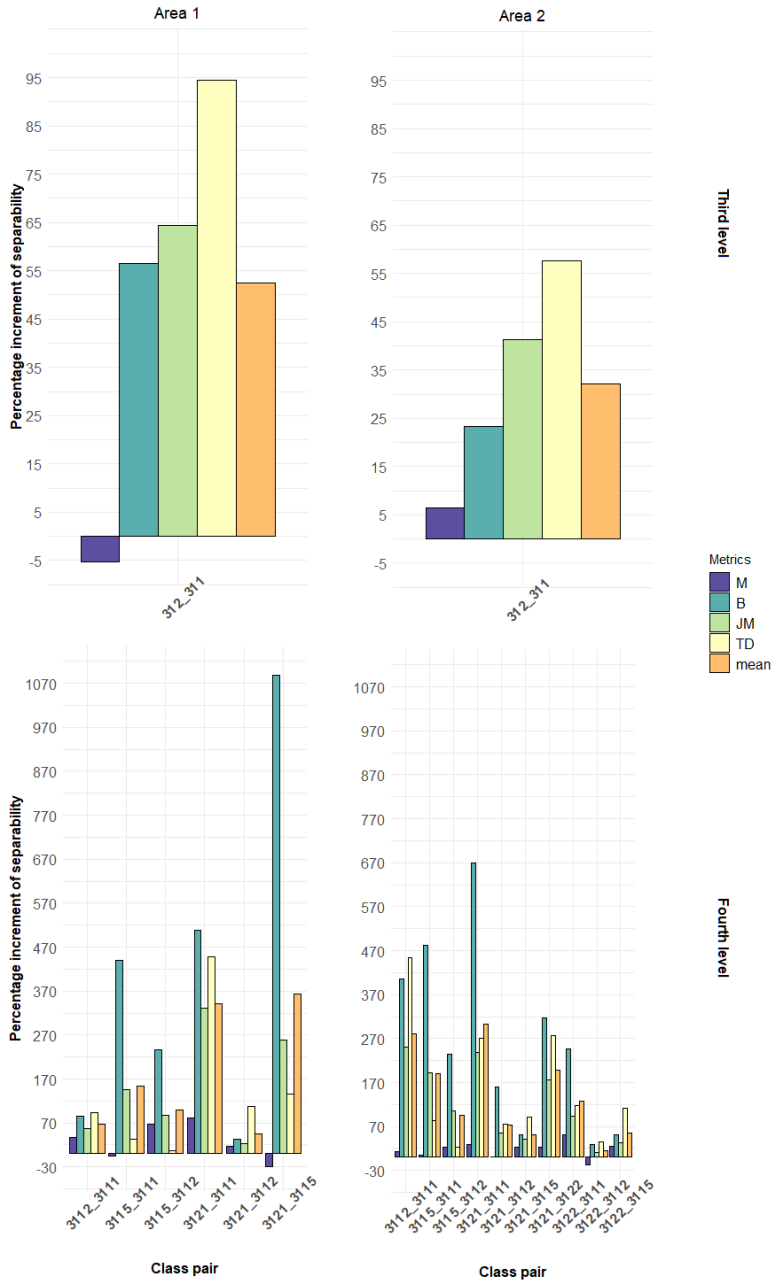
## 4. Discussion

The separability analysis revealed similar results for the two levels of the nomenclature system and the two study areas. At both levels of the nomenclature system, PRISMA overcame Sentinel-2, but with different scores.

At the third level of the nomenclature system, the broadleaf–coniferous class was well separated by PRISMA, in a narrow range of wavelengths not sensed by the Sentinel-2 MSI, corresponding to the blue (450 nm) and SWIR (1841 nm) bands in Areas 1 and 2, respectively. The differences between the two study areas were most probably due to the characteristics of the terrain. Area 2 presents a more complex topography, with steep slopes and a wide range of elevation, which influence the backscatter of the sensors [50,51]. Therefore, in regions of rapid slope or aspect changes, a large radiometric noise can be expected [51]. In addition, the presence of many shadow areas, due to the forest characteristics, where high and low height trees are mixed, has surely affected the results of the separability analysis and could explain most of the differences between the study areas.

In addition, the effects of varying atmospheric and illumination conditions, due to the time lag between the scene acquisitions, may be of considerable impact. It is worth noticing that the separability was higher in the SWIR channel of PRISMA than in Sentinel-2. Thanks to its spectral resolution and band numbers, hyperspectral images have many advantages in distinguishing the different forest types.

For the fourth level of the nomenclature system, the performance of PRISMA data was even better when compared to Sentinel-2. We found that the separability of forest types was higher in a narrow range of wavelength in the blue channel (430–440 nm) for Area 1, in the NIR-plateau (approximately at 1370 nm), and in the SWIR spectrum at 1822 nm in Area 2. These wavelengths were not sensed by the Sentinel-2 MSI, which primarily relies on the red-edge bands (b6, b7) to discriminate the forest types, because of their high sensitivity to pigment concentration in most leaves and canopies [21]. Our study confirms previous results [17,52,53] where the broadleaves were best separated in the SWIR and NIR spectral ranges, and the coniferous specifically in the SWIR, in bands located directly beyond the water absorption features of the spectrum. This region was also critical for the separation of coniferous–broadleaf combinations, probably due to the differences in leaf water content and total leaf mass between species, which produces a typical species-dependent spectral behavior [53]. The blue channel (450–550 nm), associated with the chlorophyll and other pigments content, was useful for all comparisons between coniferous and broadleaf forest types in Area 1. The

better performance of PRISMA at the fourth level of the nomenclature system derived from the combination of the fine spectral resolution and the structural complexity of the forest stand. A forest area with a mixed tree species composition with very similar spectral signatures needs the use of data with finer spectral resolution, while in a forest with few spectrally different species, a coarser spectral resolution can also be used [7]. At the pixel level, the structural complexity of the Mediterranean forest, and the fraction of non-photosynthetic vegetation (that is, bark, branches, wood) affects the extraction of pure spectral signatures.

The low number of field references, observer bias, and time differences between field observation and image acquisition could also influence the results.

Regarding the spatial resolution, it does not appear that the coarser resolution of PRISMA has negatively affected the separability of the classes. As found by Ghosh et al. [54] and Liu et al. [55] a finer spatial resolution is not necessarily better. The former authors obtained better classification accuracy using Hyperion hyperspectral imagery at 30 m spatial resolution than HyMAP imagery at 8 m resolution. Roth et al. [56] demonstrated that 40 and 60 m resolution hyperspectral data can be used to reliably classify most dominant species and plant functional types, in different ecosystem types, including a Mediterranean climate region in California. Moreover, other studies [57,58] have proven that hyperspectral data are less sensitive than multispectral ones in coarsening spatial resolution, due to their greater spectral coverage and finer spectral resolution. In Area 1, the use of the PRISMA sensor improved the recognition between the coniferous and the broadleaves of the third level, in three metrics out of four. In addition, for the fourth level, the fine spectral resolution of the hyperspectral sensor leads to a better separation in all the combinations of forest types. In Area 2, the differences in the performances between the two sensors were generally lower than in Area 1, probably due to the more complex topography and the higher number of forest classes. An in-depth analysis of the slope revealed that here most of the vegetation categories were on a very steep slope, up to 120%, characterized by abrupt changes that caused backscatter interferences and augmented the signal-to-noise ratio of the narrow hyperspectral bands. However, the PRISMA sensor allowed better discrimination in all class pairs, achieving an average improvement among forest types of over 120% in

Area 1 and 84% in Area 2, with maximum improvements for some types of 170% in Area 1 and 130% in Area 2.

## 5. Conclusion

In this paper, we evaluated the spectral separability of forest types in two study areas in Italy using the new hyperspectral satellite PRISMA, contrasted against the well-known Sentinel-2 multispectral sensor. The analysis was carried out in the spectral range between 400 and 2500 nm, and with two levels for forest type nomenclature systems. The main findings of this study are:

1. Hyperspectral data were effective in discriminating forest types in both study areas and nomenclature system levels (average normalized separability higher than 0.50 for four out of six classes in Area 1, and nine out of 10 class pairs in Area 2). Only in Area 1 for the third level of nomenclature system the Sentinel-2 MSI was comparable with the PRISMA sensor.

2. The SWIR spectral zone resulted as the most suitable for forest type discrimination. Other remarkable zones were the blue channel (in Area 1) for the broadleaf–coniferous class pair, the red-edge and the NIR-plateau (in Area 2) for most of the considered class pairs. Sentinel-2 relies primarily on the red-edge region (b6, b7) in separating the forest classes.

3. The PRISMA sensor improved the separation between coniferous and broadleaves by 50% in Area 1 and 30% in Area 2. At the fourth level, the average separability of was 120% higher in Area 1 and 84% in Area 2.

This study showed that in the two investigated study areas, the PRISMA hyperspectral sensor had the capability to better discriminate forest types than Sentinel-2 MSI. This was true when the classification requested is for differentiating different forest types, while when aggregated forest classes are used (broadleaves/coniferous). Sentinel-2 MSI can still compete with the hyperspectral sensor. This study also demonstrated that where PRISMA images were not available, Sentinel-2 MSI can be used to separate simple forest classes.

In the future, as the PRISMA data will increase in availability, the new hyperspectral time series can pave the path for more accurate research in plant phenology, forest species classification, the recognition of forest disturbances and change detection studies, making these data very attractive for the forestry sector and beyond. Other fields of expected benefits can be precision agriculture (e.g., crop mapping, crop rotation, crop stress analysis, fertilization), inland and coastal waters (e.g., water quality, chlorophyll monitoring, alga bloom), as well as climate change and environmental research (e.g., desertification, deforestation, vegetation stress, environmental degradation, and hazards).

However, further investigations were needed to explore the full capabilities of the new hyperspectral sensor, for example, testing new algorithms for feature selection and band extraction, the use of vegetation indices, the possibility of automatic segmentation, and object-based classification.

## 6. Reference

1. Kumar, B.; Dikshit, O.; Gupta, A.; Singh, M.K. Feature extraction for hyperspectral image classification: a review. *Int. J. Remote Sens.* **2020**, *41*, 6248–6287, doi:10.1080/01431161.2020.1736732.
2. Li, S.; Wu, H.; Wan, D.; Zhu, J. An effective feature selection method for hyperspectral image classification based on genetic algorithm and support vector machine. *Knowl. Based Syst.* **2011**, *24*, 40–48, doi:10.1016/j.knosys.2010.07.003.
3. Acquarelli, J.; Marchiori, E.; Buydens, L.M.C.; Tran, T.; Van Laarhoven, T. Spectral spatial classification of hyperspec-tral images: Three tricks and a new supervised learning setting. *Remote Sens.* **2018**, *10*, 1156.
4. Defourny, P.; D'Andrimont, R.; Maugnard, A.; Defourny, P. Survey of Hyperspectral Earth Observation Applications from Space in the Sentinel-2 Context. *Remote Sens.* **2018**, *10*, 157, doi:10.3390/rs10020157.
5. Liu, H.; Zhang, F.; Zhang, L.; Lin, Y.; Wang, S.; Xie, Y. UNVI-Based Time Series for Vegetation Discrimination Using Separability Analysis and Random Forest Classification. *Remote Sens.* **2020**, *12*, 529, doi:10.3390/rs12030529.
6. Guarini, R.; Loizzo, R.; Longo, F.; Mari, S.; Scopa, T.; Varacalli, G. Overview of the prisma space and ground segment and its hyperspectral products. In Proceedings of the 2017 IEEE International Geoscience and Remote Sensing Symposium (IGARSS), Fort Worth, TX, USA, 23–28 July *2017*.
7. Rees, G. *The Remote Sensing Data Book*; Cambridge University Press: Cambridge, UK, 2005.
8. Travaglini, D.; Barbati, A.; Chirici, G.; Lombardi, F.; Marchetti, M.; Corona, P. ForestBIOTA data on deadwood monitoring in Europe. *Plant Biosyst.* **2007**, *141*, 222–230, doi:10.1080/11263500701401778.

9. Hao, X.; Wu, Y.; Wang, P. Angle Distance-Based Hierarchical Background Separation Method for Hyperspectral Imagery Target Detection. *Remote Sens.* **2020**, *12*, 697, doi:10.3390/rs12040697.

10. Adams, J.B.; Smith, M.O.; Gillespie, A.R. Imaging spectroscopy: Interpretation based on spectral mixture analysis. In *Remote Geochemical Analysis: Elemental and Mineralogical Composition*; Pieters, C.M., Englert, P.A.J., Eds.; Press Syndicate of University of Cambridge: Cambridge, UK, 1993; pp. 145–166.

11. Guo, B.; Damper, R.; Gunn, S.R.; Nelson, J. A fast separability-based feature-selection method for high-dimensional remotely sensed image classification. *Pattern Recognit.* **2008**, *41*, 1653–1662, doi:10.1016/j.patcog.2007.11.007.

12. Staenz, K.; Held, A. Summary of current and future terrestrial civilian hyperspectral spaceborne systems. In Proceedings of the 2012 IEEE International Geoscience and Remote Sensing Symposium, Munich, Germany, 22–27 July 2012; pp. 123–126.

13. Verrelst, J.; Romijn, E.; Kooistra, L. Mapping Vegetation Density in a Heterogeneous River Floodplain Ecosystem Using Pointable CHRIS/PROBA Data. *Remote Sens.* **2012**, *4*, 2866–2889, doi:10.3390/rs4092866.

14. Cook, B.; Corp, L.; Nelson, R.; Middleton, E.; Morton, D.; McCorkel, J.; Masek, J.; Ranson, K.; Ly, V.; Montesano, P. NASA Goddard's LiDAR, Hyperspectral and Thermal (G-LiHT) Airborne Imager. *Remote Sens.* **2013**, *5*, 4045–4066.

15. Middleton, E.M.; Ungar, S.G.; Mandl, D.J.; Ong, L.; Frye, S.W.; Campbell, P.E.; Landis, D.R.; Young, J.P.; Pollack, N.H. The Earth Observing One (EO-1) Satellite Mission: Over a Decade in Space. *IEEE Sel. Top. Appl. Earth Obs. Remote Sens.* **2013**, *6*, 427–438.

16. Yin, J.; Wang, Y.; Hu, J. A New Dimensionality Reduction Algorithm for Hyperspectral Image Using Evolutionary Strategy. *IEEE Trans. Ind. Inf.* **2012**, *8*, 935–943, doi:10.1109/tii.2012.2205397.

17. Adams, J.B.; Smith, M.O.; Johnson, P.E. Spectral mixture modeling: A new analysis of rock and soil types at the Vi-king Lander 1 site. *J. Geophys. Res. Atmos. Solid Earth Planets* **1986**, *91*, 8098–8112.

18. Adam, E.; Mutanga, O.; Rugege, D. Multispectral and hyperspectral remote sensing for identification and mapping of wetland vegetation: a review. *Wetl. Ecol. Manag.* **2010**, *18*, 281–296, doi:10.1007/s11273-009-9169-z.

19. Kussul, N.; Lavreniuk, M.; Skakun, S.; Shelestov, A. Deep Learning Classification of Land Cover and Crop Types Using Remote Sensing Data. *IEEE Geosci. Remote Sens. Lett.* **2017**, *14*, 778–782, doi:10.1109/lgrs.2017.2681128.

20. Vali, A.; Comai, S.; Matteucci, M. Deep Learning for Land Use and Land Cover Classification based on Hyperspectral and Multispectral Earth Observation Data: A Review. *Remote Sens.* **2020**, *12*, 2495, doi:10.3390/rs12152495.

21. Roberts, D.A.; Ustin, S.L.; Ogunjemiyo, S.; Greenberg, J.A.; Dobrowski, S.Z.; Chen, J.; Hinckley, T.M. Spectral and Structural Measures of Northwest Forest Vegetation at Leaf to Landscape Scales. *Ecosystems* **2004**, *7*, 545–562, doi:10.1007/s10021-004-0144-5.

22. Vaiphasa, C.; Ongsomwang, S.; Vaiphasa, T.; Skidmore, A.K. Tropical mangrove species discrimination using hyperspec-tral data: A laboratory study. *Estuar. Coast. Shelf Sci.* **2005**, *65*, 371–379.

23. Dalponte, M.; Orka, H.O.; Gobakken, T.; Gianelle, D.; Naesset, E. Tree Species Classification in Boreal Forests With Hyperspectral Data. *IEEE Trans. Geosci. Remote Sens.* **2013**, *51*, 2632–2645, doi:10.1109/tgrs.2012.2216272.

24. Dalponte, M.; Bruzzone, L.; Gianelle, D. Tree species classification in the Southern Alps based on the fusion of very high geometrical resolution multispectral/hyperspectral images and LiDAR data. *Remote Sens. Environ.* **2012**, *123*, 258–270, doi:10.1016/j.rse.2012.03.013.

25. Zeng, W.; Lin, H.; Yan, E.; Jiang, Q.; Lu, H.;; Wu, S. Optimal selection of remote sensing feature variables for land cov-er classification. In Proceedings of the 2018 Fifth International Workshop on Earth Observation and Remote Sensing Applications (EORSA), Xi'an, China, 18–20 June 2018.

26. Aria, S.E.H.; Menenti, M.; Gorte, B. Spectral discrimination based on the optimal informative parts of the spectrum. In Proceedings of the Image and Signal Processing for Remote Sensing XVIII, Edinburgh, UK, 8 November 2012; Volume 8537, p. 853709.

27. Attarchi, S.; Gloaguen, R. Classifying Complex Mountainous Forests with L-Band SAR and Landsat Data Integration: A Comparison among Different Machine Learning Methods in the Hyrcanian Forest. *Remote Sens.* **2014**, *6*, 3624–3647, doi:10.3390/rs6053624.

28. Huang, H.; Roy, D.; Boschetti, L.; Zhang, H.K.; Yan, L.; Kumar, S.S.; Gomez-Dans, J.; Li, J. Separability Analysis of Sentinel-2A Multi-Spectral Instrument (MSI) Data for Burned Area Discrimination. *Remote Sens.* **2016**, *8*, 873, doi:10.3390/rs8100873.

29. Ba, R.; Song, W.; Li, X.; Xie, Z.; Lo, S. Integration of Multiple Spectral Indices and a Neural Network for Burned Area Mapping Based on MODIS Data. *Remote Sens.* **2019**, *11*, 326, doi:10.3390/rs11030326.

30. Chang, C.-I.; Wang, S. Constrained band selection for hyperspectral imagery. *IEEE Trans. Geosci. Remote Sens.* **2006**, *44*, 1575–1585, doi:10.1109/tgrs.2006.864389.

31. Büttner, G.; Feranec, J.; Jaffrain, G.; Mari, L.; Maucha, G.; Soukup, T. The corine land cover 2000 project. *EARSeL eProc.* **2004**, *3*, 331–346.

32. FAO. Global Forest Resources Assessment 2010. Terms and Definition. Working Paper 144/E. Available online: http://www.fao.org/docrep/014/am665e/am665e00.pdf (accessed on 12 March 2020).

33. Forest Europe. Streamline Global Forest Reporting and Strengthen Collaboration among International Criteria and Indicator Processes; 2011; Proceedings of the Joint Workshop. Victoria, British Columbia Canada. ISBN978-1-100-20248-8.

34. Vizzarri, M.; Chiavetta, U.; Chirici, G.; Garfì, V.; Bastrup-Birk, A.; Marchetti, M. Comparing multisource harmonized forest types mapping: a case study from central Italy. *iFor. Biogeosci.* **2015**, *8*, 59–66, doi:10.3832/ifor1133-007.

35. Chiavetta, U.; Camarretta, N.; Garfì, V.; Ottaviano, M.; Chirici, G.; Vizzarri, M.; Marchetti, M. Harmonized forest categories in central Italy. *J. Maps* **2016**, *12*, 98–100, doi:10.1080/17445647.2016.1161437.

36. ASI. Prisma Products Specification Document Issue 2.3. Available online at http://prisma.asi.it/missionselect/docs/PRISMA%20Product%20Specifications_Is2_3.pdf: (accessed on 12 March 2020).

37. Loizzo, R.; Guarini, R.; Longo, F.; Scopa, T.; Formaro, R.; Facchinetti, C.; Varacalli, G. Prisma: The Italian Hyperspectral Mission. In Proceedings of the IGARSS 2018—2018 IEEE International Geoscience and Remote Sensing Symposium, Valencia, Spain, 22–27 July 2018; pp. 175–178.

38. Fattorini, L.; Marcheselli, M.; Pisani, C. A three-phase sampling strategy for largescale multiresource forest invento-ries. *J. Agric. Biol. Environ. Stat.* **2006**, *11*, 296–316.

39. Busetto, L. Prismaread: An R Package for Imporing PRISMA L1/L2 Hyperspectral Data and Convert Them to a More User Friendly Format—v0.1.0. 2020. Available online: https://github.com/lbusett/prismaread, https://doi.org/10.5281/zenodo.3727671 (accessed on 02 March 2020).

40. Mohan, B.K.; Porwal, A. Hyperspectral image processing and analysis. *Curr. Sci.* **2015**, *108*, 833–841.

41. Somers, B.; Asner, G.P. Multi-temporal hyperspectral mixture analysis and feature selection for invasive species mapping in rainforests. *Remote Sens. Environ.* **2013**, *136*, 14–27, doi:10.1016/j.rse.2013.04.006.

42. Yeom, J.; Han, Y.; Kim, Y. Separability analysis and classification of rice fields using KOMPSAT-2 High Resolution Satellite Imagery. *Res. J. Chem. Environ.* **2013**, *17*, 136–144.

43. Hu, Q.; Sulla-Menashe, D.; Xu, B.; Yin, H.; Tang, H.; Yang, P.; Wu, W. A phenology-based spectral and temporal feature se-lection method for crop mapping from satellite time series. *Int. J. Appl. Earth Obs. Geoinf.* **2019**, *80*, 218–229.

44. Evans, J.; Murphy, M.A.; Ram, K. Spatialeco: Spatial Analysis and Modelling Utili-Ties. 2020. Available online: https://CRAN.R-project.org/package=spatialEco (accessed on 15 March 2020).

45. Kaufman, Y.; Remer, L. Detection of forests using mid-IR reflectance: an application for aerosol studies. *IEEE Trans. Geosci. Remote Sens.* **1994**, *32*, 672–683, doi:10.1109/36.297984.

46. Bhattacharyya, A. On a measure of divergence between two statistical populations defined by their probability dis-tributions'. *Bull. Calcutta Math. Soc.* **1943**, *35*, 99–109.

47. Bruzzone, L.; Roli, F.; Serpico, S.B. An extension to multiclass cases of the Jefferys-Matusita distance. *IEEE Trans. Pattern Anal. Mach. Intell.* **1995**, *33*, 1318-1321.

48. Moik, J.G. *Digital Processing of Remotely Sensed Images Scientific and Technical Information Branch*; National Aero-Nautics and Space Administration: Washington, DC, USA, 1980.

49. Du, H.; Chang, C.I.; Ren, H.; D'Amico, F.M.; Jensen, J.O. New Hyperspectral Discrimination Measure for Spectral Characterization. *Opt. Eng.* **2004**, *43*, 1777–1786.

50. Teillet, P.; Guindon, B.; Goodenough, D. On the Slope-Aspect Correction of Multispectral Scanner Data. *Can. J. Remote Sens.* **1982**, *8*, 84–106, doi:10.1080/07038992.1982.10855028.

51. Richter, R. Correction of satellite imagery over mountainous terrain. *Appl. Opt.* **1998**, *37*, 4004–4015, doi:10.1364/ao.37.004004.

52. Van Aardt, J.A.N.; Wynne, R.H. Examining pine spectral separability using hyperspectral data from an airborne sensor: An extension of field-based results. *Int. J. Remote Sens.* **2007**, *28*, 431–436, doi:10.1080/01431160500444772.

53. Fassnacht, F.E.; Neumann, C.; Forster, M.; Buddenbaum, H.; Ghosh, A.; Clasen, A.; Joshi, P.K.; Koch, B. Comparison of Feature Reduction Algorithms for Classifying Tree Species With Hyperspectral Data on Three Central European Test Sites. *IEEE J. Sel. Top. Appl. Earth Obs. Remote Sens.* **2014**, *7*, 2547–2561, doi:10.1109/jstars.2014.2329390.

54. Ghosh, A.; Fassnacht, F.E.; Joshi, P.K.; Koch, B. Aframework for mapping tree species combining hyperspectral and LiDAR data: Role of selected classifiers and sensor across three spatial scales. *Int. J. Appl. Earth Obs. Geoinf.* **2014**, *26*, 49–63.

55. Liu, M.; Yu, T.; Gu, X.; Sun, Z.; Yang, J.; Zhang, Z.; Mi, X.; Cao, W.; Li, J. The Impact of Spatial Resolution on the Classification of Vegetation Types in Highly Fragmented Planting Areas Based on Unmanned Aerial Vehicle Hyperspectral Images. *Remote Sens.* **2020**, *12*, 146, doi:10.3390/rs12010146.

56. Roth, K.L.; Roberts, D.A.; Dennison, P.E.; Peterson, S.; Alonzo, M. The impact of spatial resolution on the classification of plant species and functional types within imaging spectrometer data. *Remote Sens. Environ.* **2015**, *171*, 45–57, doi:10.1016/j.rse.2015.10.004.

57. Herold, M.; Roberts, D.A. Multispectral Satellites—Imaging Spectrometry—LIDAR: Spatial—Spectral Tradeoffs in Urban Mapping. *Int. J. Geoinform.* **2006**, *2*, 1–13.

58. Goodenough, D.; Dyk, A.; Niemann, K.; Pearlman, J.; Chen, H.; Han, T.; Murdoch, M.; West, C. Processing hyperion and ali for forest classification. *IEEE Trans. Geosci. Remote Sens.* **2003**, *41*, 1321–1331, doi:10.1109/tgrs.2003.813214.

# 5. Paper II

**The Effect of Forest Mask Quality in the Wall-to-Wall Estimation of Growing Stock Volume.**

*Vangi E.[1,2], D'AmicoG. [1], Francini S:[1,2,3], Giannetti F:[1,4,*], Lasserre B. [2], Marchetti M. [2], McRoberts R.E. [5], Chirici G.[1,4,6]*

[1] Department of Agricultural, Food, Environmental and Forestry Sciences and Technologies, University of Florence, Firenze 50145, Italy;

[2] Department of Biosciences and Territory, University of Molise, Campobasso, 86100, Italy;

[3] Department for Innovation in Biological, Agri-food and Forestry systems, University of Tuscia, Viterbo, 01100, Italy

[4] ForTech Joint Laboratory, University of Florence, Firenze 50145, Italy

[5] Department of Forest Resources, University of Minnesota, Saint Paul, MN, 55108, USA

[6] Research Unit COPERNICUSUniversity of Florence, Firenze 50145, Italy

* corresponding author: francesca.giannetti@unifi.it

## Abstract

Information about forest cover and its characteristics are essential in national and international forest inventories, monitoring programs, and reporting activities. Two of the most common forest variables needed to support sustainable forest management practices are forest cover area and growing stock volume (GSV m3 ha−1). Nowadays, national forest inventories (NFI) are complemented by wall-to-wall maps of forest variables which rely on models and auxiliary data. The spatially explicit prediction of GSV is useful for small-scale estimation by aggregating individual pixel predictions in a model-assisted framework. Spatial knowledge of the area of forest land is an essential prerequisite. This information is contained in a *forest mask* (FM). The number of FMs

is increasing exponentially thanks to the wide availability of free auxiliary data, creating doubts about which is best-suited for specific purposes such as forest area and GSV estimation. We compared five FMs available for the entire area of Italy to examine their effects on the estimation of GSV and to clarify which product is best-suited for this purpose. The FMs considered were a mosaic of local forest maps produced by the Italian regional forest authorities; the FM produced from the Copernicus Land Monitoring System; the JAXA global FM; the hybrid global FM produced by Schepaschenko et al., and the FM estimated from the Corine Land Cover 2006. We used the five FMs to mask out non-forest pixels from a national wall-to-wall GSV map constructed using inventory and remotely sensed data. The accuracies of the FMs were first evaluated against an independent dataset of 1,202,818 NFI plots using four accuracy metrics. For each of the five masked GSV maps, the pixel-level predictions for the masked GSV map were used to calculate national and regional-level model-assisted estimates. The masked GSV maps were compared with respect to the coefficient of correlation ($\rho$) between the estimates of GSV they produced (both in terms of mean and total of GSV predictions within the national and regional boundaries) and the official NFI estimates. At the national and regional levels, the model-assisted GSV estimates based on the GSV map masked by the FM constructed as a mosaic of local forest maps were closest to the official NFI estimates with $\rho = 0.986$ and $\rho = 0.972$, for total and mean GSV, respectively. We found a negative correlation between the accuracies of the FMs and the differences between the model-assisted GSV estimates and the NFI estimate, demonstrating that the choice of the FM plays an important role in GSV estimation when using the model-assisted estimator.

**Keywords**: forest mask; spatial estimation; growing stock volume; Italy

## 1. Introduction

Information about forest cover and its characteristics are essential in national and international forest inventories, monitoring programs, and reporting activities (Schepaschenko et al., 2015; FAO, 2010) such as in the context of international agreements (e.g., Kyoto protocol), and restoration programs (e.g., Reducing emissions from deforestation and forest degradation projects (REDD+))(FAO UNCCD, 2015). Two of the most common forest variables needed to estimate sustainable forest management indicators as required by the national and international framework and agreements relate to forest cover area (generally according to the international definition adopted by the Food and agriculture organization (FAO) and the total growing stock volume (GSV, m3) (McRoberts et al., 2013; Witke et al., 2019). These data are usually provided by national forest inventory (NFI) programs which use probability-based approaches to infer the estimates for large areas such as countries and regions within countries. (McRoberts et al., 2013; Hansen et al., 1983; McRoberts et al., 2006). In several countries with long NFI histories such as Norway (Næsset et al., 2004), Finland (Tomppo et al., 2008), Austria (Hollaus et al., 2010), and Switzerland (Waser et al., 2006; 2015), the typical NFI ground survey is nowadays complemented by continuous spatial predictions, characterized as wall-to-wall maps of forest variables which rely on models and wall-to-wall auxiliary data such as remotely sensed data (Kangas et al., 2018; White et al., 2016; Næsset, 2014).

Wall-to-wall GSV data are useful because they can be integrated into decision support systems to assess wood production and harvesting activities at small scales (i.e., in forest properties) (Puletti et al., 2017; Chirici et al., 2020; Giannetti et al., 2020; D'Amico et al., 2021) and to produce small-scale estimates by aggregating individual pixel predictions (Särndal et al., 1992; 2003; Breidt et al., 2009; McRobetrs et al., 2016). In the probability-based framework, multiple estimators including the stratified, post-stratified, and model-assisted estimators can be used. The latter is considered asymptotically unbiased in the sense that the mean of estimates obtained using the estimator for all possible samples approaches the true value as the sample size increases (McRobetrs et al., 2016).

GSV and above-ground biomass are known to be strongly correlated with three-dimensional (3D) data such as those acquired through airborne laser scanning (ALS) or photogrammetric techniques (Wittke et al., 2019; White et al., 2016; Næsset et al., 2008; McRoberts et al., 2010; Giannetti et al., 2018; Goodbody et al., 2018). However, acquiring these data is still expensive, and some countries such as Italy still do not have wall-to-wall ALS coverage (D'Amico et al., 2021). Multispectral satellite data are often used instead of or with 3D data to predict GSV, thanks to their free availability over large areas (Barrett et al., 2016; Saarela et al., 2016; Holm et al., 2017; Nilsson et al., 2017).

Several types of models can be used to produce wall-to-wall predictions of forest attributes in a model-assisted approach. These models include both parametric and non-parametric techniques (White et al., 2016; Chirici et al., 2020; Goodbody et al., 2019; Barrett et al., 2016; Immitzer et al., 2016), with the recent prevalence of multiple linear regression and random forests (White et al., 2016; Karlson et al., 2015; Belgiu et al., 2016). Regardless of the estimation approach, spatial knowledge of the area covered by forest land is an essential prerequisite, both to restrict the establishment of field plots and to restrict the application of the models. A forest mask (FM) indicates the location of forest land and is often in a raster or a spatial polygon database format. FMs are conventionally obtained by manual delineation of aerial images, or by supervised or unsupervised classification of satellite imagery, from both optical or radar imagery (Stankiewicz et al., 2003; Hansen et al., 2013; Dostálová et al., 2016), and more recently ALS data (Eysn et al., 2012; Dalponte et al., 2014; Rudjord et al., 2016; Øivind et al., 2018). Remotely sensed data suitable for forest mapping are nowadays frequently and freely available( Woodcock et al., 2008; Wulder et al., 2019; Olofsson et al., 2020). For this reason, the number of FMs has increased exponentially, creating doubts about which is best-suited for specific purposes such as forest area and GSV estimation. National information about forest extent can be estimated from any of several FMs produced independently by different research agencies globally or for large areas, including the European Environmental Agency (EEA) (European Enviromental Agency, 2007), the European Space Agency (ESA) (Langanke, 2017), the International Institute for Applied Systems Analysis (IIASA) (Schepaschenko et al., 2015), and the Japanese Aerospace Exploration Agency (JAXA) (JAXA, 2016). Despite individual

weaknesses and strengths, spatial differences among these products are evident and can lead to substantial variation in their accuracies (Schepaschenko et al., 2015; Seebach et al., 2012). Furthermore, these FMs were developed for different aims and thus have different characteristics in terms of minimum mapping unit (MMU) and minimum mapping width (MMW), reference forest definition, and year of production.

Multiple studies have compared land cover maps at global and local levels. Fritz and See (2005) and Giri et al. (2005) compared the Global Land Cover 2000 data set and the MODIS global land cover product and highlighted areas with strong disagreements. Hoyos et al. (2017) compared four global satellite-based land cover maps and showed a worsening of area agreements as the spatial scale increases. Neumann et al. (2007) provided an assessment of compatibilities and differences between the CORINE2000 and GLC2000 datasets and reported general disagreement due to the combination of thematic similarities, spatial heterogeneity, and classification accuracy. Seebach et al. (2011) compared the advantages and limitations of four pan-European forest cover maps for the reference years 2000, demonstrating that the spatial agreement between the maps ranged between 50% to 70% within a large study area in Europe. The authors found the greatest spatial differences among all maps in the Alpine and Mediterranean regions. Here, the vulnerability to climate change and anthropogenic disturbance is extremely large and will cause an increased demand for accurate wall-to-wall maps (Chirici et al., 2020). Only a few studies have analyzed the effects of using different FMs on the uncertainty of forest parameter estimates. Rodríguez-Veiga et al. (2016) reported a large impact on estimates of national carbon stocks in Mexico caused by discrepancies in forest extent estimated from different FMs. In their study, Li et al. (2017) considered the uncertainty of the MODIS land cover products, finding substantial differences in the regional climate modeling outputs when the uncertainty was not considered. Esteban et al. (2020) estimated the effects of the uncertainty of forest species maps used in the sampling and forest parameter estimation processes in a Spanish study area. Their study revealed that the effects of map uncertainty are not negligible, especially for less common Mediterranean forest species.

The choice of FM can heavily impact the estimation of forest parameters in two different manners: i) it affects the number of plots selected for the construction of the

predictive model and ii) it affects the total area to which the model is applied (Esteban et al., 2020).

The aim of this paper is to evaluate the impacts of the accuracies of different FMs on the estimation of GSV based on the integration of field information and remotely sensed data. We constructed a national wall-to-wall GSV map with an optimized procedure based on a random forests model with remotely sensed imagery and auxiliary data as predictors (Chirici et al., 2020). We used five different FMs to mask out non-forest areas from the GSV map and then used the model-assisted regression estimator to estimate total and mean GSV (m3 ha−1) for the forest portion of the GSV map. We then investigated the relationship between mask accuracy and agreement between the model-assisted total GSV estimates and the official NFI estimates. The test was carried out for the entire area of Italy. Finally, we clarified which product was best-suited for total and mean GSV estimation, both at national and regional levels.

## 2. Materials and Methods

### 2.1. Study area

The study was carried out in Italy which covers 301,408 km2 (Figure 1). Italy has extreme variations in climatic conditions due to proximity to the sea and elevation ranges between coastal areas and the Alpine region with elevations as great as 4000 m asl.

The territory falls within the temperate zone of a Mediterranean climatic region (Pinna, 1970). On the coasts of the main islands, the average annual rainfall is 250 mm but reaches more than 3000 mm in the Alpine and pre-Alpine belts. Average yearly temperatures vary between 16 °C in the southern coastal areas to 10 °C in the inner central regions and the pre-Alps, with temperatures less than 5 °C in the mountain ranges and on the highest peaks.
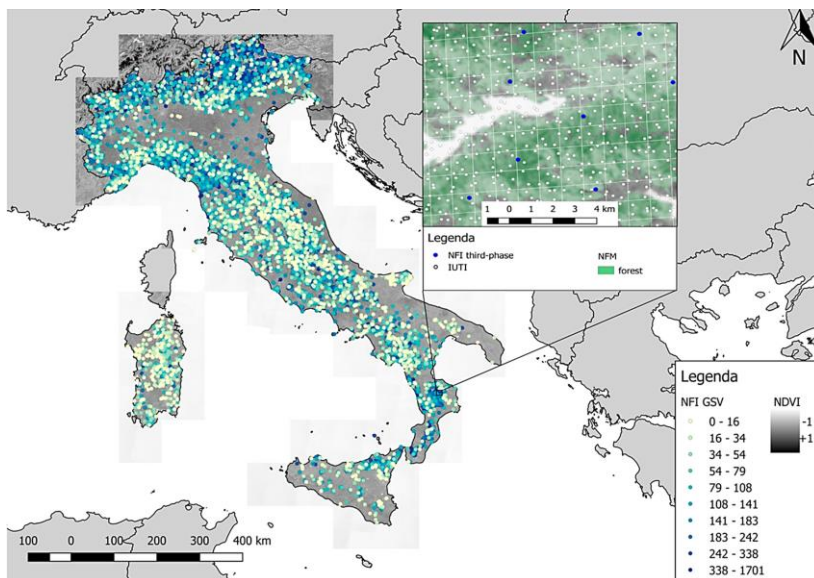
Figure 1. The study area with the distribution of the national forest inventories (NFI) plots colored by growing stock volume (GSV) expressed in m3 ha−1. On the right, a detail of the distribution of sample points used in the study within the NFI 1 x 1 km grid where the third-phase NFI plots (Section 2.2.2) are depicted in blue and the Inventario dell'Uso delle Terre in Italia (IUTI) points (Section 2.2.2) in white.

According to the last Italian NFI (INFC, 2007), forest vegetation and other wooded lands occupy 10,467,533 ha, about 34% of the national territory. Forests are dominated by deciduous trees (68%), mainly Quercus oak (Q. petrea (M.) L., Q. pubescens W., Q. robur L., Q. cerris L.), and European beech (Fagus sylvatica L.). The dominant conifers are Norway spruce (Picea abies K.) and pines (Pinus sylvestris L., P. nigra A., P. pinae L., P. pinaster A.), which are mainly artificial plantations located in mountain areas or near the coast (Figure 1). Seven of the 14 European forest types occur in Italy, of which the most common is the thermophilous deciduous forest (White et al., 2016, Barbati et al., 2014).

Italy is divided into 20 administrative regions (NUTS2) for each of which the NFI produces estimates of forest area, total and mean GSV, and their standard errors (SEs). The average GSV is 144 m3 ha−1 (Gasparini et al., 2009).

## 2.2. Field Data

### 2.2.1. Second Italian National Forest Inventory

The field reference data for the wall-to-wall spatial prediction of GSV were acquired in the framework of the second Italian NFI (INFC, 2007) based on a three-phase, systematic, unaligned sampling design with 1 x 1 km grid cells (Fattorini et al., 2006). In the first phase, N = 301,300 points were selected and classified with respect to 10 coarse land-use strata using aerial orthophotos. In the second phase, for an $n < N$ sub-sample of the points in the "forest" stratum of the first-phase points, qualitative information such as forest type, management, and property were collected during a field survey. In the third phase, for a sub-sample of 6782 points extracted from the second-phase points, a quantitative survey was carried out for circular plots of 13 m radius (530 m2). All tree stems with a DBH of at least 2.5 cm were callipered, and for a subsample, height was measured. For all 6782 third-phase plots, allometric models (Tabacchi et al., 2011) were used to predict GSV (m3) which was then aggregated at plot-level and scaled to a per unit area basis. For this study, allometric model prediction uncertainty and uncertainty due to Global Navigation Satellite System (GNSS) position error were expected to be negligible for the spatial resolution adopted (McRobetrs et al., 2015; Chirici et al., 2020; McRoberts et al., 2016; McRoberts et al., 2018). The third-phase plots have a mean GSV of 145.75 m3 ha−1, with a median value of 102.82 m3 ha−1.

Official design-based NFI estimates of total forest area and mean and total GSV at national and regional NUTS2 levels were acquired online at https://www.sian.it/inventarioforestale/ (accessed on: 02-10-2020) (McRoberts et al., 2018), for the reference year 2005.

The study area was tessellated into a 23 x 23 m national grid whose pixel area matched the area of the NFI ground plots, for a total of 569,769,690 pixels (D'Amico et al., 2021). The national grid was used as a spatial reference grid for resampling the predictor variables and the FM to 23 x 23 m resolution.

### 2.2.2. Inventory of Land Use in Italy

To evaluate the accuracy of the FMs, we used the sample points from the Italian land use inventory (Inventario dell'Uso delle Terre in Italia, IUTI). The IUTI has adopted

the methodology of approach number three of the Good Practices Guidance for Land Use, Land Use Change, and Forestry (GPG-LULUCF) of the Intergovernmental Panel on climate change (Penman et al., 2003; Romano et al., 2011; Corona et al., 2012). IUTI is a permanent monitoring system that estimates the extent of six land use categories identified in the GPG-LULUCF. The IUTI is based on a systematic unaligned sampling design with 0.5 x 0.5 km grid cells which is an intensification of the NFI sample grid, for a total of 1,202,828 points of which 301,300 are the first-phase points of the NFI. The six categories reported by IUTI are urban, agriculture, forest land, grassland, wetland, other (Masek et al., 2006). Each point is photo-interpreted in three time periods (1990, 2008, 2012) for estimating land-use change using aerial orthophotos with spatial resolution ranging between 1 x 1 m for 1990 and 0.5 x 0.5 m for 2008. We combined the six land use categories into forest and non-forest and assigned the value 1 to all the points classified as forest (class 1.1, 1.2) and 0 to all other categories. Subsequently, the forest class included 32% of the total observations with 387,085 of 1,202,818 points.

For this study, we used the IUTI points as an independent dataset to evaluate the accuracies of the FMs. We used the 2008 photointerpretation to be as consistent as possible with the 2005 NFI ground surveys.

### 2.2.3. Predictor Variables

To predict GSV as described in section 3.1, we used predictors obtained from multiple sources including remotely sensed variables from multiple sensors, climate, and soil characteristics (Table 1). The variables were selected based on their availability throughout the national territory as reported by (Chirici et al., 2020). All variables were resampled from the original resolution to the 23 x 23 m pixel size of the national grid. A more detailed description of the database is provided by (Chirici et al., 2020).

Table 1. Predictor variables based on remotely sensed and auxiliary data.

| Database | Band/information | Predictor variables | Original spatial resolution |
|---|---|---|---|
| Landsat 7 ETM+ | 3 years median of Band 1 | Landsat_B1 | 30 m |
| | 3 years median of Band 2 | Landsat_B2 | 30 m |
| | 3 years median of Band 3 | Landsat_B3 | 30 m |
| | 3 years median of Band 4 | Landsat_B4 | 30 m |

| | 3 years median of Band 5 | Landsat_B5 | 30 m |
|---|---|---|---|
| | 3 years median of Band 6 | Landsat_B6 | 30 m |
| | 3 years median of Band 7 | Landsat_B7 | 30 m |
| Global PALSAR/ PALSAR-3 | HH polarization | SAR_HH | 25 m |
| | HV polarization | SAR_HV | 25 m |
| Climate data | Total annual precipitation | Prec | 1 km |
| | Mean annual temperature | temp_mean | 1 km |
| | Maximum annual temperature | temp_max | 1 km |
| | Minimum annual temperature | temp_min | 1 km |
| European Soil Database v2.0 | Subsoil available water capacity | AWC_SUB | 1 km |
| European Soil Database v2.1 | Topsoil available water capacity | AWC_TOP | 1 km |

### 2.2.4. Landsat Composite Image

We constructed a cloud-free composite image across Italy based on 848 Landsat 7 Enhanced Thematic Mapper Plus (ETM+) images acquired in the same year as the field survey (2005) +/- 1 year (Figure 2).

We used Landsat 7 Surface Reflectance Tier 1 imagery from the Earth Engine Data Catalog, acquired in the vegetation period (1st April– 30th September), atmospherically corrected using Landsat Ecosystem Disturbance Adaptive Processing System LEDAPS (Masek et al., 2006). We masked out cloud pixels based on the quality assessment (QA) band provided with the Landsat 7 database, using the C function of mask algorithm (CFMask) (Foga et al., 2017). Finally, for each 23 x 23 m national grid pixel, we calculated the median values for each Landsat band (Kennedy et al., 2018).
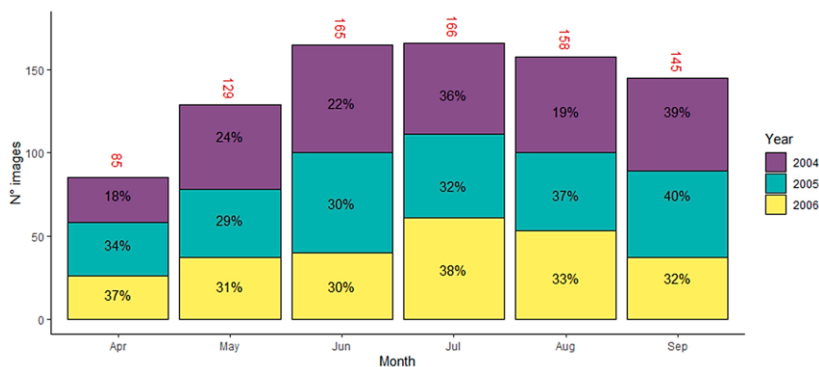
Figure 2. Distribution of Landsat 7 ETM+ images per month, divided by acquisition years.

### 2.2.5. SAR Variables

We used SAR data from PALSAR-2/PALSAR from the Advanced Land Observing Satellite (ALOS) and Advanced Land Observing Satellite-2 (ALOS-2) freely available at the global level online from the Japan Aerospace Exploration Agency (JAXA) at 25 x 25 m resolution. We rescaled the raw backscattering coefficients for each polarization HH and HV for the year 2007 to the 23 x 23 m pixel of the national grid. For more information on this data we refer to https://www.eorc.jaxa.jp/ALOS/en/palsar_fnf/fnf_index.htm (accessed on: 05-11-2019)

### 2.2.6. Climate and Soil Variables

We derived climate data from the 1 x 1 km downscaled climatological maps obtained by Maselli et al. (2012) which is representative of the period 1981–2010. The dataset includes the following variables: total annual precipitation, mean annual temperature, maximum annual temperature, minimum annual temperature. For more details on these climate data, we refer to Chirici et al. (2020).

Soil variables were from the harmonized soil geodatabase of Europe (European Soil Database v2.0 - 2004) (Penagis et al., 2004). The subsoil available water capacity and topsoil available water capacity soil variables used for this study were selected using the optimization phase described in Chirici et al. (2020).

### 2.3. Forest Masks

We obtained five FMs available for the entire Italian territory that potentially reflect the forest FAO FRA definition (FAO, 2010). These masks can be divided into two main categories: i) FMs obtained by semi-automated classification of remotely sensed data; ii) FMs obtained by manual delineation and classification of fine-resolution images. All the FMs were first reprojected in the WGS 84 / UTM zone 32 North (EPSG:32632) reference system to make them comparable and then resampled at the 23 x 23 m resolution of the national grid resulting to produce five comparable FMs.

### 2.3.1. National Forest Mask (NFM)

We used the national forest mask (NFM) which is based on the mosaic of local forest maps produced by manual photointerpretation by the Italian regional forest authorities (D'Amico et al., 2021). The mosaic was constructed by merging 16 fine resolution forest maps with nominal reference scales varying between 1:5,000 and 1:25,000 and five land use maps specifically filtered to produce forest cover maps. All the maps were based on manual photointerpretation of aerial orthophotos. The local forest maps were reclassified into Boolean masks using code 1 for pixels classified as "forest", and code 0 for pixels classified as "non-forest". The NFM is a mosaic of 20 fine-resolution regional forest maps resampled at the 23 x 23 m national grid resolution. The mask is also available on-line at www.forestinfo.it

### 2.3.2. Copernicus Land Monitoring System (CLMS) Forest Mask

To construct the Copernicus FM, we first used the 2012 Forest Type map (https://land.copernicus.eu/pan-european/high-resolution-layers/forests/forest-type-1/status-maps/2012?tab=download) that uses the Tree Cover Density layer (https://land.copernicus.eu/pan-european/high-resolution-layers/forests/tree-cover-density/status-maps/2012?tab=download) (accessed on: 05-11-2020) to classify all 20 x 20 m pixels of European lands as forest when the tree cover density is at least 10% and when such pixels are aggregated into a continuous patch of at least 0.52 hectares (Langanke et al., 2017). We excluded pixels in agricultural and urban contexts from the Forest Type map, using the Forest Additional Support Layer also available from Copernicus at https://land.copernicus.eu/pan-european/high-resolution-layers/forests/forest-type-1/status-maps/2012?tab=download (accessed on: 05-11-2020). The resulting map reflects as closely as possible the international forest definition in a raster layer having 23 x 23 m resolution

### 2.3.3. JAXA Forest Mask

JAXA constructed an FM for the reference years 2007±1 with a spatial resolution of 25 x 25 m based on the HV-polarization backscatter images acquired by the PALSAR and PALSAR 2 sensors carried by the ALOS and ALOS2 satellites. The JAXA declares to adopt the FAO forest definition (JAXA, 2016) and is available online at

https://developers.google.com/earthengine/datasets/catalog/JAXA_ALOS_PALSAR_Y EARLY_SAR (accessed on: 05-11-2020).

### 2.3.4. Hybrid Global Forest Mask 2000 (FM00)

Schepaschenko et al. (2015) constructed a global FM using a hybrid approach combining multiple local, national, and global datasets into a single product. This map was constructed by converting the global forest probability map into a forest/non-forest map using a threshold calculated for each country. The threshold selected for this study produced area estimates that matched as closely as possible the official FAO forest area statistics. We characterized this map as "FM00". The map has a spatial resolution of 1 x 1 km, was produced for the reference year 2000, and is available online at https://application.geo-wiki.org/branches/biomass/ (accessed on: 05-11-2020).

### 2.3.5. Corine Land Cover 2006 (CLC06)

The CORINE Land Cover (CLC) project was initiated in 1990 by the European Environmental Agency (EEA) (Büttner et al., 2004) and has been updated in 2000, 2006, 2012, and 2018 to monitor land-use changes in the 39 participating countries (EEA, 2007). It consists of land cover maps based on a nomenclature system of 44 classes produced by photointerpretation of fine-resolution satellite imagery. CLC uses a MMU of 25 hectares and a MMW of 100 m. For this study, we acquired the CLC map for the reference year 2006±1 (referred to as "CLC06") obtained by photo-interpretation of SPOT-4/5 and IRS P6 LISS III dual data images (EEA, 2007) and available online in vector format at https://land.copernicus.eu/pan-european/corine-land-cover/clc-2006?tab=download (accessed on: 05-11-2020). To derive the CLC mask, we first rasterized the vector product to the 23 x 23 m spatial resolution of the national grid, and then we assigned the categories 2.4.4, 3.1.1, 3.1.2, 3.1.3, 3.2.3, 3.2.4 to the "forest" class and all the remaining categories to the "non-forest" class.

## 2.4. Overview of the Method

A concise overview of the methodology followed is presented: i) a wall-to-wall GSV map was constructed using a random forests model with the NFI plot GSV data and the predictor variables; ii) the accuracies of the five FMs were assessed; iii) the wall-to-

wall GSV map was masked in turn with each of the five FMs, obtaining five masked GSV maps; iv) for each masked GSV maps we estimated the mean and total GSV with the model-assisted regression estimator, at the national and regional level; v) we compared model-assisted estimations for each FM with the official estimation from the Italian NFI, in terms of correlation coefficient; vi) we assessed the relationship between FMs accuracy and GSV estimates in terms of the correlation coefficient.

## 2.5. Wall-to-Wall National GSV Map

To estimate the effects of FM accuracy on the model-assisted GSV estimates, we constructed a GSV map consisting of GSV predictions for all 23 x 23 m pixels of the national grid (569,769,690 pixels) using the random forests (RF) prediction technique with the NFI plot GSV data and the predictor variables described in Table 1. RF was optimized following Chirici et al. (2020) by selecting the combination of predictor variables and parameter values (ntree and mtry) that minimized the root mean square error (RMSE) calculated using the leave one out cross-validation (LOOCV) technique (McRoberts et al., 2015). RMSE was calculated as:

$$RMSE = \sqrt{\frac{\sum_{i=1}^{n}(y_i - \hat{y}_i)^2}{n}} \tag{1}$$

where n is the number of third-phase NFI plots (i.e., 6782), $y_i$ is the i-th GSV associated with the plots and $\hat{y}_i$ is the i-th GSV predicted by the random forests model. The most accurate combination resulting from LOOCV was used to predict the GSV for all N pixels of the study area to produce a 23 x 23 m resolution GSV map. The model fitting and optimization phase was performed using the randomForest package within the statistical software package R 3.6.3 (Devarriva et al., 2020) (https://www.r-project.org, accessed on: 05-11-2020). For the 6,782 NFI plots, the pixel-level GSV predictions ranged between 0 and 690 m3 ha−1 with a standard deviation of 68.5 m3 ha−1 while the original NFI values ranged between 0.3 and 701 m3 ha−1 with a standard deviation of 147 m3 ha−1. The map was found to have a mean deviation of −4.3 m3 ha−1.

## 2.6. Accuracy Assessment of FMs

We first assessed the five FMs with respect to thematic accuracy using the IUTI dataset as reference data. For each of the 1,202,828 points of the IUTI database, we extracted the forest/non-forest classification from the five FMs and constructed the respective five confusion matrices. For each matrix we calculated four metrics:

$$\text{Overall Accuracy} = \frac{\sum True\ positive + \sum True\ negative}{\sum Total\ population} \tag{2}$$

$$\kappa = \frac{p_0 - p_e}{1 - p_e} \tag{3}$$

Where:

$p_0 = \text{Overall Accuracy}$

$$p_e = \frac{1}{N^2} \sum_k \sum True\ positive * \sum True\ negative \tag{4}$$

for k categories and N observations.

$$\text{Precision} = \frac{\sum True\ positive}{\sum True\ positive + \sum False\ positive} \tag{5}$$

$$\text{Recall} = \frac{\sum True\ positive}{\sum True\ positive + \sum False\ negative} \tag{6}$$

These metrics need to be used together to correctly describe the quality of classification in the case of unbalanced datasets. This is the case for forest masks when the forest and non-forest classes cover the land area with very different proportions. In such cases, many classification performance indicators including overall accuracy may provide misleading information (Devarriva et al., 2020; Jaafor et al., 2012). For this reason, the model accuracy comparison should focus on recall as per Equation (6) and, most importantly, precision as per Equation (5).

## 2.7. Impact of FMs Accuracy on Model-Assisted GSV Estimation

The five FMs were used to mask out all non-forest pixels in the national GSV map. The pixel-level predictions for the resulting five masked GSV maps were used with a model-assisted, generalized regression estimator to infer mean and total GSV at both national (NUTS1) and regional levels (NUTS2) (Särndal et al., 1992; 2003; Breidt et al., 2009). An initial estimate of GSV can be calculated from the masked GSV maps as,

$$\hat{\mu}_{\text{initial}} = \frac{1}{n} \sum_{i=1}^{N} \hat{y}_i \tag{7}$$

where $N$ is the number of forest pixels within the masked GSV map and $\hat{y}_i$ is the GSV prediction obtained using the RF model for the i-th pixel. However, this estimator may be biased because of systematic prediction error. The bias can be estimated as,

$$\widehat{\text{Bias}}(\hat{\mu}_{\text{initial}}) = \frac{1}{n}\sum_{j=1}^{n}(\hat{y}_j - y_j) \tag{8}$$

where $n$ is the NFI sample size, i.e., the number of plots used for constructing the model, $\hat{y}_j$ is the GSV model prediction for the j-th plot and $y_j$ the observed value of GSV for the j-th plot. Subtracting the estimated bias from the initial estimate yields the model-assisted estimator as,

$$\hat{\mu}_{ma} = \hat{\mu}_{\text{initial}} - \widehat{\text{Bias}}(\hat{\mu}_{\text{initial}}) = \frac{1}{N}\sum_{i=1}^{N} y_i - \frac{1}{n}\sum_{j=1}^{n}(\hat{y}_j - y_j) \tag{9}$$

where ma denotes model-assisted, $\hat{\mu}_{ma}$ is the estimate of mean GSV for the given masked GSV map, N is the number of forest pixels within the masked GSV map, $\hat{y}_i$ is the GSV prediction obtained using the RF model for the i-th pixel. The standard error (SE) for the estimator is:

$$SE(\hat{\mu}_{ma}) = \sqrt{\frac{1}{n(n-1)}\sum_{j=1}^{n}(e_j - \hat{e}_j)^2} \tag{10}$$

where $n$ is the NFI sample size, $e_j = \hat{y}_j - y_j$ and $\hat{e}_j = \frac{1}{n}\sum_{j=1}^{n} e_j$.

Similarly, the model-assisted estimator for the GSV total was:

$$\hat{\tau}_{ma} = \sum_{i=1}^{N} y_i - \frac{N}{n}\sum_{j=1}^{n}(\hat{y}_j - y_j) \tag{11}$$

where $\hat{\tau}_{ma}$ is the estimate of total GSV for the given GSV-masked map, N the number of pixels within the masked GSV map, $y_i$ the GSV prediction obtained using the RF model for i-th pixel. The SE for the $\hat{\tau}_{ma}$ is given by d'Oliviero et al. (2012):

$$SE(\hat{\tau}_{ma}) = \sqrt{N^2\left(\frac{1}{n} - \frac{1}{N}\right)\sum_{j=1}^{n}\frac{(e_j - \hat{e}_j)^2}{n-1}} \tag{12}$$

where N is the population size, n is the NFI sample size, $e_j = \hat{y}_j - y_j$ and $\hat{e}_j = \frac{1}{n}\sum_{j=1}^{n} e_j$.

It is important to note that correction for estimated bias compensates for GSV map inaccuracy and makes the model-assisted estimator asymptotically unbiased.

Using the SEs, it was possible to construct confidence intervals for both estimates of mean and total GSV for the entire study area. These intervals are expressed as

$$\hat{E}_{ma} \pm t_n * SE(\hat{E}_{ma}) \tag{13}$$

where $\hat{E}_{ma}$ denotes either the model-assisted estimate of mean GSV or total GSV, $SE(\hat{E}_m)$ is the SE of $\hat{E}_{ma}$, and the factor tn depends on the desired significance level and the distribution of the response variable. For most distributions and applications, tn = 2 produces an approximate 95% confidence interval (McRoberts et al., 2008). For purposes of constructing confidence intervals, the focus of the study was the estimation of mean and total GSV and the SEs using the model-assisted regression estimators. To compare the GSV estimates produced with the five masked GSV maps and the NFI estimates at national and regional levels, we used the t statistic calculated as follows:

$$t = \frac{\hat{E}_{ma} - \hat{E}_{NFI}}{\sqrt{SE^2(\hat{E}_{ma}) + SE^2(\hat{E}_{NFI})}} \quad\quad\quad (14)$$

where $\hat{E}_{ma}$ denotes either the model-assisted estimate of mean GSV or total GSV for the masked GSV maps, $\hat{E}_{NFI}$ denotes either the NFI estimate of mean GSV or total GSV, and $SE^2(\hat{E}_{ma})$ and $SE^2(\hat{E}_{NFI})$ are the squares of the SEs of the estimates. Values of $|t| > 2$ indicates that the two estimates are statistically significantly different. Correlations for estimates of both mean and total estimates and the corresponding NFI estimates in terms of Pearson correlation coefficient ($\hat{\rho}_{Mean}$, $\hat{\rho}_{Total}$) were also calculated.

In addition, we calculated relative efficiency (RE) to assess the quality of the model-assisted estimators, compared to the SE obtained by the NFI (Chirici et al., 2020), both at national and regional scales. RE was calculated as:

$$RE = \frac{\widehat{Var}(\hat{E}_{NFI})}{\widehat{Var}(\hat{E}_{ma})} \quad\quad\quad (15)$$

where $\widehat{Var}(\hat{E}_{NFI})$ and $\widehat{Var}(\hat{E}_{ma})$ are the estimated variances of the NFI estimates and the model-assisted estimates, respectively.

Values of RE greater than 1.0 are evidence of greater precision in the model-assisted estimates (Moser et al., 2016). RE could be interpreted as the factor by which the original sample size would have to be increased to achieve the same precision as that achieved using the remotely sensed auxiliary data (Chirici et al., 2020).

Finally, we evaluated the relationship between the accuracies of the FMs (in terms of overall accuracy, κ, precision and recall) and the SEs of the model-assisted estimates for the NUTS2 administrative level using the Pearson correlation coefficient ($\hat{\rho}$).

# 3. Results

## 3.1. Forest Masks Accuracy Assessment

At the national level, the most accurate FM was the NFM with an underestimation against the NFI estimates of only −2%, followed by the CLC06 with −3%, JAXA with −4%, CLMS with +16%, and FM00 with +51% . The same ranking was obtained from the comparison with IUTI in terms of OA, k, and precision (Table 2). For 17 of the 20 regions, the NFM was the most accurate, followed by the CLMS FM in two regions, and CLC06 in the remaining region. The confusion matrices for each one of the five FMs are shown in Figure 3.
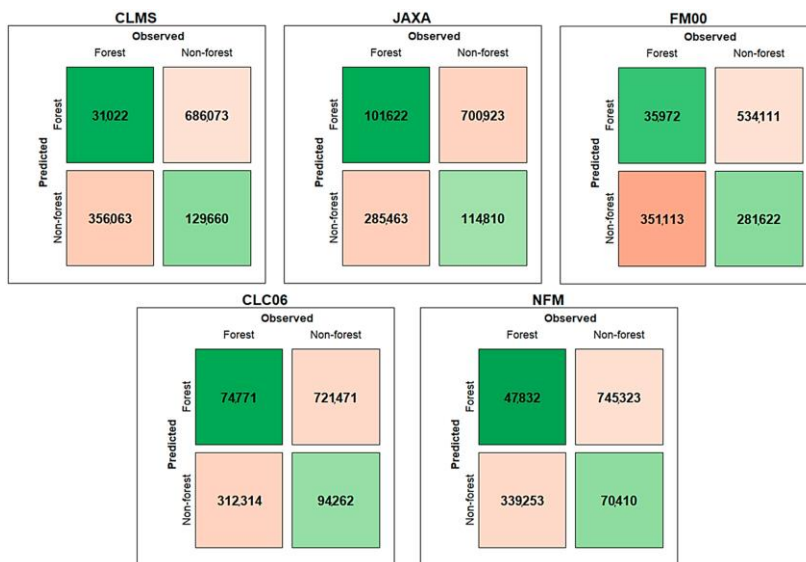


Figure 3. Confusion matrices of each forest mask.

Table 2. Accuracy assessment for the five forest masks (FMs) based on the confusion matrices with the IUTI.

| Mask | Accuracy | | | |
|------|------|------|-----------|--------|
| | OA | κ | Precision | Recall |
| CLMS | 0.88 | 0.73 | 0.73 | 0.92 |
| JAXA | 0.85 | 0.61 | 0.71 | 0.74 |
| FM00 | 0.76 | 0.51 | 0.55 | 0.91 |
| CLC06 | 0.87 | 0.70 | 0.77 | 0.81 |
| NFM | 0.91 | 0.79 | 0.84 | 0.90 |

We also noted that regardless of the FM used, the islands (Sicilia and Sardegna) and some of the southern regions (Calabria, Campania, Puglia) were characterized by small precision and recall (sensitivity), leading to numerous misclassifications of non-forest as forest (commission errors) (Figure 4).
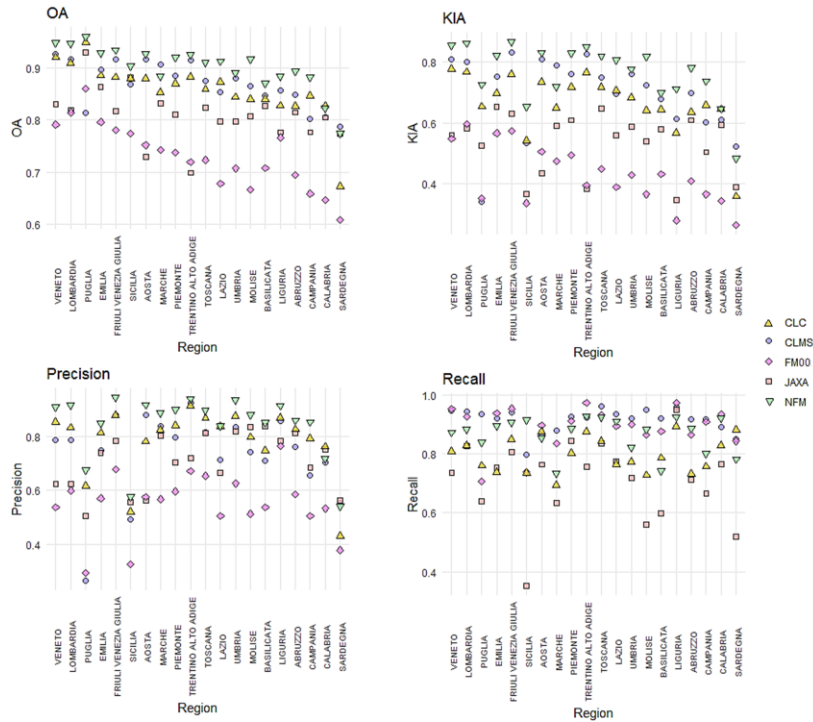


Figure 4. Comparison of four accuracy metrics among the FMs, calculated at regional level (NUTS2).

## 3.2. GSV Model-Assisted Estimations

In Figure 5, the GSV map of Italy produced with the random forests model is reported.
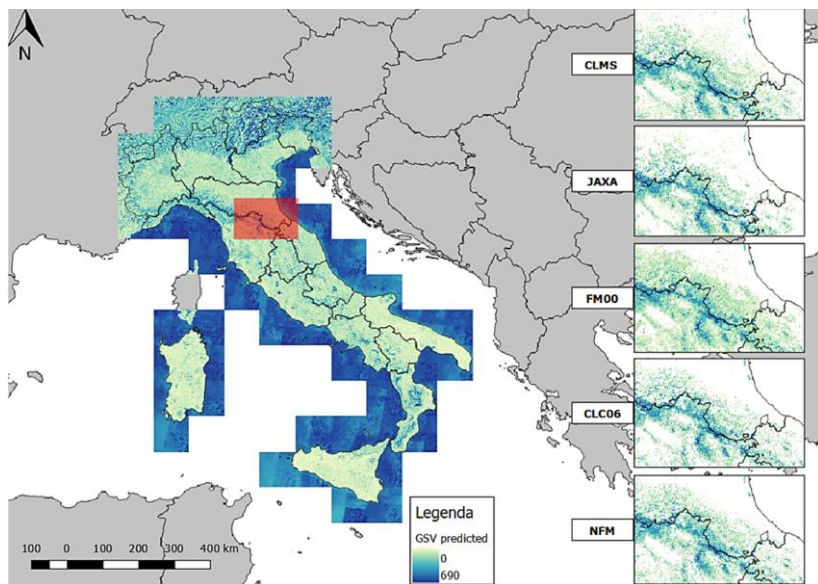
Figure 5. Growing stock map of Italy generated with random forests model. GSV in m3 ha−1. On the right, a detail of the GSV map masked with the five forest masks.

For the five masked GSV maps, $\hat{\mu}_{ma}$ ranged between 125 (CLMS) and 135 (NFM), m3 ha−1 with a $SE(\hat{\mu}_{ma})$ between 1.1 and 1.3 m3 ha−1. For comparison, the design-based estimation of mean GSV from the NFI was 131 m3 ha−1 with a SE of 1.6 m3 ha−1. Three of the five GSV-masked maps (NFM, CLC06, JAXA) produced estimates that were not statistically significantly different from the NFI estimate. The value of $\hat{\tau}_{ma}$ ranged between 1321 (JAXA) and 1525 (CLMS) millions m3, with $SE(\hat{\tau}_{ma})$ between 13 (NFM) and 17 (JAXA) million m3, while the official estimate from the NFI was 1366 million m3 with SE of 14 million m3, demonstrating a general trend towards overestimation of total volume (Table 3). The differences between the total GSV estimate for two of the five masked GSV maps (NFM, CLC06) and the NFI estimate were not statistically significantly different from 0.

Table 3. Model-assisted regression estimates for the five maps. The last row has the Italian NFI estimates.

| Forest mask | | | | Model-assisted and NFI estimates (m$^3$) | | | |
|---|---|---|---|---|---|---|---|
| | $\hat{\mu}_{ma}$ | $SE(\hat{\mu}_{ma})$ | $t(\hat{\mu})$ | $\hat{\tau}_{ma}$ | $SE(\hat{\tau}_{ma})$ | $t(\hat{\tau})$ | RE |
| CLMS | 125 | 1.2 | −3 | 1,525,000,000 | 14,487,500 | 7.9 | 1.17 |
| JAXA | 131 | 1.3 | 0 | 1,321,000,000 | 13,342,100 | −2.3 | 1.09 |
| FM00 | 113 | 1.1 | −9.5 | 1,791,000,000 | 17,014,500 | 19.3 | 1.15 |
| CLC06 | 135 | 1.3 | 1.94 | 1,387,000,000 | 13,572,900 | 1.0 | 1.12 |
| NFM | 134 | 1.2 | 1.5 | 1,371,000,000 | 13,037,800 | 0.26 | 1.16 |
| INFC (NFI) | 131 | 1.6 | 0 | 1,366,000,000 | 13,959,000 | 0 | 1 |

For the 20 NUTS2 administrative regions, the greatest correlation with the NFI estimates was achieved by the GSV map masked with the NFM mask with $\hat{\rho}$ = 0.972 and $\hat{\rho}$ = 0.986 for the mean and total GSV, respectively (Table 4). The GSV maps masked with the CLMS and FM00 masks, despite their large values of $\hat{\rho}$, show a systematic overestimation of the $\hat{\tau}_{ma}$.

Table 4. Coefficient of correlation between the mean and total model-assisted estimate and NFI estimates for administrative NUTS2 regions (*p-value=0; **p-value < 0.001).

| Forest mask | $\hat{\rho}_{Total}$ | $\hat{\rho}_{Mean}$ |
|---|---|---|
| CLMS | 0.978* | 0.963** |
| JAXA | 0.968** | 0.971** |
| FM00 | 0.979* | 0.949** |
| CLC | 0.977** | 0.970** |
| NFM | 0.986* | 0.972* |

Regarding $\hat{\mu}_{ma}$, for 16 of 20 regions, the differences between the model-assisted estimates and the NFI estimate were not statistically significantly different from 0 for the NFM masked GSV map, for 15 regions for CLMS and JAXA, for 14 regions for CLC06, and for 10 regions for FM00. Similar results were obtained for $\hat{\tau}_{ma}$ for which the differences for 16 of 20 regions were not statistically significantly different from 0 for the NFM masked GSV map, 15 for CLC06 and JAXA, six for CLMS, and two for FM00. The regions that always showed a statistically significant difference between the model-assisted estimates and the official NFI turned out to be the islands (Sardegna,

Sicilia) and two regions (Puglia, Umbria), while those which never did were seven, distributed in northern and central Italy.

RE exceeded 1 for most regions, regardless of the FM used. RE < 1 was observed in one region for the CLMS and FM00 masks (Toscana), two regions for the CLC06 mask (Toscana, Emilia Romagna), and four regions for the JAXA mask (Toscana, Emilia Romagna, Sardegna, Umbria). The only masked GSV map that leads to RE coefficient always >1 was the NFM.

3.3. Relationship Between FMs Accuracy and GSV Estimates

The relationship between the accuracies of the FMs and the SEs of the estimates with the model-assisted estimator is presented in Table 5. The correlation was calculated for the 20 administrative regions.

Table 5. Correlation coefficient between the accuracy metrics and the SEs of estimates for each FM. The overall values were calculated based on all five FMs together.

| Forest mask | $\hat{\rho}$ | | | |
|---|---|---|---|---|
| | Overall Accuracy | κ | Precision | Recall |
| CLMS | −0.26 | −0.43 | −0.48 | −0.25 |
| JAXA | 0.26 | −0.27 | −0.36 | −0.62 |
| FM00 | 0.12 | −0.24 | −0.57 | −0.68 |
| CLC | 0.09 | −0.20 | −0.39 | −0.29 |
| NFM | 0.09 | −0.26 | −0.26 | −0.58 |
| Overall | 0.03 | −0.20 | −0.32 | −0.42 |

## 4. Discussion

The aim of this study was to assess the effects of using different FMs available for Italy for the area-based estimation of GSV. We first constructed a pixel-level GSV map for the entirety of Italy based on the procedure recently proposed by Chirici et al. (2020). We then acquired five different FMs and, after evaluating their accuracies against an independent dataset (IUTI), we used them to mask out non-forest areas from the national GSV map produced with the random forest model. We then compared the five

resulting model-assisted GSV estimates aggregated at regional levels with the official design-based NFI estimates.

Four of the five FMs achieved overall accuracies > 85%, based on the 2008 land use classification of IUTI points, with the CLC06 and NFM outperforming the other products. At the national level, the FM that achieved the greatest overall accuracy, κ and precision was the NFM, followed by the CLC06. Despite the greatest recall (0.91) achieved, the FM00 was affected by systematic overestimation of the regional forest area due to the original coarse resolution (Schepaschenko et al., 2015) which made this FM unsuitable for GSV estimation.

In contrast, the JAXA FM produced the smallest recall (0.74), most probably because the SAR backscatter in the HV polarization is relatively insensitive to Mediterranean vegetation (D'Amico et al., 2021; Bartsch et al., 2020) which probably caused an underestimation of the forest area. The photointerpreted FMs, CLC06 and NFM, had the greatest precision. This is an expected result because forest land use identification is typically done by local experts. However, CLC06 produced less precision than the NFM because it was implemented for monitoring land cover, not land uses, adopting a MMU and a crown cover threshold greater than that adopted by the INFC 2005 (Seebach et al., 2011;Vizzarri et al., 2015). In fact, the CLC project did not map forest clear-cuts and other natural or anthropic disturbances as forest land use, but rather as bare soil or other non-forest classes, affecting the estimation of forest area. Conversely, the NFM, as a mosaic of local forest maps, is designed to monitor forest land use, such as the NFI. However, the small precision of the accuracy showed that false positives were the majority of classification errors.

At the regional level, OA was greater than 85% for 18 regions for the NFM mask, followed by the CLMS mask (14 regions), the CLC06 mask (12 regions), the JAXA mask (3 regions), and the FM00 mask (1 region). Regardless of the FM used, the greatest uncertainty was found in the southern regions and the islands (Campania, Calabria, Abruzzo, Basilicata, Sardegna, Sicilia), most probably because of the complex Mediterranean formations and complex agroforestry landscape tiles that characterized these regions where the NFI estimates also have larger associated SEs.

The greatest accuracies were achieved for regions characterized by greater forest cover (Liguria, Trentino-Alto Adige, Friuli-Venezia Giulia, Umbria, Toscana). These regions

are characterized by extensive forests with continuous coverage and greater accumulation of GSV, as in the Apennine and Alpine Mountains, which probably reduces the probability of forest misclassifications, regardless of the FM considered.

Conversely, the forests bordering other land uses, along rivers, and in the coastal and rural contexts are typically characterized by a sparse canopy, which makes them more difficult to correctly classify, even by manual photointerpretation.

In conclusion, regarding the qualities of the FMs, the most accurate was the NFM, which was comparable with the CLC06, but with the advantage of a finer MMU which makes it more suitable for regional and local scale applications.

Regarding the model-assisted GSV estimates, although all the masked GSV maps overestimated total GSV, the NFM masked GSV map was most accurate as a trade-off between the national and regional GSV and the SE of estimates. The general overestimation was caused by the trend of the prediction model to overpredict GSV for pixels with small observed GSV values. (i.e., GSV < 250 m3 ha−1). This evidence, along with the limited GSV that characterizes Italian forests, caused the general overestimation at the national level. One possible solution is to increase the performance of the model, for example, by integrating ALS metrics which is a well-established data source for enhancing GSV predictions (Næsset et al., 2004; Kangas et al., 2018; Næsset et al., 2014). Both the CLMS and FM00 masked GSV maps suffered from systematic prediction error which caused the overestimation of $\hat{\tau}_{ma}$, both nationally and regionally. For the CLMS masked GSV map, this can be caused by the inclusion of many agricultural and rural areas that occur in Italy (Langanke, 2017), and for FM00 because of the original coarse spatial resolution (1 x 1 km). The differences between the total GSV model-assisted estimates and the official NFI estimate for two of the five masked GSV maps (NFM, CLC06) were statistically significantly different from 0. At the national level, the mean GSV estimates were comparable for all maps, except for the GSV map masked with the FM00 mask. The JAXA masked GSV map produced the same value as the NFI for mean GSV but underestimated the total due to the underestimation of forest area. However, the SEs were almost comparable for all the GSV-masked maps considered. The SE is mainly affected by the number of NFI plots used for building the model and calculation of the correction term in the estimator.

Despite the differences among the FMs, the NFI plots falling within the forested portions of the FMs were similar, ranging between 6100 (CLMS) and 5800 (JAXA). Differences in the number of plots selected by each FM are likely to be concentrated at the forest edge, where maps are more prone to classification errors. These results confirm the findings of Esteban et al. (2020), suggesting that the FM effects on area estimates are more important than the effects of field plot sampling variability on the uncertainty of the mean and total estimates.

At the regional level, the NFM produced the greatest $\hat{\rho}$ relative to the NFI estimates, both for $\hat{\mu}_{ma}$ and $\hat{\tau}_{ma}$, with the largest number of regional estimates in accordance with the NFI (16 regions out of 20). The NFM was also the only FM that led consistently to RE > 1. The CLC06 achieved similar results, with the major exception of Sardegna and in general in the southern regions, where, as we reported before, the MMU of the CLC project is not fine enough to discern the complex patchwork in the landscape of a rural region.

$SE(\hat{\tau}_{ma})$ was smaller than $SE(\hat{\tau}_{NFI})$ for 16 regions, which represent 70% of the Italian territory. The regions with the greatest $SE(\hat{\tau}_{ma})$ were Puglia, Valle d'Aosta, Molise, Basilicata, and Marche ($SE(\hat{\tau}_{ma})$> 5%) probably because of the small number of NFI plots in these regions. Nevertheless, with the use of the model-assisted estimation approach, it was possible to decrease the error of the estimates with respect to the NFI estimates, both at the national (NUTS1), and regional levels (NUTS2).

Regarding the relationship between the FM accuracy and the SEs of the estimates, we found small correlation coefficients, in particular with the overall accuracy. The SE depends primarily on the sample size, which is less affected by the accuracy of the FMs, as reported by Esteban et al. (2020). The accuracy metric was more correlated with the SE of the estimates than was the recall, followed by the precision. This is an expected result because these metrics are strictly related to the area classified as forest which, in turn, affects the number of NFI plots included in the FMs. Of interest, the FM with the greatest recall (CLMS) was also the FM that included the greatest number of NFI plots.

However, the negative correlation with the other accuracy metrics demonstrated that a more accurate FM leads to a smaller $SE(\hat{\tau}_{ma})$.

It would be interesting to combine the available maps by aggregating their beneficial features to overcome the problems associated with each FM as per McRoberts et al. (2016). Another option would be to calibrate the FMs using the NFI data as per Næsset et al. (2007).

In conclusion, the differences in the accuracies of the FMs led to different GSV estimates, although the SEs were almost comparable. The smallest GSV difference against the official NFI estimate was obtained by the most accurate FMs, i.e., the NFM. This is likely due to the correct classification of the main, dense forests, which have the largest amount of volume and subsequently make the greatest contribution in the model-assisted estimation. Presumably, forest misclassification occurs mainly along the margins and in boundary areas between different land uses.

## 5. Conclusions

This paper presents a comparative analysis of the impacts of different forest masks on the model-assisted estimation of GSV. Several conclusions can be drawn from this study.

At national and regional levels, the masked GSV map constructed using the NFM mask produced GSV estimates that were most similar to the official NFI estimates. Regardless of the forest mask, the major disagreement with the official estimate was found in the southern regions and islands, most probably because of the presence of the Mediterranean macchia, which is difficult to classify correctly, even by manual photointerpretation of fine-resolution images. These were the regions with the least classification accuracies. Regions with abundant forest components (central and northern regions) produced the most accurate masks and the most accurate and most precise GSV estimates.

Despite the small correlation coefficients, we found a negative relationship between forest mask accuracy and the standard error of the GSV estimate, demonstrating that the accuracy of the FM must be considered in the GSV estimation through the model-assisted estimator.

The quality of the model-assisted estimation mostly depends on the performance of the prediction model. A more accurate FM can compensate for systematic model prediction

errors, leading to a greater agreement with official NFI GSV estimates, both at national and regional levels.

In conclusion, we recommend using the NFM, both at regional and national levels, for studies aimed at estimating forest parameters related to variables such as forest area, GSV, AGB, and carbon stock. However, it is plausible to assume that as the accuracy of the model predictions increases thanks to the growing availability of 3D data, the NFM will always produce more accurate and precise estimates of total GSV. In this regard, we hope that in the future, wall-to-wall ALS coverage will be finally available in Italy, to enhance the prediction of forest variables with even greater accuracy.

Finally, we strongly recommended that the different forest mapping and monitoring programs currently active in Italy converge on a common method and lead to harmonized, multiscale systems in line with the international forest definition.

# 6. Reference

Barbati, A.; Marchetti, M.P.; Chirici, G.; Corona, P. European Forest Types and Forest Europe SFM indicators: Tools for monitoring progress on forest biodiversity conservation. For. Ecol. Manag. 2014, 321, 145–157, doi:10.1016/j.foreco.2013.07.004.

Barrett, F.; McRoberts, R.E.; Tomppo, E.; Cienciala, E.; Waser, L.T. A questionnaire-based review of the operational use of remotely sensed data by national forest inventories. Remote. Sens. Environ. 2016, 174, 279–289, doi:10.1016/j.rse.2015.08.029.

Bartsch, A.; Widhalm, B.; Leibman, M.; Ermokhina, K.; Kumpula, T.; Skarin, A.; Wilcox, E.J.; Jones, B.M.; Frost, G.V.; Höfler, A.; et al. Feasibility of tundra vegetation height retrieval from Sentinel-1 and Sentinel-2 data. Remote. Sens. Environ. 2020, 237, 111515, doi:10.1016/j.rse.2019.111515.

Belgiu, M.; Drăguţ, L. Random forest in remote sensing: A review of applications and future directions. Isprs J. Photogramm. Remote Sens. 2016, 114, 24–31, doi:10.1016/j.isprsjprs.2016.01.011.

Breidt, F.J.; Opsomer, J.D. Chapter 27-nonparametric and semiparametric estimation in complex surveys. In Handbook of Statistics; Rao, C.R., Ed.; Elsevier: Amsterdam, The Netherlands, 2009; pp. 103–119, doi:10.1016/S0169-7161(09)00227-2.

Büttner, G.; Feranec, J.; Jaffrain, G.; Mari, L.; Maucha, G.; Soukup, T. THE CORINE LAND COVER 2000 PROJECT. EARSeL eProceedings 3, 3/2004 331. 2004 available online at http://citeseerx.ist.psu.edu/viewdoc/download?doi=10.1.1.618.9940&rep=rep1&type=pdf (accessed on 06/02/2021).

Chirici, G.; Giannetti, F.; McRoberts, R.E.; Travaglini, D.; Pecchi, M.; Maselli, F.; Chiesi, M.; Corona, P. Wall-to-wall spatial prediction of growing stock volume based on Italian National Forest Inventory plots and remotely sensed data. Int. J. Appl. Earth Obs. Geoinf. 2020, 84, 101959, doi:10.1016/j.jag.2019.101959.

Corona, P.; Barbati, A.; Tomao, A.; Bertani, R.; Valentini, R.; Marchetti, M.; Fattorini, L.; Perugini, L. Land use inventory as framework for environmental accounting: An application in Italy. Iforest Biogeosci. For. 2012, 5, 204–209. Available online: http://www.sisef.it/iforest/contents? id=ifor0625-005 (accessed on 06/11/2020).

D'Amico, G.; Vangi, E.; Francini, S.; Giannetti, F.; Nicolaci, A.; Travaglini, D.; Massai, L.; Giambastiani, Y.; Terranova, C.; Chirici, G. Are We Ready for a Web-Based National Forest Information System? State of the Art of for-Est Maps and Airborne Laser Scanning Data Availability in Italy. iForest.

Dalponte, M.; Ørka, H.O.; Ene, L.T.; Gobakken, T.; Næsset, E. Tree crown delineation and tree species classification in boreal forests using hyperspectral and ALS data. Remote. Sens. Environ. 2014, 140, 306–317, doi:10.1016/j.rse.2013.09.006.

Devarriya, D.; Gulati, C.; Mansharamani, V.; Sakalle, A.; Bhardwaj, A. Unbalanced breast cancer data classification using novel fitness functions in genetic programming. Expert Syst. Appl. 2020, 140, 112866, doi:10.1016/j.eswa.2019.112866.

D'Oliveira, M.V.; Reutebuch, S.E.; McGaughey, R.J.; Andersen, H.-E. Estimating forest biomass and identifying low-intensity logging areas using airborne scanning lidar in Antimary State Forest, Acre State, Western Brazilian Amazon. Remote Sens. Environ. 2012, 124, 479–491, doi:10.1016/j.rse.2012.05.014.

Dostálová, A.; Hollaus, M.; Milenković, M.; Wagner, W. FOREST AREA DERIVATION FROM SENTINEL-1 DATA. Isprs Ann. Photogramm. Remote. Sens. Spat. Inf. Sci. 2016, III-7, 227–233, doi:10.5194/isprs-annals-iii-7-227-2016.

Esteban, J.; McRoberts, R.E.; Fernández-Landa, A.; Tomé, J.L.; Marchamalo, M. A Model-Based Volume Estimator that Accounts for Both Land Cover Misclassification and Model Prediction Uncertainty. Remote. Sens. 2020, 12, 3360, doi:10.3390/rs12203360.

European Enviromental Agency. Enviromental Statement; Office for Official Publications of the European Communities: Luxembourg, 2007; ISBN 978-92-9167-936-2.

Eysn, L.; Hollaus, M.; Schadauer, K.; Pfeifer, N. Forest Delineation Based on Airborne LIDAR Data. Remote. Sens. 2012, 4, 762–783, doi:10.3390/rs4030762.

FAO, UNCCD. Sustainable Financing for Forest and Landscape Restoration: The Role of Public Policy Makers; FAO, Rome 2015; p. 12.

FAO. Global forest resources assessment 2010. Terms and definition. Working paper 144/E. 2010. Available online: http://www.fao.org/3/am665e/am665e00.pdf (accessed on 07/10/2020).

Fattorini, L.; Marcheselli, M.; Pisani, C. A three-phase sampling strategy for large-scale multiresource forest inventories. J. Agric. Biol. Environ. Stat. 2006, 11, 296–316, doi:10.1198/108571106x130548.

Foga, S.; Scaramuzza, P.L.; Guo, S.; Zhu, Z.; Dilley, R.D.; Beckmann, T.; Schmidt, G.L.; Dwyer, J.L.; Hughes, M.J.; Laue, B. Cloud detection algorithm comparison and validation for operational Landsat data products. Remote. Sens. Environ. 2017, 194, 379–390, doi:10.1016/j.rse.2017.03.026.

Fritz, S.; See, L. Comparison of land cover maps using fuzzy agreement. Int. J. Geogr. Inf. Sci. 2005, 19, 787–807, doi:10.1080/13658810500072020.

Giannetti, F.; Chirici, G.; Gobakken, T.; Næsset, E.; Travaglini, D.; Puliti, S. A new approach with DTM-independent metrics for forest growing stock prediction using UAV photogrammetric data. Remote. Sens. Environ. 2018, 213, 195–205, doi:10.1016/j.rse.2018.05.016.

Giannetti, F.; Puletti, N.; Puliti, S.; Travaglini, D.; Chirici, G. Modelling Forest structural indices in mixed temperate forests: comparison of UAV photogrammetric DTM-independent variables and ALS variables. Ecol. Indic. 2020, 117, 106513, doi:10.1016/j.ecolind.2020.106513.

Giri, C.; Zhu, Z.; Reed, B. A comparative analysis of the Global Land Cover 2000 and MODIS land cover data sets. Remote. Sens. Environ. 2005, 94, 123–132, doi:10.1016/j.rse.2004.09.005.

Goodbody, T.R.H.; Coops, N.C.; White, J.C. Digital Aerial Photogrammetry for Updating Area-Based Forest Inventories: A Review of Opportunities, Challenges, and Future Directions. Curr. For. Rep. 2019, 5, 55–75, doi:10.1007/s40725-019-00087-2.

Hansen, M.C.; Potapov, P.V.; Moore, R.; Hancher, M.; Turubanova, S.A.; Tyukavina, A.; Thau, D.; Stehman, S.V.; Goetz, S.J.; Loveland, T.R.; et al. High-Resolution Global Maps of 21st-Century Forest Cover Change. Science 2013, 342, 850–853.

Hansen, M.H.; Madow, W.G.; Tepping, B.J. An evaluation of model dependent and probability-sampling inferences in sample surveys. J. Am. Stat. Assoc. 1983, 78, 776–793.

Hollaus, M.; Dorigo, W.; Wagner, W.; Schadauer, K.; Höfle, B.; Maier, B. Operational wide-area stem volume estimation based on airborne laser scanning and national

forest inventory data. Int. J. Remote. Sens. 2009, 30, 5159–5175, doi:10.1080/01431160903022894.

Holm, S.; Nelson, R.; Ståhl, G. Hybrid three-phase estimators for large-area forest inventory using ground plots, airborne lidar, and space lidar. Remote. Sens. Environ. 2017, 197, 85–97, doi:10.1016/j.rse.2017.04.004.

Hoyos, A.P.; Rembold, F.; Kerdiles, H.; Gallego, J. Comparison of Global Land Cover Datasets for Cropland Monitoring. Remote. Sens. 2017, 9, 1118, doi:10.3390/rs9111118.

Immitzer, M.; Stepper, C.; Böck, S.; Straub, C.; Atzberger, C. Use of WorldView-2 stereo imagery and National Forest Inventory data for wall-to-wall mapping of growing stock. For. Ecol. Manag. 2016, 359, 232–246, doi:10.1016/j.foreco.2015.10.018.

INFC. 2007. Le stime di superficie 2005-seconda parte. In Inventario Nazionale delle Foreste e dei Serbatoi Forestali di Carbonio; Tabacchi, A.G., De Natale, F., Di Cosmo, L., Floris, A., Gagliano, C., Gasparini, P., Salvadori, I., Scrinzi, G., Tosi, V., Eds.; MiPAF–Corpo Forestale dello Stato-Ispettorato Generale, CRA-ISAFA: Trento, Italy. Available online: http://www.infc.it (accessed on 05/11/2019).

Jaafor, O.; Birregah, B. KNN-LC: Classification in Unbalanced Datasets using a KNN-Based Algorithm and Local Centralities In: Adjallah K., Birregah B., Abanda H. (eds) Data-Driven Modeling for Sustainable Engineering. ICEASSM 2017. Lecture Notes in Networks and Systems, vol 72. Springer, Cham. https://doi.org/10.1007/978-3-030-13697-0_7D'Oliveira, M.V.; Reutebuch, S.E.; McGaughey, R.J.; Andersen, H.-E. Estimating forest biomass and identifying low-intensity logging areas using airborne scanning lidar in Antimary State Forest, Acre State, Western Brazilian Amazon. Remote. Sens. Environ. 2012, 124, 479–491, doi:10.1016/j.rse.2012.05.014.

JAXA. Global 25m Resolution PALSAR-2/PALSAR Mosaic and Forest/Non-Forest Map (FNF) Dataset Description. Japan Aerospace Exploration Agency (JAXA), Earth Observation Research Center (EORC), Japan, 2016.

Kangas, A.; Astrup, R.; Breidenbach, J.; Fridman, J.; Gobakken, T.; Korhonen, K.T.; Maltamo, M.; Nilsson, M.; Nord-Larsen, T.; Næsset, E.; et al. Remote sensing and forest inventories in Nordic countries–roadmap for the future. Scand. J. For. Res. 2018, 33, 397–412, doi:10.1080/02827581.2017.1416666.

Karlson, M., Ostwald, M., Reese, H., Sanou, J., Tankoano, B., Mattsson, E. Mapping tree canopy cover and above-ground biomass in Sudano-Sahelian woodlands using landsat 8 and random forest. Remote Sens. 2015, 7, 10017.

Kennedy, R.E.; Yang, Z.; Gorelick, N.; Braaten, J.; Cavalcante, L.; Cohen, W.B.; Healey, S. Implementation of the LandTrendr Algorithm on Google Earth Engine. Remote. Sens. 2018, 10, 691, doi:10.3390/rs10050691.

Langanke, T. Copernicus Land Monitoring Service–High Resolution Layer Forest: Product Specifications Document 38;Copernicus team at EEA, 2017.

Li, Z.-W.; Xin, X.-P.; Tang, H.; Yang, F.; Chen, B.-R.; Zhang, B.-H. Estimating grassland LAI using the Random Forests approach and Landsat imagery in the meadow steppe of Hulunber, China. J. Integr. Agric. 2017, 16, 286–297, doi:10.1016/s2095-3119(15)61303-x.

Liaw, A.; Wiener, M. Classification and regression by randomForest. Nucleic Acids Res. 2002, 5, 983–999, doi:10.1023/A:101093340432.

Masek, J.G., Vermote, E.F., Saleous, N.E., Wolfe, R., Hall, F.G., Huemmrich, K.F., Gao, F., Kutler, J., Lim, T.-K. A Land-sat surface reflectance dataset for North America, 1990–2000. IEEE Geosci. Remote Sens. Lett. 2006, 3, 68–72.

Maselli, F.; Pasqui, M.; Chirici, G.; Chiesi, M.; Fibbi, L.; Salvati, R.; Corona, P. Modeling primary production using a 1 km daily meteorological data set. Clim. Res. 2012, 54, 271–285, doi:10.3354/cr01121.

McRoberts, R.E. Probability- and model-based approaches to inference for proportion forest using satellite imagery as ancillary data. Remote. Sens. Environ. 2010, 114, 1017–1025, doi:10.1016/j.rse.2009.12.013.

McRoberts, R.E.; Chen, Q.; Walters, B.F.; Kaiershot, D.J. The effects of global positioning system receiver accuracy on airborne laser scanning-assisted estimates of aboveground biomass. Remote. Sens. Environ. 2018, 207, 42–49, doi:10.1016/j.rse.2017.09.036.

McRoberts, R.E.; Naesset, E.; Gobakken, T. Accuracy and Precision for Remote Sensing Applications of Nonlinear Model-Based Inference. IEEE J. Sel. Top. Appl. Earth Obs. Remote. Sens. 2013, 6, 27–34, doi:10.1109/JSTARS.2012.2227299.

McRoberts, R.E.; Næsset, E.; Gobakken, T. Optimizing the k-Nearest Neighbors technique for estimating forest above-ground biomass using airborne laser scanning data. Remote Sens. Environ. 2015, 163, 13–22.

McRoberts, R.E.; Tomppo, E.O. Remote sensing support for national forest inventories. Remote. Sens. Environ. 2007, 110, 412–419, doi:10.1016/j.rse.2006.09.034.

McRoberts, R.E.; Vibrans, A.C.; Sannier, C.; Næsset, E.; Hansen, M.C.; Walters, B.F.; Lingner, D.V. Methods for evaluating the utilities of local and global maps for increasing the precision of estimates of subtropical forest area. Can. J. For. Res. 2016, 46, 924–932, doi:10.1139/cjfr-2016-0064.

Moser, P.; Vibrans, A.C.; McRoberts, R.E.; Næsset, E.; Gobakken, T.; Chirici, G.; Mura, M.; Marchetti, M. Methods for variable selection in LiDAR-assisted forest inventories. Forestry 2016, 90, 112–124, doi:10.1093/forestry/cpw041.

Næsset, E. Airborne laser scanning as a method in operational forest inventory: Status of accuracy assessments accom-plished in Scandinavia. Scand. J. For. Res. 2007, 22, 433–422.

Næsset, E. Area-Based Inventory in Norway–From Innovation to an Operational Reality. In Forestry Applications of Airborne Laser Scanning Concepts Case Stud.; Maltamo, M., Næsset, E., Vauhkonen, J., Eds.; Springer: Dordrecht, The Netherlands, 2014; pp. 215–240, doi:10.1007/978-94-017-8663-8_11.

Næsset, E.; Gobakken, T. Estimation of above- and below-ground biomass across regions of the boreal forest zone using airborne laser. Remote. Sens. Environ. 2008, 112, 3079–3090, doi:10.1016/j.rse.2008.03.004.

Næsset, E.; Gobakken, T.; Holmgren, J.; Hyyppä, H.; Hyyppä, J.; Maltamo, M.; Nilsson, M.; Olsson, H.; Persson, Å.; Söderman, U. Laser scanning of forest resources: The nordic experience. Scand. J. For. Res. 2004, 19, 482–499, doi:10.1080/02827580410019553.

Neumann, K.; Herold, M.; Hartley, A.; Schmullius, C. Comparative assessment of CORINE2000 and GLC2000: Spatial analysis of land cover data for Europe. Int. J. Appl. Earth Obs. Geoinf. 2007, 9, 425–437, doi:10.1016/j.jag.2007.02.004.

Nilsson, M.; Nordkvist, K.; Jonzén, J.; Lindgren, N.; Axensten, P.; Wallerman, J.; Egberth, M.; Larsson, S.; Nilsson, L.; Eriksson, J.; et al. A nationwide forest attribute map of Sweden predicted using airborne laser scanning data and field data from the National Forest Inventory. Remote. Sens. Environ. 2017, 194, 447–454, doi:10.1016/j.rse.2016.10.022.

Øivind, D.T.; Salberg, A.-B.; Kermit, M.; Øystein, R.; Gobakken, T.; Næsset, E.; Aarsten, D. Tree species classification in Norway from airborne hyperspectral and

airborne laser scanning data. Eur. J. Remote. Sens. 2018, 51, 336–351, doi:10.1080/22797254.2018.1434424.

Olofsson, P.; Arévalo, P.; Espejo, A.B.; Green, C.; Lindquist, E.; McRoberts, R.E.; Sanz, M.J. Mitigating the effects of omission errors on area and area change estimates. Remote. Sens. Environ. 2020, 236, 111492, doi:10.1016/j.rse.2019.111492.

P.; Gasparini, F.; De Natale, L.; Di Cosmo, C.; Gagliano, I.; Salvadori, G.; Tabacchi e.V.; Tosi. INFC, 2009–I caratteri quantitativi–parte 1, vers. 2. Inventario Nazionale delle Foreste e dei Serbatoi Forestali di Carbonio; MiPAAF–Ispettorato Generale Corpo Forestale dello Stato, CRA-MPF: Trento, Italy,.2009

Panagos, P. The European Soil Database; GEO: 2006; pp. 32–33.

Penman, J.; Gytarsky, M.; Hiraushi, T.; Krug, T.; Kruger, D.; Pipatti, R.; Buendia, L.; Miwa, K.; Ngara, T.; Tanabe, K.; et al. Good Practice Guidance for Land Use, Land Use Change and Forestry. Chapter 3: Annex 3A.1 Biomass Default Tables for Section 3.2 Forest Land Good Practice Guidance for Land Use, Land-Use Change and Forestry; The Institute for Global Enviromental Strategies for the IPCC and the Intergovernmental Panel on Climate Change, Hayama: Kanagawa, Japan, 2003; p. 21.

Puletti, N.; Floris, A.; Scrinzi, G.; Chianucci, F.; Colle, G.; Michelini, T.; Pedot, N.; Penasa, A.; Scalercio, S.; Corona, P.; et al. CFOR: A spatial decision support system dedicated to forest management in Calabria. For. Riv. Selvic. Ed Ecol. For. 2017, 14, 135–140, doi:10.3832/efor2363-014.

Rodríguez-Veiga, P.; Saatchi, S.; Tansey, K.; Balzter, H. Magnitude, spatial distribution and uncertainty of forest biomass stocks in Mexico. Remote. Sens. Environ. 2016, 183, 265–281, doi:10.1016/j.rse.2016.06.004.

Romano D, Arcarese C, Bernetti A, Caputo A, Condor RD, Contaldi M, Lauretis R, Di Cristofaro E, Federici S, Gagna A, Gonella B, Lena F, Liburdi R, Taurino, E., Vitullo, M. Italian Greenhouse Gas Inventory 1990–2009. National Inventory Report; ISPRA: Rome, Italy, 2011.

Rudjord, O.; Trier, O.D. Tree species classification with hyperspectral imaging and lidar. In Proceedings of the 2016 8th Workshop on Hyperspectral Image and Signal Processing: Evolution in Remote Sensing (WHISPERS),Los Angeles, CA, USA, 12/02/2016; p. 4, doi:10.1109/whispers.2016.8071665.

Saarela, S.; Holm, S.; Grafström, A.; Schnell, S.; Næsset, E.; Gregoire, T.G.; Nelson, R.F.; Ståhl, G. Hierarchical model-based inference for forest inventory utilizing three sources of information. Ann. For. Sci. 2016, 73, 895–910, doi:10.1007/s13595-016-0590-1.

Särndal, C.-E.; Swensson, B.; Wretman, J. Model Assisted Survey Sampling; Springer: New York, NY, USA, 1992; p. 402, p. 694.

Särndal, C.-E.; Swensson, B.; Wretman, J. Model Assisted Survey Sampling; editor, Springer: Berlin, Germany, 2003.

Schepaschenko, D.; See, L.; Lesiv, M.; McCallum, I.; Fritz, S.; Salk, C.; Moltchanova, E.; Perger, C.; Shchepashchenko, M.; Shvidenko, A.; et al. Development of a global hybrid forest mask through the synergy of remote sensing, crowdsourcing and FAO statistics. Remote. Sens. Environ. 2015, 162, 208–220, doi:10.1016/j.rse.2015.02.011.

Seebach, L.; McCallum, I.; Fritz, S.; Kindermann, G.; LeDuc, S.; Böttcher, H.; Fuss, S. Choice of forest map has implications for policy analysis: A case study on the EU biofuel target. Environ. Sci. Policy 2012, 22, 13–24, doi:10.1016/j.envsci.2012.04.010.

Seebach, L.M.; Strobl, P.; Miguel-Ayanz, J.S.; Gallego, J.; Bastrup-Birk, A. Comparative analysis of harmonized forest area estimates for European countries. Forests 2011, 84, 285–299, doi:10.1093/forestry/cpr013.

Stankiewicz, K.; Dąbrowska-Zielińska, K.; Gruszczynska, M.; Hoscilo, A. Mapping vegetation of a wetland ecosystem by fuzzy classification of optical and microwave satellite images supported by various ancillary data In Proceedings of the Remote Sensing for Agriculture, Ecosystems, and Hydrology IV, 17 March 2003; doi:10.1117/12.462423.

Tabacchi, G.; Di Cosmo, L.; Gasparini, P.; Morelli, S. Stima Del Volume E Della Fitomassa Delle Principali Specie Forestali Italiane, Equazioni Di Previsione, Tavole Del Volume E Tavole Della Fitomassa Arborea Epigea; Consiglio per la ricerca e sperimentazione in agricoltura, Unità di ricerca per il monitoraggio e la pianificazione forestale, Trento 2011.

Tomppo, E.; Olsson, H.; Ståhl, G.; Nilsson, M.; Hagner, O.; Katila, M. Combining national forest inventory field plots and remote sensing data for forest databases. Remote. Sens. Environ. 2008, 112, 1982–1999, doi:10.1016/j.rse.2007.03.032.

Vizzarri, M.; Chiavetta, U.; Chirici, G.; Garfì, V.; Bastrup-Birk, A.; Marchetti, M. Comparing multisource harmonized forest types mapping: A case study from central Italy. Iforest-Biogeosci. For. 2015, 8, 59–66. Available online:http://www.sisef.it/iforest/contents/?id=ifor1133-007 (accessed on 05/11/2020).

Waser, L.T.; Fischer, C.; Wang, Z.; Ginzler, C. Wall-to-Wall Forest Mapping Based on Digital Surface Models from Image-Based Point Clouds and a NFI Forest Definition. Forests 2015, 6, 4510–4528, doi:10.3390/f6124386.

Waser, L.T.; Schwarz, M. Comparison of large-area land cover products with national forest inventories and CORINE land cover in the European Alps. Int. J. Appl. Earth Obs. Geoinf. 2006, 8, 196–207, doi:10.1016/j.jag.2005.10.001.

White, J.C.; Coops, N.C.; Wulder, M.A.; Vastaranta, M.; Hilker, T.; Tompalski, P. Remote Sensing Technologies for Enhancing Forest Inventories: A Review. Can. J. Remote. Sens. 2016, 42, 619–641, doi:10.1080/07038992.2016.1207484.

Wittke, S.; Yu, X.; Karjalainen, M.; Hyyppä, J.; Puttonen, E. Comparison of two-dimensional multitemporal Sentinel-2 data with three-dimensional remote sensing data sources for forest inventory parameter estimation over a boreal forest. Int. J. Appl. Earth Obs. Geoinf. 2019, 76, 167–178, doi:10.1016/j.jag.2018.11.009.

Woodcock, C.E.; Allen, R.; Anderson, M.; Belward, A.; Bindschadler, R.; Cohen, W.; Gao, F.; Goward, S.N.; Helder, D.; Helmer, E.; et al. Free Access to Landsat Imagery. Science 2008, 320, 1011a, doi:10.1126/science.320.5879.1011a.

Wulder, M.A.; Loveland, T.R.; Roy, D.P.; Crawford, C.J.; Masek, J.G.; Woodcock, C.E.; Allen, R.G.; Anderson, M.C.; Belward, A.S.; Cohen, W.B.; et al. Current status of Landsat program, science, and applications. Remote Sens. Environ. 2019, 225, 127–147, doi:10.1016/j.rse.2019.02.015.

# 5. Paper III

**GEDI4R: an R package for NASA's GEDI level 4A data downloading, processing and visualization**

*Vangi E.[1,2], D'Amico G.[2], Francini S.[1,2,3], Chirici G.[2,4]*

[1] Department of Bioscience and Territory (DiBT), University of Molise. Pesche 86090, (IS), Italy

[2] Department of Agriculture, Food, Environment and Forestry (DAGRI), University of Florence. Florence 50145, Italy

[3] Department of Innovation in Biological, Agro-Food and Forest System (DIBAF), University of Tuscia.Viterbo 01100, (VT), Italy

[4] ForTech, University of Florence joint laboratory, Florence, Italy

* corresponding author saverio.francini@unifi.it

Earth Science Informatics-

## Abstract

1.      Forest ecosystems' structure and biomass monitoring are crucial for understanding the contribution of forests to the global greenhouse gas balance. NASA's Global Ecosystem Dynamics Investigation (GEDI) mission collects waveform lidar data to estimate Above Ground Biomass Density (AGBD). While of great interest, GEDI data are challenging to download and pre-process and require coding expertise, limiting their usage.

2.      In this paper, we introduce GEDI4R, an open-source R package providing efficient methods for downloading, reading, clipping, visualizing, and exporting GEDI data.

3.      GEDI4R was tested throughout Italy, and more than 11 million GEDI pulses were downloaded in less than 10 hours. The GEDI pulse density in forests ranged between 132 per km2 (in the Friuli Venezia Giulia Italian administrative region) and 61 pulses per km2 (in Trentino Alto-Adige). A regional-level comparison between the official growing stock volume estimates reported in the last Italian forest inventory and

the AGBD extracted from the GEDI data acquired over the forest revealed significant correlations (r2 = 0.77).

4.      Our package contributes to improving the GEDI AGBD data usage, which provides innovative information to monitor carbon cycle dynamics at the global scale.

**Keywords**: Lidar, Forest, Biomass, Ecosystem, Remote sensing, Open access

## 1. Introduction

Forest ecosystems cover about one-third of the Earth's lands and play a crucial role in the global carbon balance (FAO, 2018), absorbing almost 3 billion tons of anthropogenic carbon annually, or 30% of the total emissions associated with fossil fuel burning and net deforestation (Canadell & Raupach, 2008). Accurate measurements of forest variables at large spatial scales are essential for understanding the global carbon cycle and achieving effective carbon mitigation strategies (Chen et al., 2016). Indeed, three-dimensional forest structure data acquired by Light Detection And Ranging (lidar) sensors are the most valuable to assess forest biomass and biomass changes due to human activities or natural hazards mainly related to climate change (Silva et al., 2021). On the other hand, the extensive survey and processing cost limit such information, which, as a result, is usually available just over small areas limiting consistent and large-scale monitoring of forest height and biomass (Dubayah et al., 2020).

The Global Ecosystem Dynamics Investigation (GEDI) is the first satellite mission conceived explicitly for retrieving vertical vegetation structure and has been collecting unique data on vegetation structure since April 2019 for a nominal two-year mission onboard the International Space Station (ISS). GEDI is equipped with a geodetic-class laser altimeter/waveform lidar comprised of three lasers that produce eight transects (beams) of structural information, providing 25-meters resolution measurements of forest height in temperate and tropical forests (between 51.6° N and 51.6° S latitude). GEDI data have already been used to derive various forest-related essential products, including canopy height, foliar canopy profiles, Leaf Area Index (LAI), sub-canopy topography, and biomass (Coops et al., 2021). Also, GEDI forest canopy height measurements have been extrapolated using Landsat data to create a 30 m spatial

resolution global forest canopy height map for 2019 (Potapov et al., 2021). Recently, GEDI data were related to lidar and forest disturbances predicted using Landsat data to study the biomass regrowth following the disturbance (Francini et al., 2022).

Despite a few studies exploiting GEDI potential, GEDI data present limitations that may complicate their further research applicability. First, each GEDI file is represented by the sensor track on Earth, which depends on the orbit of the ISS. For this reason, to acquire information in a small Area of Interest (AOI), despite the full orbit granules being divided in sub-orbit since version 2.0, it is required to download continental-scale files, which complicates the analysis. Second, GEDI products are provided at different levels and spatial resolutions and correspond to different amounts of pre-processing (table 1).

Table 1. GEDI level data features

| Level | Data products | Resolution |
|-------|---------------|------------|
| 1A | Raw waveforms | 25 m Ø |
| 1B | Geolocated waveforms | 25 m Ø |
| 2A | Ground elevation, canopy top height, relative height (RH) metrics | 25 m Ø |
| 2B | Canopy Cover Fraction (CCF), CCF profile, Leaf Area Index (LAI), LAI profile | 25 m Ø |
| 3 | Gridded level 2 metrics | 1 km grid |
| 4A | Footprint level aboveground biomass | 25 m Ø |

GEDI level 4A data version 2.1 was recently released for 2019-04-18 to 2021-11-23 (Dubayah et al., 2022, Duncanson et al., 2022) and is the most up-to-date GEDI product corresponding to the highest processing level available to date. They represent the

output of models in which footprint metrics derived from level 2 products are used to estimate the aboveground biomass density (AGBD). Specifically, AGBD was derived from parametric models that relate GEDI level 2A (L2A) waveform relative height (RH) metrics to field plot estimates of AGBD (Dubayah et al., 2021). For each level of pre-processing, specific software or dedicated functions are required to download and elaborate the data. While the *rGEDI* R package (Silva et al., 2020) allows downloading and processing level 1 and 2 data, no software has been implemented to work with GEDI level 4A data. Although GEDI level 4 data is of great interest, very few studies are published as of now using not simulated data (Francini et al., 2022), possibly due to the lack of ready-to-use analysis procedures specifically conceived for GEDI level 4 data.

This paper aims to (i) present the *GEDI4R* R package for GEDI level 4 data processing and (ii) test the package in Italy. First, we provide a detailed description of *GEDI4R* functions and features (section 2.). Second, we show an illustrative example by applying *GEDI4R* over the whole of Italy and by comparing GEDI AGBD estimates to estimates produced by the most recent (2015) Italian national forest inventory (NFI) (section 3.). Third, we explore the impact of this new package by highlighting the scientific and operative contribution of *GEDI4R* (section 4.).

## 2. Design and implementation

### 2.1. Workflow summary

*GEDI4R* is an R package written in R 4.0 (R Core team 2017) designed to facilitate the download and pre-processing of the GEDI level 4A data (figure 1). The package follows a simple name convention: all function names start with the prefix "l4_" and are followed by a verb indicating the function's primary purpose. *GEDI4R* uses the *data.table* package (https://r-datatable.com) for the data structure, allowing fast and memory-efficient data aggregation and manipulation. Typically slower operations, such as downloading and reading files, are performed in parallel thanks to the functionalities of the *snowfall* and *foreach* R packages. The output of each function is standardized to be compatible with the most common R packages for spatial analysis and plotting, such

as *raster*, *sf*, and *ggplot2*. *GEDI4R* provides functions for i) downloading, ii) reading, iii) clipping, and iv) visualizing data (figure 1), for which we provide a summary below and detailed information in subsequent sections.
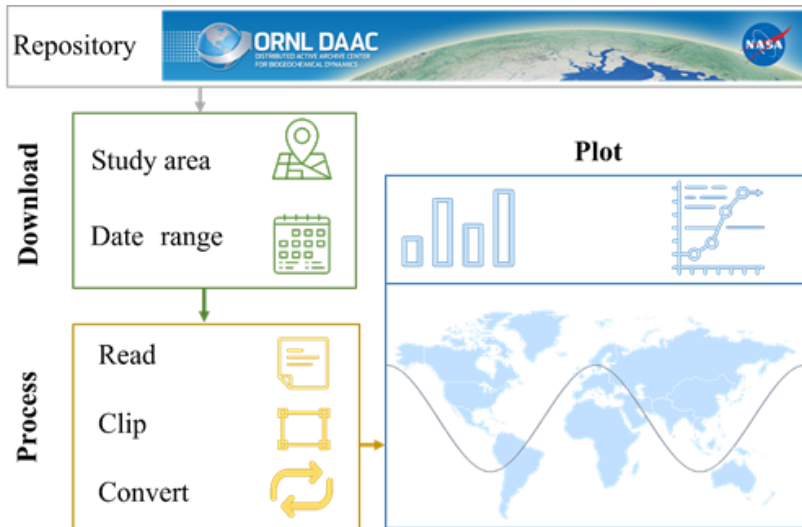


Figure 1. Workflow of the package

Following the connection to the GEDI level 4A repository using the user's Earth Explorer Login Information, the *l4_download* function can download data based on a user-defined Area Of Interest (AOI) and time range (section 2.2.). Then, the package provides a function to read the original h5 file format (section 2.3.). Using the *l4_clip,* GEDI data can be constrained over the AOI (section 2.4.) and then saved on a local machine (section 2.5.). All the mentioned steps can be executed at once using the *l4_process* function (section 2.6.). Finally, two functions are available to plot footprints location and biomass distribution as a function of elevation (section 2.7.). Please refer to the package documentation for detailed information on the functions and their use.

## 2.2. Downloading

The first step of *GEDI4R* is to establish a connection to the GEDI level 4A repository using the user's Earth Explorer Login Information (please see the package readme or functions documentation for more detail about the registration), from which data can be downloaded. The *GEDI4R* function *l4_download* interfaces with the NASA-developed Earth Observing System (EOS) Common Metadata Repository (CMR)

101

(https://cmr.earthdata.nasa.gov/search) to find and access GEDI level 4 data through the doi value and concept ID of the GEDI level 4 collection. It allows finding GEDI level 4A data paths intersecting a user-defined study area and date range. The resulting file paths are then downloaded in parallel using the *foreach* package. At the first run of *l4_download*, users will need to enter their NASA Earth Explorer Login Information in a pop-up window. The function will create a text file in the user-defined directory that stores the login credentials to the ORNL DAAC database, where GEDI level 4A datasets are stored. The function is called for its side effects and returns the path of the downloaded GEDI level 4A files.

## 2.3. Reading

After the download, files can be read into the R environment from the original file format with the function *l4_getmulti* as *data.table* objects. The function can read one file at a time or accept a list or a vector of file paths (as the output of *l4_download*) and read them in parallel, using the *snowfall* package. *l4_getmulti* offers the option to merge files into one single database of class data.table, preserving the information of the file source for each footprint.

The function removes by default footprints with AGBD values corrupted (AGBD <0) and can be used to filter footprints based on the tree cover threshold derived for the year 2010 from Hansen et al. (2013) and encoded as a percentage per output grid cell.

The function returns a *data.table* object with AGBD of each GEDI footprint, along with other auxiliary information. See the details section of *l4_getmulti* documentation for more details of the default variables returned and other variables that can be added to the default output dataset.

## 2.4. Clipping

In their first version, GEDI products were released in files containing all the footprints that constitute the ground track during the entire orbit of the ISS (full-orbit granules). Starting from version 2.0, each GEDI product has been divided into four sub-orbit granules covering an extent of the order of one continent. The *l4_clip* function clips footprints over an AOI. Currently, the AOI can be a path to Shapefiles or Tif files but

also an object of class *sf*, *Raster*, numeric vector of coordinates, or other objects from which an extent can be extracted, specified with the argument *clip*. The function will convert the extent of the spatial object to the GEDI default coordinate system (longitude/latitude, WGS84 - EPSG 4326) to ensure compatibility during the clip. Depending on the *usegeometry* argument, footprints can be clipped on the boundary of the geometry or the extent of the file defining the AOI. Depending on the *usegeometry* argument, the function returns a *data.table* object or an *sf* object. In particular, if *usegeometry=TRUE* the function returns an sf object. It returns a data.table otherwise.

## 2.5 Saving

After the above pre-processing step, usually, data are converted and saved in a user-defined vector format. The function *l4_convert* reprojects footprint coordinates to a user-defined coordinate reference system (by specifying the EPSG code), converts data to an *sf* object, and exports them in vector format (l4_convert uses sf::st_write to save files in vector format, so all file formats supported by sf::st_write are possible. See https://gdal.org/drivers/vector/index.html for full driver documentation and the help page of sf::st_write). Note that column names will be abbreviated with a warning when converting data to ESRI Shapefile. Use other formats such as gpkg to avoid this behavior.

## 2.6. Full processing chain

The processing steps of *l4_getmulti, l4_clip,* and *l4_convert* can be easily performed in chunks of files with the function *l4_process*. This function is designed to be used in real case studies, where files to be processed can be hundreds or thousands, and allows a faster application of functions already described. The function allows the processing of each chunk in parallel. Users can specify the number of cores and the dimension of chunks that should depend on the maximum available RAM: the larger the RAM, the larger the number of per-chunk files that could be processed at once. By default, this function automatically guesses the best number of cores based on the number of available cores and the number of files to be processed. Footprints are clipped on the geometry boundary by default in the clipping step, which is usually the desired choice.

## 2.7. Plotting

The package implements two functions for creating default plots from the processed data: *l4_plotagb* and *l4_plotprofile*. The former returns the location of footprints, the distribution of AGBD against the elevation, or both. The latter produces the plot of AGBD against the elevation profile along the GEDI track. These functions simplified the visualization and interpretation of the GEDI level 4A data. Figures 2 and 3 show the default output of the two plot functions, using a single GEDI track acquired over Italy as input.

It has to be noted that plotting elevation profiles from GEDI data (i.e., with the function *l4_plotprofile*) is only advisable for single beam/track pairs. Plotting profiles from multiple GEDI files (orbits) can be misleading by forcing overlapping data from tracks at different locations.
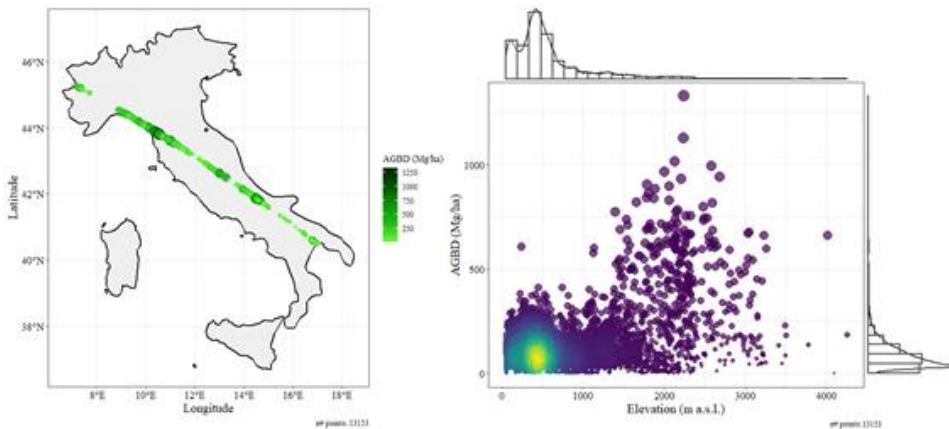


Figure 2. Example plots generated with the function l4_plotagb. Left panel: the location of footprints; right panel: the distribution of AGBD against the elevation. Points color encoded the

point density, while points size encoded the amount of AGBD
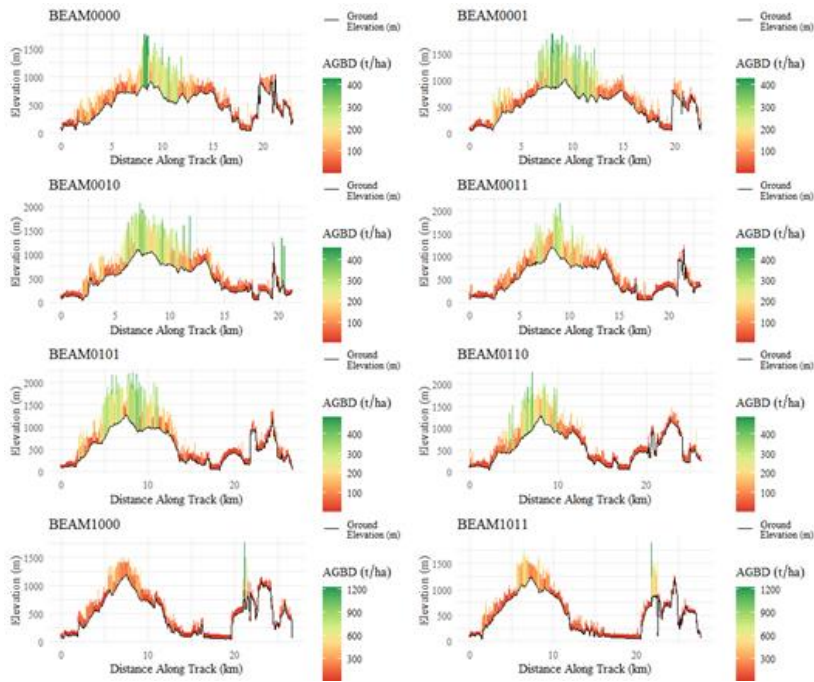


Figure 3. Example plots generated with the function l4_plotprofile. Each panel corresponds to one of the eight laser beams.

## 3. GEDI4R application

The following section illustrates the capabilities of the GEDI4R package with a real-case application aimed at downloading and pre-processing all GEDI level 4A tracks available in Italy.

### 3.1. Study area

The study was carried out in Italy (figure 4), which has a considerable climate and geomorphological variability, with a flat coastal strip, hilly hinterland part, and two main mountain ranges, the Apennines along the peninsula length and the Alps in the north with peaks over 4800 m a.s.l. The country is divided into 20 local administrations (called Regions) or NUTS2 according to the Nomenclature of Territorial Units for

Statistics, following the European Statistical Office. According to the finest national forest mask, Italian forests cover about 11 million hectares (D'Amico et al., 2021; Vangi et al., 2021). Forests are distributed mainly in hills and mountains (INFC, 2007), mainly with broadleaf species (68% of forest area).
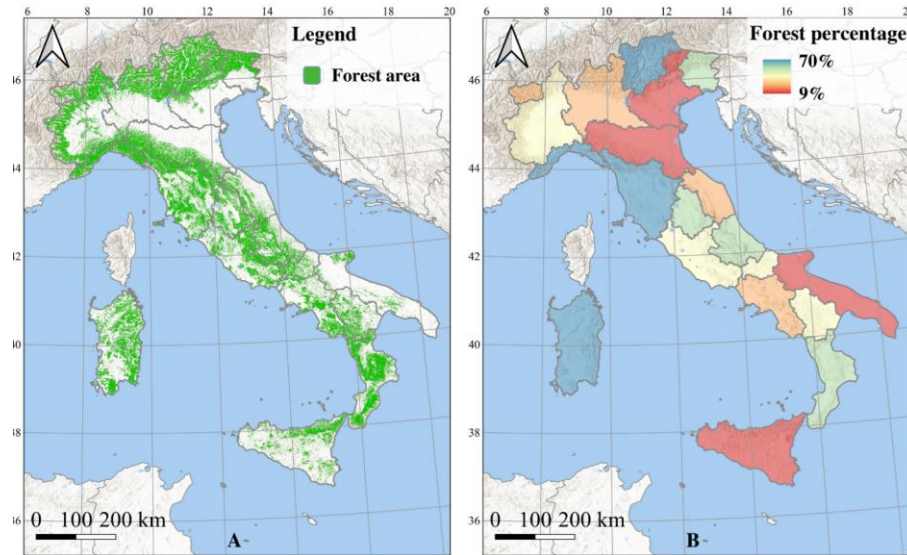


Figure 4. A: Italian forest area; B: Percentage of forest area per region.

## 3.2. Methods

All the analyses were performed using an AMD Ryzen workstation with 3.00Ghz of clock speed, 64 Gb RAM, a Hard disk drive of 4 Tb, 48 logical cores, and 640 Mbps in download. Using the *l4_download* function, we downloaded all GEDI footprints acquired between 2019-04-18 and 2021-11-23 over Italy. Downloading was performed in parallel using 47 cores out of the 48 available. Then, all preprocessing steps were performed using the *l4_process* function. We set 10% as the tree canopy threshold, 20 as the number of files to be processed in each chunk, and ESRI Shapefile as the format to save each chunk. With this parameters configuration, 20 cores out of 48 were used to read each chunk of files, and two cores to loop over chunks. The resulting files were merged in a single layer with all pulses.

### 3.3. Results

2175 files were downloaded, requiring approximately 3 hours and a storage capacity of 620 Gb (average file sizes of 280 Mb). A total of 107 Shapefile were created in about 6 hours, for a total of 8.36 Gb of data (average file sizes of 3 Mb).

Based on the processing settings, more than 11 million pulses (11,427,184) fall on the Italian territory (figure 5), of which 3,144,283 were acquired in 2019, 5,246,897 in 2020, and 3,037,077 in 2021. A total of 9,758,758 pulses fall within the national high-resolution forest mask produced by D'Amico et al. (2021) for Italy.

The Italian Region with the highest number of pulses was Tuscany with 1,183,864 pulses, while the lowest was Aosta Vally with 79,434. The Italian Region with the highest percentage of forests covered by GEDI pulses was Friuli Venezia Giulia (with a pulse density of 132 per $km^2$), while the one with the lowest was Trentino Alto-Adige (with 61 pulses per $km^2$). The mean AGBD in the forest was 124.3 t $ha^{-1}$ with a standard deviation of 7.5 t $ha^{-1}$. For instance, the official estimation of AGBD from the last Italian NFI (INFC 2015) was 114.9 t $ha^{-1}$, with an increase of 19% between 2005 and 2015 (De Laurentis et al., 2021), which is consistent with the one estimated with the GEDI L4 data.
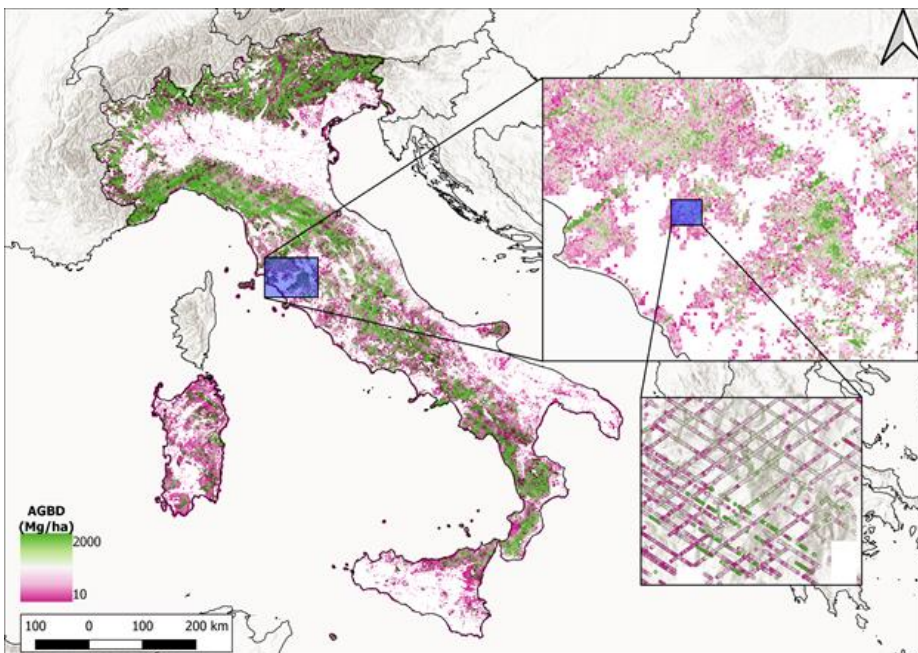
Figure 5. The forest coverage of GEDI level 4A footprints in Italy.

Finally, a regional-level comparison between the official growing stock volume (GSV) data reported in the last Italian NFI (INFC, 2015) and the AGBD extracted from the GEDI data fallen in the forest mask was performed (figure 6), resulting in a coefficient of determination ($r^2$) of 0.77. It was impossible to compare AGBD between GEDI and NFI due to the lack of available biomass data at the regional level.
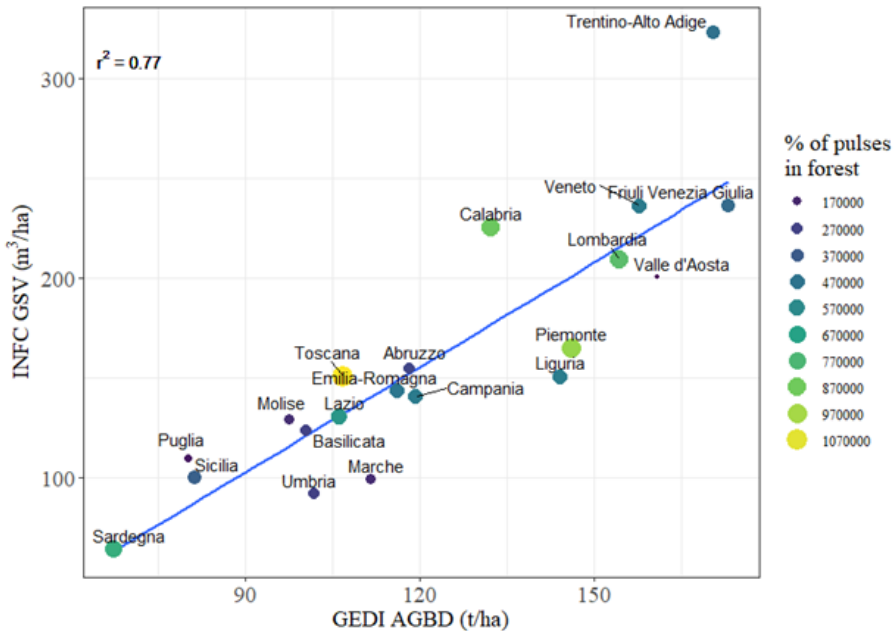


Figure 6. Comparison between NFI GSV density and GEDI AGBD at the regional level.

## 4. Final consideration

Accurate measurements of the forests ecosystem's vertical structure are essential for assessing forests biomass variations due to natural growth but mainly to decline related to human activities or events often connected to the evolution processes related to climate changes (Dubayah et al., 2020). On the other hand, due to data acquisition's high costs, lidar coverage was constrained in both time and space before the launch of the GEDI in December 2018.

Recent studies confirm GEDI data as a game-changer for three-dimensional forest structure and biomass monitoring. In addition, starting from August 2021, GEDI provides an additional product related to the AGBD (Dubayah et al., 2020), data that are crucial for studying forest ecology and forest ecosystems evolution over time and space. However, very few studies using not simulated GEDI level 4 data exist so far. Sharing knowledge and experience on lidar data acquired from space should allow a complete understanding of its strengths and limitations. To do this, as many people as possible should have easy access to every piece of information provided by the GEDI mission, the benchmark for future and more advanced lidar missions from space.

GEDI represents critical advancement in earth observation for forest monitoring, but some tasks - such as downloading GEDI data - are challenging due to the global coverage of each acquisition, which implies huge file sizes. Our package provides a ready-to-use tool that enables getting pre-processed data, allowing many researchers, students, technicians, foresters, or managers worldwide to make the most from GEDI level 4A, focusing on scientific research and avoiding repeating the work we did related to data understanding organization, download, and pre-processing. In addition, the simplicity of the developed functions allows even people with minimal knowledge of the R programming language to successfully interact with GEDI level 4 data. Plus, the function's parameters settings are intuitive, straightforward, and documented in detail within the package.

A first version of the presented GEDI4R package was recently used to analyze the forest ecosystems' biomass trend following forest disturbances (Francini et al., 2022). Data obtained using our package can be further used to derive various forest products,

such as wall-to-wall maps of biomass, carbon stock, and plant functional types.. Using it with multispectral satellite data such as Landsat or Sentinel-2 can improve the forest variables estimates at local and global scales (Potapov et al., 2021), and integrating GEDI data with Landsat time-series is expected to enable a multidecadal historical analysis of forest ecosystems dynamics and disturbance trend. Our package is designed to simplify and facilitate all mentioned tasks and help research in the ecological field, enhance biomass and carbon stock estimates, and answer how forests contribute to carbon sequestration, habitat restoration, and global biodiversity.

*GEDI4R* represents the first step toward several future advancements in forest monitoring, from which researchers can take advantage and minimize the effort to make the most of innovative and groundbreaking GEDI level 4 data.

## 5. Code availability

The source code of the GEDI4R package is accessible via GitHub at https://github.com/VangiElia/GEDI4R. After the download and installation disk occupancy of the GEDI4R package is approximately 3MB and it works on Microsoft Windows and Apple macOS platforms (Table 2).

*Table 2. Package metadata*

| Code metadata description | |
|---|---|
| Current code version | v0.0.1 |
| Operating system and platform | Microsoft Windows10 and above, Apple macOS. |
| Permanent link to code/repository used for this code version | https://github.com/VangiElia/GEDI4R |
| Legal code license | GNU GPLv3.0 |
| Code versioning system used | git |
| Software code languages, tools, and services used | R version 4.0.3 |
| Compilation requirements, operating environments, and dependencies | R packages: data.table, httr, hdf5r, rGEDI, snow, snowfall, doParallel, foreach, raster, sf, ggplot2, proj4, ggExtra, gridExtra, viridis |
| If available, link to developer documentation/manual | https://github.com/VangiElia/GEDI4R |
| Support email for questions | elia.vangi@unifi.it, saverio.francini@unifi.it, giovanni.damico@unifi.it |

# 6. Reference

Canadell, J. G., & Raupach, M. R. (2008). Managing forests for climate change mitigation. science, 320(5882), 1456-1457. doi: 10.1126/science.1155458

Chen, Q., McRoberts, R. E., Wang, C., Radtke, P. J., 2016. Forest aboveground biomass mapping and estimation across multiple spatial scales using model-based inference. Remote Sens. Environ. 184, 350–360. doi: https://doi.org/10.1016/j.rse.2016.07.023

Coops, N. C., Tompalski, P., Goodbody, T. R., Queinnec, M., Luther, J. E., Bolton, D. K., White, J. C., Wulder, M. A., van Lier, O. R., Hermosilla, T. (2021). Modelling lidar-derived estimates of forest attributes over space and time: A review of approaches and future trends. Remote Sensing of Environment, 260, 112477. doi: https://doi.org/10.1016/j.rse.2021.112477

D'Amico G, Vangi E, Francini S, Giannetti F, Nicolaci A, Travaglini D, Massai L, Giambastiani Y, Terranova C, Chirici G, Submitted. Are we ready for a National Forest Information System? State of the art of forest maps and airborne laser scanning data availability in Italy. IForest 14:144-154. doi: https://doi.org/10.3832/ifor3648-014

De Laurentis D., Papitto G., Gasparini P., Di Cosmo L., Floris A., 2021. Italian Forests, Selected results of the third National Forest Inventory INFC 2015. Carabinieri Command for the Protection of Biodiversity and Parks. Roma, Italia. Available online:
https://www.inventarioforestale.org/sites/default/files/datiinventario/pubb/Sintesi_INFC2015.pdf

Dubayah, R., Blair, J. B., Goetz, S., Fatoyinbo, L., Hansen, M., Healey, S., Hofton, M., Hurtt, G., Keller, J., Luthcke, S., Armston, J., Tang, H., Duncanson, L., Hancock, S., Jantz, P., Marseils, S., Patterson, P. L., Qi, W., Silva, C. (2020). The Global Ecosystem Dynamics Investigation: High-resolution laser ranging of the Earth's forests and topography. Science of remote sensing, 1, 100002. doi: https://doi.org/10.1016/j.srs.2020.100002

Dubayah, R.O., J. Armston, J.R. Kellner, L. Duncanson, S.P. Healey, P.L. Patterson, S. Hancock, H. Tang, M.A. Hofton, J.B. Blair, and S.B. Luthcke. 2021. GEDI L4A Footprint Level Aboveground Biomass Density, Version 1. ORNL DAAC, Oak Ridge, Tennessee, USA. doi: https://doi.org/10.3334/ORNLDAAC/1907

Dubayah, R.O., J. Armston, J.R. Kellner, L. Duncanson, S.P. Healey, P.L. Patterson, S. Hancock, H. Tang, J. Bruening, M.A. Hofton, J.B. Blair, and S.B. Luthcke. 2022. GEDI L4A Footprint Level Aboveground Biomass Density, Version 2.1. ORNL DAAC, Oak Ridge, Tennessee, USA. https://doi.org/10.3334/ORNLDAAC/2056

Duncanson, L.; Kellner, J.R.; Armston, J.; Dubayah, R.; Minor, D.M.; Hancock, S.; Healey, S.P.; Patterson, P.L.; Saarela, S.; Marselis, S.; et al. (2022). Aboveground biomass density models for NASA's Global Ecosystem Dynamics Investigation (GEDI) lidar mission. Remote Sensing of Environment. 270, 112845. https://doi.org/10.1016/j.rse.2021.112845.

FAO, 2018. The State of the World's Forests 2018 - Forest Pathways to Sustainable Development. Rome. License: CC BY-NC-SA 3.0 IGO. Accessed on August 15, 2019. Available at. http://www.fao.org/3/I9535EN/i9535en.pdf.

Francini, S.; D'Amico, G.; Vangi, E.; Borghi, C.; Chirici, G. Integrating GEDI and Landsat: Spaceborne Lidar and Four Decades of Optical Imagery for the Analysis

of Forest Disturbances and Biomass Changes in Italy. Sensors 2022, 22, 2015. https://doi.org/10.3390/s22052015

Hansen, M.C.; Potapov, P.V.; Moore, R.; Hancher, M.; Turubanova, S.A.; et al. (2013). High-resolution global maps of 21st-century forest cover change. Science, 342, 850–853. https://doi.org/10.1126/science.1244693.

Potapov, P., Li, X., Hernandez-Serna, A., Tyukavina, A., Hansen, M. C., Kommareddy, A., et al. (2021). Mapping global forest canopy height through integration of GEDI and Landsat data. Remote Sensing of Environment, 253, 112165. doi: https://doi.org/10.1016/j.rse.2020.112165

R Core Team (2017). R: A language and environment for statistical computing. R Foundation 499 for Statistical Computing, Vienna, Austria. URL https://www.R-project.org/

Silva,C.A; Hamamura,C.; Valbuena, R.; Hancock,S.; Cardil,A.; Broadbent, E. N.; Almeida,D.R.A.; Silva Junior, C.H.L; Klauberg, C. rGEDI: NASA's Global Ecosystem Dynamics Investigation (GEDI) Data Visualization and Processing. version 0.1.9, accessed on October. 22 2020, available at: https://CRAN.R-project.org/package=rGEDI

Silva, C. A., Duncanson, L., Hancock, S., Neuenschwander, A., Thomas, N., Hofton, M., Fatoyinbo, L., Simard, M., Marshak, C.Z., Armston, J., Lutchke, S., Dubayah, R. (2021). Fusing simulated GEDI, ICESat-2 and NISAR data for regional aboveground biomass mapping. Remote Sensing of Environment, 253, 112234. doi: https://doi.org/10.1016/j.rse.2020.112234

# 7. Paper IV

**Large-scale high-resolution yearly modeling of forest growing stock volume and above-ground carbon pool**

*Vangi E.[1,2] ,D'Amico G.[2], Francini S.[1,2,3,*], Borghi C.[2],Giannetti F.[2], Corona P.[3,4],Marchetti M.[1] Pellis G.[5], Vitullo M.[5], Travaglini D.[2], Chirici G.[2]*

[1] Dipartimento di Bioscienze e Territorio, Università degli Studi del Molise, Contrada Fonte Lappone, 86090 Pesche, Italy

[2] Department of Agriculture, Food, Environment and Forestry, Università degli Studi di Firenze, Via San Bonaventura, 13, 50145 Firenze, Italy

[3] Dipartimento per l'Innovazione dei sistemi Biologici, Agroalimentari e Forestali, Università degli Studi della Tuscia, Via San Camillo de Lellis, 01100 Viterbo, Italy

[4] CREA, Research Centre for Forestry and Wood, Viale Santa Margherita 80, 52100 Arezzo, Italy

[5] Istituto Superiore per la Protezione e la Ricerca Ambientale

* corresponding author giovanni.damicoi@unifi.it

## Abstract

Within the Paris Agreement's Enhanced Transparency Framework, consistent data collections are the prerequisite for a successful reporting of GHG emissions. For such purposes, NFIs are usually the primary source of information, even if they are frequently not designed for producing estimations on a yearly basis and in the form of wall-to-wall high-resolution maps. In this framework, we present a new spatial model to produce yearly growing stock volume (GSV), above-ground biomass (AGB), and carbon stock wall-to-wall estimates. We tested the model in Italy for the period 2005–2018, obtaining a time-series of yearly maps at 23 meters spatial resolution. Results were validated against the 2015 Italian NFI reaching an average RMSE% of 19% for aggregated areas. Results were also compared against data reported by the Italian GHG inventory, reaching an RMSE% of 28% and 20% for GSV and carbon stock respectively.

We demonstrated that the modeling approach can be successfully used for setting up a forest monitoring system to meet the interests of governments in inventories of GHG emissions and private entities in carbon offset investments.

## 1. Introduction

Under the enhanced transparency framework of the Paris Agreement, each country Party must report every two years an inventory of their anthropogenic greenhouse gases (GHGs) emissions by sources and removals by sinks following the Intergovernmental Panel on Climate Change (IPCC) guidelines and guidance (IPCC, 2006). The GHG emission inventory has to fulfill the IPCC key principles: transparency, accuracy, completeness, consistency, and comparability while providing helpful information for assessing the climate impacts. The "Land Use, Land-Use Change and Forestry" (LULUCF) is exceptionally demanding, dealing with natural carbon dynamics and aiming to assess emissions and removals related to the impact of anthropogenic activities. The LULUCF sector is responsible for significant GHG emissions globally, mainly due to deforestation activities. In this framework, forests are pivotal ecosystems, being a substantial and growing atmospheric carbon sink (Sellers et al., 2018). Forests are estimated to sequester 30% of the total global $CO_2$ released into the atmosphere annually (Houghton and <u>Nassikas</u>, 2017), corresponding to 7.6 Gt $CO_2$ $y^{-1}$, reflecting a balance between gross carbon removals and gross emissions from deforestation and other disturbances (Harris et al., 202; Xu et al., 2021). Increasing the carbon stored in the above and below-ground forest biomass is a mitigation mechanism to fight climate change and offset anthropogenic emissions worldwide (Di Cosmo et al., 2016).

Despite the UNFCCC requirements related to the provision by Parties of biennial forestry-related carbon stock change, many National Forest Inventories (NFI) are not designed for continuous yearly reports and cannot cope with the required reporting

frequency due to longer update cycles (McRoberts et al., 2018). Estimating carbon stock changes between consecutive NFIs is a pivotal step in accomplishing the reporting requirements. The methodology should be based on year-to-year measured forest variables or prediction models to extend NFI-based estimates to assessment years rather than a simple interpolation between estimates produced by NFIs at different years (Federici et al., 2008).

Even if the main source of information for such reporting activities are NFIs (Tomppo et al., 2010, Condes and McRoberts, 2017; Kulbokas et al., 2019), in recent times, considerable efforts have been laid out to integrate remotely sensed (RS) data in the process. Examples are available to provide spatially continuous (also referred to as wall-to-wall maps) and updated estimations of several forest variables such as: the growing stock volumes (GSV), the above-ground biomass (AGB) (Kangas et al., 2018; Chirici et al., 2020; Vangi et al., 2021), and the rate of forest disturbances (Hansen et al., 2013; van der Werf et al., 2017; Francini et al., 2021; Francini et al., 2022, a; Francini et al., 2022, b). Coupling traditional NFI information acquired in the field with such wall-to-wall maps based on remotely sensed data is the basis for evolving from traditional NFIs to the new so called Enhanced Forest Inventory (EFI) framework (White et al., 2016). This has already been carried out by Countries with a long history in NFIs, such as those in the Scandinavian area (Næsset et al., 2004; Nord-Larsen and Schumacher, 2012; Tomppo et al., 2008), Canada (White et al., 2016), Austria (Hollaus et al., 2009) and Switzerland (Waser et al., 2017). The EFI approach has several benefits (Chirici et al., 2020): it enables the estimation of forest attributes from a local to national scale to support local management and national planning; it can provide estimates of forest removals due to logging and other disturbances, which are essential in the context of carbon cycle assessments (Francini et al., 2021). But evolving from traditional NFIs to EFIs requires elaborating a huge amount of remotely sensed (RS) data which in turn requires investments in software and hardware resources for their processing (D'Amico et al., 2021). Conversely, field activities can be reduced by optimizing the sampling strategy by integrating RS data (Corona, 2010). For example biomass density maps constructed from remotely sensed data can be used to enhance

the stratification of ground inventories, to supply carbon stock changes estimates in poorly-sampled or unapproachable areas, or for verification purposes (ISPRA, 2021, a).

Coming more specifically to the problem of how to estimate forest carbon stock changes, there are at least three approaches reported in literature that are based on different level of data availability (Williams et al., 2012). The first one is the gain-loss method, a process-based approach, which estimates emissions and removals from changes in carbon stocks due to forest land and related land-use changes. Default data are provided in each land-use category chapter to allow the estimation of biomass carbon stock changes in case of missing country-specific data. This is the method recommended only for countries without an NFI and poor data collection.

In the second approach, forest carbon sinks are estimated by coupling estimates of forest age with age-specific carbon sequestration models. These models are derived from yield tables, expressing carbon stocks as a function of age stand.

The third approach, called the stock-change approach, requires bi-temporal biomass carbon stock measurements; therefore, its application is suitable in countries having NFI systems and other land-use categories, where stocks of different biomass pools are surveyed with a regular frequency. This method results in considerably less uncertainty (McRoberts et al., 2018; ISPRA, 2021a).

Examples of these approaches are presented by Harris et al. (2021) and Xu et al. (2021), they both integrated spatially explicit datasets and ground-measured forest inventories data to provide global estimates of temporally averaged global forest carbon emissions and removals for the 21st century, founding that woody carbon stocks increased slowly but significantly at a local and regional scale.

Saatchi et al. (2011) presented a benchmark map of biomass carbon content across the world's tropical forests for 2000 by combining ground data with airborne laser scanning (ALS), multispectral, and radar data: their map provided estimations of carbon stocks for countries where prior estimates were scarce or not complete. With the stock-change approach, Paul et al. (2021) assessed the carbon stock and changes in New Zealand using the NFI data from 2002 to 2014, showing that national forests are carbon-neutral but with wide variation in carbon stocks between different forest categories. In Russia,

Shepashenko et al. (2021) used multiple RS-based maps and NFI data to estimate $CO_2$ sequestration founding figures 47% higher than the national GHG inventory.

In Italy, Dalponte and Coomes (2016) developed an approach to map the carbon density of the Italian Alps through ALS and hyperspectral data. Nonini and Fiala (2020) developed a model to assess the forest biomass and carbon stock at stand-level with a gain-loss approach in a northern region in Italy.

Federici et al. (2008) developed a model to estimate carbon stock change data for the carbon pools to be reported under the forest land category in the LULUCF sector in the GHG inventory. The *For-est* (***For***est – ***est***imates) is a bookkeeping model that calculates the above-ground biomass pool C stock annually by adding the annual net increment and subtracting yearly losses associated with harvest (industrial roundwood and fuelwood), forest fires, and other mortality. A detailed description of the modeling approach is reported in IMELS, 2019 (section 3.3). The annual GSV is converted to AGB and then to carbon stock by species-specific parameters. The model is currently used by Italy to estimate carbon stock changes for the national GHG inventory under UNFCCC (ISPRA, 2021, b).

The aim of this study is to present the development of a spatial approach for the wall-to-wall estimation of GSV and carbon stock to fill the information gaps left by the long updating cycle of the periodic Italian NFI, under the framework for a new EFI that better fits the international reporting requirements.

To do so, we propose a new methodology to produce a yearly high-resolution (23 m) forest above-ground carbon pools and GSV maps. Our approach is initiated by a 23 m resolution wall-to-wall GSV map of 2005 constructed by combining Landsat imagery with NFI data (Vangi et al., 2021). We then applied yearly increments with species-specific growth models derived from yield tables driven by the forest GSV to estimate the annual current increment (Federici et al., 2008). We take into account removals due to forest disturbances predicted using Landsat imagery and the 3I3D forest disturbance detection algorithm (Francini et al., 2021; Francini et al., 2022, a). The approach was tuned against a set of independent field observations, and the final pixel-level estimates were aggregated at the regional level and validated against the design-based estimation

from the last Italian NFI completed in 2015, obtaining an RMSE% at a regional level of 19% and 17% for GSV and carbon stock, respectively. Our estimates were also compared with official data reported in the Italian GHG inventory.

To the best of the author's knowledge, this represents the first attempt to provide high-resolution wall-to-wall yearly time-series maps of forest growing stock volume and carbon stock in Italy. These new products allow the spatial analysis of the annual Italian forest carbon stock changes, consistently with the IPCC guidelines.

## 2. Materials

The study was carried out in Italy, covering 301,408 km$^2$ (Figure 1). Italy has a wide range of climatic conditions due to its proximity to the sea and the presence of two main mountain belts with elevations ranging between sea level up to 4000 m a.s.l. Italy has mainly a temperate Mediterranean climate (Pinna, 1970). According to the 2015 Italian NFI (INFC, 2021), forest vegetation and other wooded lands occupy 11,054,458 ha, about 36% of the national land. Deciduous species cover 68% of the forest area and are represented mainly by Quercus oak (*Q. petraea* (Matt.) Liebl., *Q. pubescens* Willd., *Q. robur* L., *Q. cerris* L.), and European beech (*Fagus sylvatica* L.). Coniferous species, such as Norway spruce (*Picea abies* (L.) H.Karst.) and pines (*Pinus sylvestris* L., *P. nigra* J.F.Arnold, *P. pinae* L., *P. pinaster* Aiton), form vast plantations, especially in the northern regions and coastal areas (Figure 1).

Italy is divided into 20 administrative regions (NUTS2); the NFI produces every ten years regional estimates for several variables including forest area, total and average GSV, and biomass with the relative associated standard errors (SE) with a traditional design-based approach. According to NFIs, at the country level, the average GSV was 121 m$^3$ ha$^{-1}$ and 135 m$^3$ ha$^{-1}$ in 2005 and 2015, respectively.
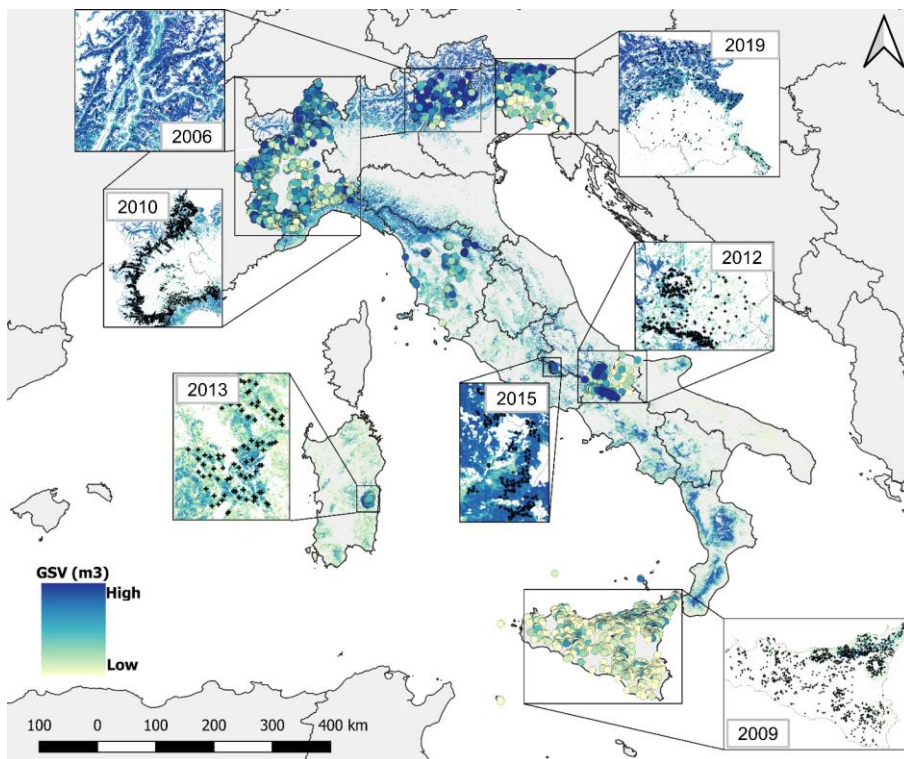
Figure 1. The study area (the whole of Italy) with the location of the independent plots was used for optimizing and validating the model.

In this area, poplar plantations are intensively managed and primarily targeted to plywood production, with rotations usually about 10-12 years and tree spacing between 36 m$^2$ (6 x 6 m) and 49 m$^2$ (7 x 7 m) (Corona et al., 2018b, Puletti et al., 2019). In about three-fourth of the poplar plantations, the 'I-214' (*Populus × euroamericana*) hybrid clone is used (Chianucci et al. 2020a, 2020b).

## 2.2. Growing stock volume baseline map

For the assessment of forest GSV and above-ground carbon stock in the years following the last NFI, we used the 2005 GSV map produced by Vangi et al. (2021) for Italy as the initial GSV baseline data (GSV$_{2005}$). This map consists of GSV predictions by Landsat and other RS imagery at 23x23 m resolution for all forest pixels. The full description of the methodology is available from Chirici et al. (2020). The model fitting and tuning steps were carried out using the *randomForest* package in the statistical

software R 4.0.5 (Liaw and Wiener, 2002) (https://www.r-project.org, accessed on: June 16th, 2021). The pixel-level estimations of the GSV range between 0 and 690 $m^3ha^{-1}$ with a mean value of 134 $m^3ha^{-1}$ and a standard deviation of 41.5 $m^3ha^{-1}$ (for comparison the official NFI estimates range between 0 and 950 with a mean value of 145 and a standard deviation of 69 $m^3ha^{-1}$). Using a model-assisted estimation approach (Corona, 2010), the 2005 growing stock volume map led to a standard error of 1.2% and 1% for the mean and total national GSV estimation, respectively (Vangi et al., 2021).

## 2.3. Forest category maps

In Italy, a forest category map with a spatial resolution consistent with the input GSV map used in this study is not yet available. For this reason, the distribution of forest categories was derived from the Corine Land Cover (CLC) maps, which are available for the reference years 2006, 2012, and 2018. In Italy, CLC is the only spatial source that provides consistent information on forest category distribution across different years on a national scale. The CLC project was started in 1990 by the European Environmental Agency (Buttner et al., 2004) and consists of a European-scale land-use monitoring program with a 44-class nomenclature system produced by photointerpretation of high-resolution satellite imagery. CLC uses a minimum mapping unit (MMU) of 25 hectares and a minimum mapping width (MMW) of 100 meters (EEA, 2007). The original CLC nomenclature system classifies the forest into three classes: broadleaves, coniferous, and mixed forests. In the Italian implementation the CLC maps produced by the *Istituto Superiore per la Protezione e la Ricerca Ambientale* (ISPRA) classify forests into 28 classes (Bologna et al., 2004). In this study, we re-classified forests into 18 classes (Annex I). Forest category maps were obtained from the original CLC vector products by rasterizing at the same spatial resolution as the baseline GSV map. Then we masked out the non-forest categories by assigning them to the "non-forest" class.

Our spatial approach requires for each year a newly updated forest category map. Since the CLC project is not updated yearly, we used the forest category map of 2006 for the years 2005-2009, that of 2012 for 2010-2014, and that of 2018 for 2015-2018 (Figure

2). This procedure was considered appropriate since the percentual change of forest area based on the CLC maps is limited. In the period 2006-2012, considering both increments and decrements, the forest area changed only by 741 km$^2$ (the 0.74 % of the forest area) while in the period 2012-2018, it changed only by 705 km$^2$ (the 0.70% of the forest area).
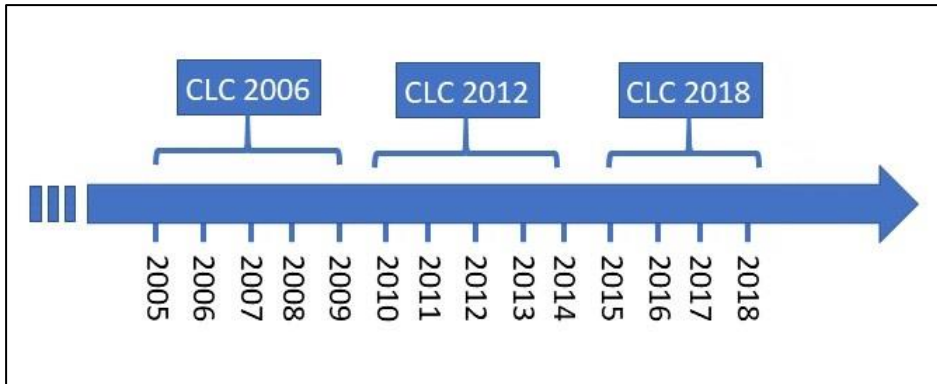


Figure 2. Corine Land Cover (CLC) forest category maps used for each year of the study period.

## 2.4. National collection of yield tables

The national collection of yield tables from Federici et al. (2001) was used to model the current increment of forests as a function of GSV and the GSV as a function of forest age. Yield tables reported the GSV and current increment as a function of forest age for 27 species within 13 genera. The 27 species were linked to the 18 forest categories derived from CLC (see section 2.3), with *ad-hoc* harmonization bridges developed for this study. Bridges preserve data attributes based on different definitions, allowing their comparison at a higher hierarchical level (Annex I).

## 2.5. Forest disturbances time series maps

Data on the spatial distribution of forest disturbances in the period 2004-2018 were needed to account for forest harvesting and other disturbances in GSV and the carbon stock estimation process. These data were produced with the 3I3D algorithm (Francini et al., 2021) recently implemented in Google Earth Engine (GEE) (Francini et al., 2022,

a), a cloud-based platform that can process massive amounts of remotely sensed data (Gorelick et al., 2017).

3I3D is an unsupervised algorithm that predicts forest disturbances requiring no input parameters or calibration. It analyses the pattern over three sequential years of three indexes (3I) of photosynthetic activity used as three-dimensional (3D) space axes. 3I3D was applied using yearly cloud-free composites of Landsat surface reflectance images atmospherically corrected with LEDAPS (Wolfe et al., 2004) and acquired with a solar zenith angle smaller than 76°. Candidate images were acquired during the vegetative season (between Jun and Aug), with a cloud cover lower than 50% in the scene. As a result, we obtained a collection of about 800 images per year. We excluded those pixels covered by clouds, shadows, water, and snow (Foga et al., 2017) and pixels with an opacity value greater than 0.3. For each year, we then selected the "best" pixels among the remaining ones using the Best Available Pixel procedure (BAP) (Griffiths et al., 2013; White et al., 2014), obtaining a BAP-collection of cloud-free composite for each year between 2004 and 2018. Specifically, the BAP pixel selection is based on a set of scores, among which i) the sensor, ii) the day of the year, iii) the distance to cloud or cloud shadows, and iv) the opacity. The BAP was recently implemented in GEE, with the full code openly available. A detailed description of the application, guidance, and suggestions on BAP parameters setting is provided on GitHub (https://code.earthengine.google.com/?accept_repo=users/sfrancini/bap).

We used BAP cloud-free composites as input for the 3I3D algorithm to predict forest disturbances with a MMU of 500 m$^2$ over the study period. Official forest data on burned areas, annually produced and released for the same period by the Italian Forest Service (Comando Unità Forestali, Ambientali e Agroalimentari of Carabinieri), have been also used. This dataset includes burnt areas from forest fires acquired through a ground survey with the Global Navigation Satellite System (GNSS).

We merged the official national database of forest fires with the forest disturbances map produced by 3I3D (with an OR logical operator), classifying forest pixels for each investigated year in "disturbed" or "undisturbed". Based on these maps, we finally produced the "age" of disturbed forests for each investigated year as the number of years since the last disturbance event (YSLD).

### 2.6. Calibration data

To optimize and calibrate the procedure, we used 9258 circular plots where the GSV was measured in the field between 2006 and 2019 in the framework of local forest inventories (Figure 1). The plots are distributed under different environmental conditions and forest categories over the whole country. The same survey protocol of the Italian NFI was adopted in all these plots. The tree-level GSV was determined by the allometric models used for the Italian NFI (Tabacchi et al., 2011), and then tree-level data were aggregated at the plot level. For this study, allometric model prediction and GNSS position uncertainties are expected to be negligible for the spatial resolution adopted (McRoberts et al., 2013, 2016, 2018; Chirici et al., 2020). The mean GSV in this calibration dataset is 216 $m^3$ $ha^{-1}$, with a maximum of 1482.4 and a standard deviation of 155 $m^3$ $ha^{-1}$. To find the most appropriate solution, we evaluated the models in terms of RMSE% at the plot level, comparing GSV estimates with the observed one.

### 2.7. Validation data

To validate the results, we compared aggregated regional GSV and carbon stock estimates for 2015 based on the pixel level values we produced (the $GSV_{2015}$ 23 m resolution map) with official regional estimates from the Italian NFI. We also compared aggregated values of GSV and carbon stock produced by our method with the official estimates reported in the Italian 2006-2019 GHG inventory. Just as in the calibration, we compared the accuracy of our results in terms of RMSE%, calculated as the percent of RMSE against the mean official values.

## 3. Methods

### 3.1. Overview of the spatial approach

For the years not covered by the periodic Italian NFI, our spatial approach for predicting GSV and carbon stocks was carried out differently for pixels belonging to disturbed and undisturbed forests. Annual stock changes were predicted for each

23 m pixel, using the GSV$_{2005}$ mapped for 2005 and the YSLD as unique drivers. The GSV$_{2005}$ was selected since it is strictly related to the above-ground biomass and carbon stock, and it is directly measured by the NFI in the field. While the YSLD was selected because it can be easily obtained based on change detection algorithms, such as the 3I3D, and it is the primary driver of forest variables in yield tables.

Our approach uses the first derivative of the Richards function (Eq. 1) to calculate the current increment (Eq. 2) as a function of the GSV in undisturbed forests for each of the 18 CLC forest categories (Federici et al. 2008). The following equation defines the Richards function:

$$\frac{dy}{dt} = \frac{k}{v} \cdot y \left[ 1 - \left( \frac{y}{a} \right)^v \right] + y_0 \quad \textit{first derivative} \qquad (1)$$

its analytical solution defines the Richards growth curve:

$$y = a \cdot \left[ 1 - e^{(\beta - kt)} \right]^{-\frac{1}{v}} \qquad (2)$$

Where the general constraints for the parameters are a, k > 0; $-1 \leq \beta \leq \infty$; $v \neq 0$.

The curve is bounded and monotonic, highly flexible thanks to its four parameters. It can be efficiently approximated to a logistic (a→∞, v>0), exponential (v>1), or other most used growth curves. However, due to the number of parameters and their high covariance, the curve is difficult to fit and can cause problems during the non-linear regression (Federici et al., 2008). The current increment represents the dependent variable, while the independent variable is the GSV map.

In disturbed forest areas, different potential models were evaluated for estimating GSV as a function of YSLD for each forest category. Using the data in the yield tables collection, we tested four regression models, two non-parametric, random forests and Support Vector Machine (SVM), and two parametric, polynomial, and linear regression. The GSV represents the dependent variable, while the independent variable is the forest age from yield tables.

The optimization was fine-tuned by picking the most accurate model based on the correlation coefficient ($r^2$). All four regression models yielded comparable results with

only slight differences. The SVM model slightly outperformed other approaches, with an average $r^2$ among the forest categories of 0.91, against 0.90 of random forests and 0.88 of polynomial and linear regression.

After the model fitting for each category in undisturbed and disturbed forest areas, the above-ground carbon stock is predicted in the five steps described below:

1.  Starting from the initial $GSV_{2005}$ map, the current increment is estimated via the Richards function in undisturbed forest areas for each year and for each forest category, based on the relationships between GSV and current increment derived from yield tables.

2.  Similar to point 1, GSV in disturbed forest areas is estimated for each year, and forest category with the corresponding SVM model, based on the relationships between YSLD and GSV derived from the yield tables.

3.  For each year and forest category, the GSV is calculated as the sum of the previous year's GSV and the estimated current increment, subtracting the losses due to natural mortality and adding the GSV in disturbed forest areas calculated in step 2.

4.  For each year and forest category, the GSV ($m^3$ $ha^{-1}$) is converted in above-ground biomass (AGB) (Mg d.m. $ha^{-1}$) with the equation:

$$AGB = GSV * BEF * WBD \qquad\qquad (3)$$

Where GSV is the growing stock volume calculated in step 3, BEF is the category-specific biomass expansion factor (dimensionless), and WBD is the wood basal density (Mg d.m. $m^{-3}$).

5.  Carbon stocks are derived from AGB by applying the default carbon fraction factor of 0.47 (IPCC, 2006).

Following the IPCC Good Practice Guidance for LULUCF (IPCC, 2003), the average rate of natural mortality was set equal to 0.116% for evergreen categories, 0.117% for deciduous categories, and 0.1165% for mixed categories, while BEF and WBD are those applied by the *For-est* model (Federici et al., 2008).

The detailed methodology is described here below.

### 3.2. GSV estimation in undisturbed forests

In undisturbed forests, the GSV for the year $n$ was computed at pixel level by adding the current increment of the year $n$-$1$ to the GSV of the year $n$-$1$ and subtracting losses due to natural mortality. We used an age-independent model to create annual maps of the current increment. Category-specific growth models were constructed using the data of the national yield tables collection to calculate the current increment ($m^3$ $ha^{-1}$ $y^{-1}$) as a function of GSV ($m^3$ $ha^{-1}$), using the first derivative of the Richards function (eq. 1). The GSV represents the independent variable $x$, while the dependent variable $y$ is the correspondent current increment. The forest category-specific Richards functions were fitted using all the fertility classes of the yield tables. The parameterization was based on a 25 iterations-bootstrap-cross-validation procedure. For each bootstrap iteration and species, the RMSE was calculated, and the model which reported the lowest RMSE was chosen as the final model,. RMSE was calculated as:

$$RMSE_{sp} = \sqrt{\frac{\sum_{i=1}^{n}(y_i - \hat{y_i})^2}{n}} \qquad (4)$$

where $n$ is the number of observations in the yield tables for the species $sp$, $y_i$ is the current increment value reported in the yields table for the i-th observation and $\hat{y_i}$ is the current increment predicted from the model for the i-th observation.

We started the process based on the $GSV_{2005}$ map produced by Vangi et al. (2021), and we produced the updated $GSV_{2006}$ map applying, for each 23 x 23 m undisturbed forest pixel, the current increment per hectare predicted for each forest category with the corresponding growth curves and subtracting the natural mortality. Then, the process was repeated for 2007 based on $GSV_{2006}$ and so on until 2018.

By applying the Richard first derivative approach, the current increment was estimated with an average RMSE (as per eq. 4) of 49.4% across all forest categories, with significant variations among forest categories, mainly due to the number of observations and fertility classes available in the yield tables. Some of the most

frequent forest categories in Italy obtained the best results, such as the maple-ash-hornbeam mixed forests (RMSE = 22%), the Mediterranean maquis (RMSE = 13%), and the chestnut forests (RMSE = 26%), which altogether represent more than 25% of the national forest area.

The best results were obtained by the exotic plantations category with an RMSE of 3.2%, most probably because of their homogeneous growth behaviour. In comparison, the mixed conifers category obtained the worst result with an RMSE of 95% (but they cover only 4.4 % of the forest area), most probably because of their heterogeneous composition.

### 3.3. GSV estimation in disturbed forests

We already know that forest age is not an appropriate predictor for estimating the productivity of undisturbed forests in Italy since they are mainly uneven-aged and are characterized by a complex mosaic of different ages or cohorts (Federici et al., 2008; Frate et al., 2015). Instead, in most disturbed forests, trees regrowing after the disturbance results in even-aged stands, at least for the first years after the disturbance. This is particularly true for clearcuts in coppice forest (Chirici et al., 2020), which represent the most common forest disturbance in Italy, based on Francini et al. (2022, a), representing 80% of all forest loggings in Italy. In such a situation, forest age can be used to predict GSV growth in disturbed stands using the data in the national yields table collection. We used forest categories-specific SVM models to predict the GSV based on forest age with a radial basis kernel function. SVM approaches are known to be robust against outliers and overfitting and are well-suited for approaching problems with a limited amount of training data. These algorithms can generate non-linear decision surfaces by mapping the data into a high-dimensional space through non-linear mapping functions called kernel functions (Cortes and Vapnik, 1995; Pal and Mather, 2003), allowing the separation of the data through linear hyperplanes (Dixon and Candade, 2008). Among the kernel functions, one of the most used is the radial basis function, which has two tuning parameters C (regularization parameter) and ɣ (kernel width) (Kavzoglu and Colkesen, 2009). An in-depth explanation of SVM-based models and kernels is presented in Smola and Schölkopf (2004) and Kavzoglu and Colkesen

(2009). Implementations of SVM models in RS can be found in Mountrakis et al. (2011). In this study, the parameters of SVM and radial kernel (C, ɣ) were determined by bootstrap cross-validation with 25 iterations using the grid search method, by selecting the pairs of parameters that produce the lowest cross-validation RMSE among an exponentially growing sequence of the parameters (C=21/2, 21, …, 25; ɣ=2-5, 2-4, …, 20). For each bootstrap iteration and species, the RMSE was calculated as per eq. 4, and the model which obtained the lowest RMSE was chosen as the final model.

In disturbed areas identified by the 3I3D algorithm, the GSV was computed for each year and forest category by applying the category-specific SVM models fitted from the yield tables data. The YSLD for the year n was used as the independent variable to predict the GSVn in each disturbed pixel, obtaining a GSV map of forest disturbances for each year between 2005 and 2018.

The complete GSVn map was produced by overlaying the GSVn maps of disturbed and undisturbed forests.

The SVM models led to an average RMSE of 35.9%, with a maximum of 64% for the mixed forests with the prevalence of coniferous and a minimum of 5% for the maple-ash-hornbeam mixed forest. As for the Richard models, we observed significant variations depending on the number of fertility classes in yield tables.

### 3.4. Carbon stock conversion

Once estimated the GSV, amounts of AGB are consequently assessed. For every forest typology, starting from the GSV, the AGB (Mg d.m. ha$^{-1}$) is calculated, through equation (3), following the approach presented in Federici et al. (2008).

Carbon stock maps were derived from AGB maps by applying the default factor for carbon fractions of 0.47 (IPCC, 2006).

The pixel-level predictions of GSV and stocked carbon were aggregated at the regional level for each year.

## 4. Results

### 4.1. GSV and carbon stock estimation

The spatial approach for estimating annual GSV and above-ground carbon pool was applied to produce 23 m resolution yearly pixel-level estimates from 2005 – 2018. Based on our results, the GSV increased in Italy by 522 million $m^3$ moving from an average of 130 $m^3\,ha^{-1}$ to 180 $m^3\,ha^{-1}$. GSV and above-ground carbon stocks time series are reported in Annex II. Carbon stock increased by 206 million of t in the same period, moving from 36.9 Mg C $ha^{-1}$ to 59.3 Mg C $ha^{-1}$, with an average accumulation rate of 14.7 mln Mg C $y^{-1}$. Regionally, most of the GSV and carbon gains dominate mountain landscapes of the Alps and Apennines mountains. In the years 2005-2018, among all forest categories, beech forests accumulated the most GSV, with about 3926 mln of $m^3$ corresponding to 54 mln Mg C of above-ground carbon stored (about 28.3 % of the total carbon absorbed by national forests), followed by mixed broadleaf forests (34 mln Mg C, about 18 % of the total) and the fir/spruce forests (23 mln Mg C, 12% of the total). Regardless of the forest category, in the study period, carbon accumulation is reflected mainly in the increase of the carbon density rather than the increase of the total forest area, which amounts to 145,000 ha according to the CLC maps.

Northern regions (Trentino-Alto Adige, Piemonte, Lombardia, Veneto, Friuli Venezia Giulia) have the highest GSV accumulation in terms of absolute and per hectare figures, accounting for 54% of the national total. Other regions with significant GSV accumulation are Toscana, Sardegna, and Emilia-Romagna, contributing 20% to the national GSV growth (each up to 20 mln $m^3$ in the study period). In contrast, most southern regions (Molise, Campania, Puglia, Basilicata, Sicilia) show the least accumulation of GSV, less than 8 mln $m^3$ between 2005 and 2018. Carbon uptake has similar patterns, exhibiting higher absolute and per hectare storage in many northern regions (Trentino-Alto Adige, Piemonte, Lombardia, Veneto) and lower in the southern ones (Molise, Puglia, Umbria) (Figure 4). Also, at the regional level, the accumulation of GSV and carbon stock is primarily driven by the increase of GSV and carbon density rather than the total forest area. This is probably due to a decrease in the harvested area

over the last two decades, which allowed for significant growth in GSV per unit area (Francini et al., 2022, b).

In figure 3 is reported the overall absolute accumulation of GSV and carbon stock at the regional level over the study period.
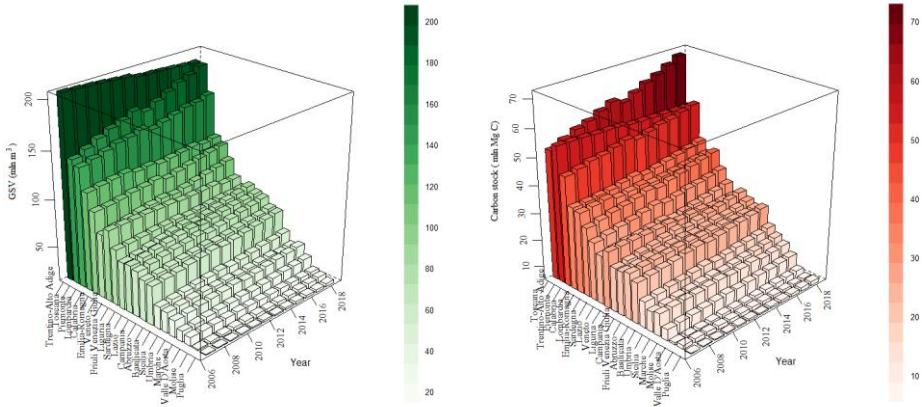


Figure 3. Annual GSV (left) and carbon stock (right) at the regional level from 2005-2018.
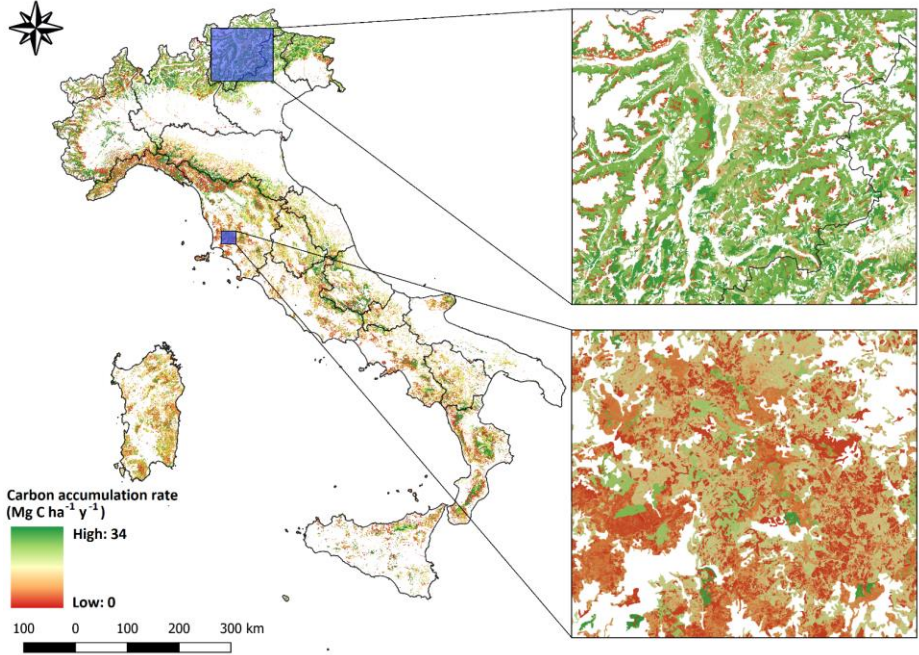


Figure 4. Left: Pixel-level carbon accumulation rate in forests (Mg C ha$^{-1}$ y$^{-1}$) for 2005-2018.

## 4.2. Validation and comparison of results

During the optimization phase the 23 m resolution pixel level estimations of GSV estimates obtained applying the best configuration of our models where compared against the GSV measured in the field in 9258 independent plots acquired in different years in the period 2006-2018. From such comparison the average RMSE% was 57% ranging between 89.6% in 2009 and 34% in 2015, (Figure 5). The bias across years was -3.7 $m^3$ $ha^{-1}$, with the minimum in 2010 (-0.2 $m^3$ $ha^{-1}$) and the maximum in 2013 and 2015 (-70.3 and -60.2 $m^3$ $ha^{-1}$). These values are in the range of previous experiences (Immitzer et al., 2016; Chirici et al., 2020; Vangi et al., 2021).
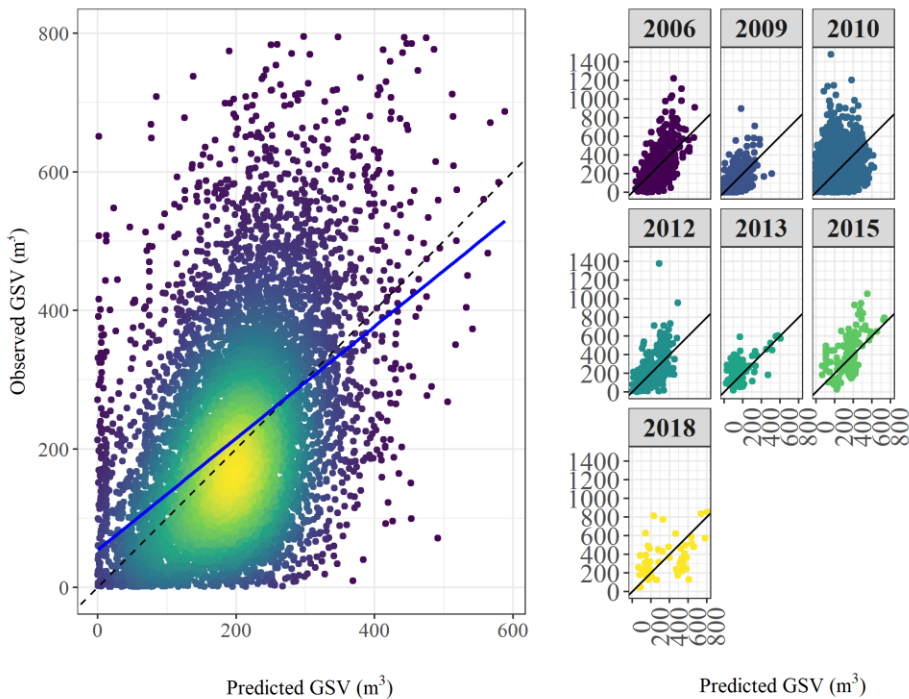


Figure 5. Left: observed GSV in the field plot against predicted GSV; Right: observed against predicted GSV for each year. Blue is the regression line.

Pixel level estimations for the year 2015 where aggregated for administrative Regions and compared with the official 2015 NFI estimates (INFC 2015), resulting in a 6.2 % and 1.1% difference at the national level for GSV and carbon stock, respectively (calculated as the mean value of the difference between predicted and observed results).

We obtained an RMSE of 19.5% and 17.8% at the regional level and an $r^2$ of 0.94 and 0.92 for GSV and carbon stock, respectively (Figure 6). RMSE was calculated as:

$$RMSE_{NFI} = \sqrt{\frac{\sum_{i=1}^{n}(y_{NFI_i}-\hat{y}_i)^2}{n_{rg}}} \qquad (5)$$

where $n_{rg}$ is the number of Italian regions, $y_{NFI_i}$ is the official NFI value (of GSV and carbon stock) for the $i$-th region and $\hat{y}_i$ is the aggregated estimation (of GSV and carbon stock) produced by the spatial approach for the $i$-th region.

The data for the comparison against the 3rd Italian NFI (INFC 2015) are presented in Annex III.
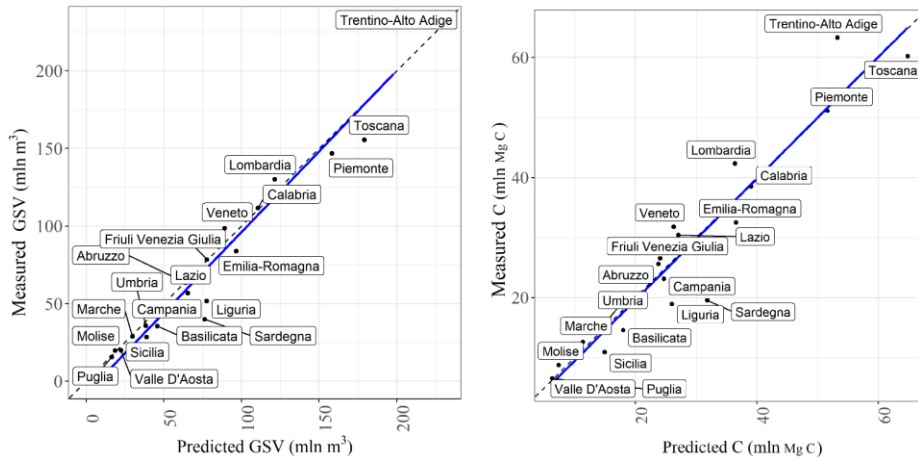


Figure 6. Left: INFC 2015 GSV against predicted GSV; Right: INFC 2015 carbon stock against predicted carbon stock. The dotted line is the y=x line, and the blue is the regression line.

Finally, following the same procedure, our GSV predictions aggregated for Italian Regions were compared with official estimates of Italian GHG inventories for 2005-2018, obtaining an overall RMSE% of 28.6% and an $r^2$ of 0.77 with a growing trend over time. Here the RMSE was calculated as:

$$RMSE_{GHG} = \sqrt{\frac{\sum_{i=1}^{n}(y_{GHG_i}-\hat{y}_i)^2}{n_{rg}}} \qquad (6)$$

where $n_{rg}$ is the number of Italian regions, $y_{GHG_i}$ is the official GHG inventoriy value (of GSV and carbon stock) for the $i$-th region and $\hat{y}_i$ is the aggregated estimation (of GSV and carbon stock) produced by the spatial approach for the $i$-th region.

The carbon stock was also compared against the official Italian GHG inventory (LULUCF sector, forest land remaining forest land category) for the same period (ISPRA, 2021, b), yielding an $r^2$ of 0.88 and an overall RMSE% (as per equation 6) of 23.1% and 17.2% among years and regions, respectively. As for the GSV, consistency with official estimates has worsened over the years, while at the regional level reached the minimum in Piemonte (RMSE 2.5%) and the maximum in Trentino-Alto Adige (RMSE 48.6%). Thirteen out of 20 regions showed an RMSE% less than 15%, with seven regions less than 10%. Figure 7 reports the regional comparison between our results and the official estimates from the national GHG inventory (ISPRA, 2021, b) regarding GSV and carbon stock.
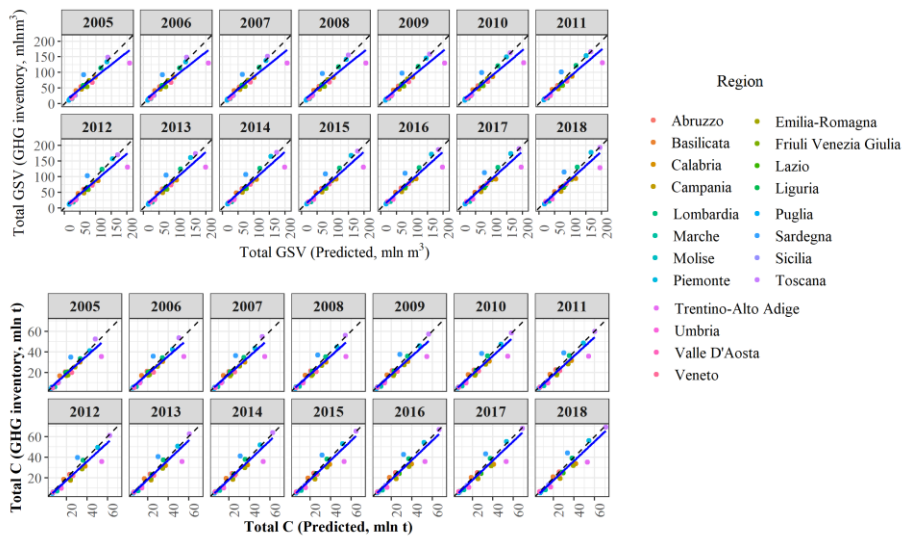


Figure 7. Comparison of GSV (right) and carbon stock (left) at the regional level against the Italian GHG inventory LULUCF sector, forest land remaining forest land category) for each year of the study period.

## 4. Discussion

The main objective of the study was to develop a new spatial approach for producing wall-to-wall high-resolution yearly GSV and carbon stock predictions between consecutive NFI field measurements, exploiting remotely sensed and auxiliary data, which could be used for operational application and to respond to international reporting tasks. Empirical models developed by interpolating data from NFI field plots could produce updated estimates only for short-term predictions, for which growth conditions such as climate and management regimes are expected to be stable (Peng, 2000). Moreover, in such models, stand variables are driven by the age of the forest, but in natural conditions, growth is strictly related to species and local environmental conditions. For these reasons, our novel approach for estimating carbon stocks and changes at the national and regional level in the above-ground carbon pool is driven only by NFI GSV data and yield models.

The yearly wall-to-wall maps of GSV and carbon stock can support reporting activities and forest management at any scale by aggregating pixel-level predictions producing small-area estimations, for example, using the estimators proposed by Chirici et al. (2020).

Our results agreed with those reported by the official Italian GHG inventory and show an increasing trend in the above-ground carbon pool that reflects both the expansion of forest areas (according to NFI, in the period 2005-2015, forest areas increased by 58,692 ha y$^{-1}$, approximatively 0.5% of total forest area in 2015) and the increased growing stock resulting from a forest harvest rate lower than the current increment. The organic carbon in the above-ground biomass of the Italian forest exceeded 566 million Mg C in 2018, with a different contribution of regions and forest categories in terms of fixed organic carbon. GSV and carbon stock distribution among forest categories comply with the 2020 Italian FAO FRA report for 2005 and 2010, with beech and spruce/fir forests accounting for 40% and 36% of the total GSV and carbon stock, respectively. Due to their limited area nationwide, the forest categories contributing the least to carbon storage (less than 0.5% of the total) are exotic conifers, broadleaf plantations, wood arboriculture, and riparian formations. It is worth noting that other

wooded vegetation in open and shrublands has a relatively significant contribution to terrestrial carbon sinks, storing more than seven mln of Mg C of carbon (approximately 5% of the national total).

Large forest areas characterize regions with the most GSV and carbon stock and highly carbon-storing forest categories (beech, mixed broadleaf, fir/spruce, larch, Mediterranean pines, exotic plantations), despite most of these categories are subject to intense forest harvesting, as resulted from 3I3D disturbances maps. In this regard, it is worth noting that the major disagreement between our approach and the official ISPRA estimates is found in the northern regions and particularly in Trentino-Alto Adige, which leads to the maximum relative RMSE (for which the GHG inventories estimate a decrease in GSV and carbon stock over the study period). This mismatch is primarily due to underestimating the number of forest disturbances, especially in high-forest stands of the main mountain ranges, where silvicultural treatments are based on continuous canopy cover approaches that are difficult to detect by optical satellite imagery. The lack of fire data compounds the underestimation of disturbances before 2007 and after 2017.

Moreover, for the Autonomous Provinces of Trento and Bolzano, the database of forest fires includes only fires greater than 20 ha, potentially increasing the underestimation of the total number of disturbances. Without offsetting for forest harvests and forest fires, the GSV builds up rapidly, driven by the increase of the current increment of highly productive forest categories, leading to significant overestimates and large values of RMSE. However, in Trentino-Alto Adige, the mismatch between our results and the 2015 NFI is less evident, with an underestimation of only 13% and 15% for GSV and carbon stock, respectively.

Another source of uncertainty is the overestimation of the current increment with the Richard first derivative compared to the 2nd NFI field measurement. This finding contrasts with the underestimation reported by Federici et al. (2008) compared to the 1st NFI data. The discrepancy between the predicted and reported current increment of NFI is likely driven by three factors: i) an outdated collection of national yield tables which no longer reflect the country's real average quality of forest sites; ii) Richard's first derivatives were fitted against all species quality class data in yield tables, and since

species data were aggregated to match the species composition of each forest category as closely as possible, the predicted current increment of less productive species can be overestimated, especially for mixed forest categories; iii) the overestimation of the GSV in the initial 2005 GSV map, used as the independent variable for Richards functions. This evidence was reported by Vangi et al. (2021). SVM models generally performed better than the Richards function for the same forest categories, except for chestnut, hygrophilous formations, exotic broadleaf plantations, larch, and stone pine categories. For those forest categories, the SVM model underestimates GSV for older age classes, for instance, over ten years for exotic broadleaf plantations and riparian formations, 25 years for chestnut, and more than 80 years for the remaining forest categories. Hence, the effect of underestimation only affects categories of hygrophilous formations and non-native species plantations, as the years since the last disturbance can be at most equal to 13 years (2018-2005).

During the optimization phase using the dataset of independent field plots the differences between pixel-level measured and estimated GSV increased over time. This bias with under-predictions for plots with high values of GSV, especially for years 2009, 2012, and 2015, can be caused by the well-known saturation effect, especially in dense crown cover and steep terrain (Nilsson et al., 2017; Giannetti et al., 2018; Chirici et al., 2020). Such dataset was acquired for those years in forests managed for productive purposes or, more in general, with an average GSV much greater (420 m$^3$ ha$^{-1}$) than those measured in INFC plots (140 m$^3$ ha$^{-1}$). In this phase the largest bias was observed in southern regions and in the islands, that are characterized by sparse Mediterranean vegetation where modelling the GSV resulted more difficult in previous experiences too (D'Amico et al., 2021; Vangi et al., 2021). But it is important to note that wall-to-wall spatial predictions from NFI field observations should never be used at the pixel level since the single pixel predictions may be affected by a consistent bias (McRoberts and Tomppo, 2007).

However, when we aggregated the pixel level estimations at the regional level, we obtained very satisfying results consistent both with the Italian GHG inventory and the 3rd NFI (INFC, 2021). It is worth noting that, concerning the 3rd NFI in 2015, the carbon stock difference at the regional level was minor than the GSV difference (Fig. 7). This

is interesting because it proves that the species-specific BEF and WBD together with the spatial distribution of forest categories can compensate for the overestimation of GSV. Under this point of view, our estimates are conservative since the approach neither overestimates increases nor underestimates decreases in carbon stocks with respect to the NFI official estimations.

As soon as new high-resolution forest types maps will be available, the use of the CLC maps should be reconsidered. Several studies have already highlighted the limitations of CLC maps in forestry, primarily because of the wide MMU of 25 ha (Seebach et al., 2011; Vizzarri et al., 2015; Vangi et al., 2021).

## 5. Conclusion

To the best of our knowledge, this is the first study to provide yearly high-resolution GSV, AGB, and carbon stock wall-to-wall time-series maps for the whole national territory in Italy, allowing an in-depth analysis of the forest carbon stock changes, consistently with the IPCC guidelines. The spatial nature of our results enables small-scale estimates by aggregating individual pixel predictions, enhancing the spatial resolution of traditional NFI design-based estimates (Chirici et al., 2020), and can be embedded into decision support systems to support sustainable forest management and precision forestry activities. Furthermore, the knowledge of the spatial distribution of carbon among forest categories can be of fundamental importance under the climate mitigation goals of the Paris Agreement (UNFCC, 2015).

The growing need for new information and technological advances is driving the rapid evolution of forest monitoring and assessment. However, the exploitation of the latter and their implementation within international reporting processes should be evidence-based (Corona, 2018).

This study provides an innovative spatial framework to track GSV and carbon stock changes between NFI surveys at local to national scales, providing a reliable monitoring approach to meet the increasing interests of non-government and private entities in carbon offset investments. Our new method incorporates forest disturbance between surveys, such as forest fires and harvesting, thanks to Landsat-based

time-series metrics exploited by the 3I3D unsupervised change detection algorithm, which has already proved to be a better solution in the Mediterranean environment than previous algorithms (Francini et al., 2021). The 3I3D algorithm here demonstrated to be a valid solution for deriving forest age to track the GSV regrowth after disturbances by applying age-dependent relationships in yield tables.

The approach could be improved with 2015 NFI data, as well as updated information on allometric models and yield tables, allowing better model calibration and quality assurance routines. It is worth remembering that although GHG inventories are not measured on the ground, they represent official data sources used for national and international reporting activities.

Nevertheless, the availability of ground-based carbon content data to calibrate and validate the method is desirable. For this reason, as soon as they will be available 2015 NFI carbon stock ground data will allow the evaluation of the pixel-level performance for the carbon stock map for 2015, providing insight into the method's effectiveness. The availability of an official high-resolution national forest map and wall-to-wall multitemporal ALS data could also be fundamental for improving the quality of GSV and carbon stock spatial estimations.

## Funding

## 6. Reference

Bologna, S., Chirici, G., Corona, P., Marchetti, M., Pugliese, A., Munafò, M., 2004. Sviluppo e implementazione del IV livello Corine Land Cover per i territori boscati e ambienti semi-naturali in Italia. Paper presented at the annual meeting for the Society of ASITA. Pp. 467–472

Barbati, A., Marchetti, M., Chirici, G., Corona, P., 2014. European Forest Types and Forest Europe SFM indicators: tools for monitoring progress on forest biodiversity conservation. Forest Ecology and Management. 321, 145‑157. https://doi.org/10.1016/j.foreco.2013. 07.004.

Büttner, G.; Feranec, J.; Jaffrain, G.; Mari, L.; Maucha, G.; Soukup, T. The corine land cover 2000 project. EARSeL eProceedings 3, 3/2004 331. 2004. Available online:http://citeseerx.ist.psu.edu/viewdoc/download?doi=10.1.1.618.9940&rep=rep1&type=pdf

Chang, C.-C., and Lin, C.-J. 2011. LIBSVM: a library for support vector machines. ACM Transactions on Intelligent Systems and Technology, 2(3):27:1–27:27. Software available at http://www.csie.ntu.edu.tw/~cjlin/libsvm

Chirici G., Giannetti F., McRoberts R.E., Travaglini D., Pecchi, M., Maselli F., Chiesi M., Corona P. 2020. Wall-to-wall spatial prediction of growing stock volume based on Italian National Forest Inventory plots and remotely sensed data. International Journal of Applied Earth Observation and Geoinformation 84, 101959. https://doi.org/10.1016/J.JAG.2019.101959

Corona P., 2010. Integration of forest mapping and inventory to support forest management. iForest – Biogeosciences and Forestry 3, 59-64. DOI: 10.3832/ifor0531-003

Corona P., 2018. Communicating facts, findings and thinking to support evidence-based strategies and decisions. Annals of Silvicultural Research 42, 1-2. DOI: 10.12899/ASR-1617

Condés, S.and McRoberts, R.E., 2017. Updating national forest inventory estimates of growing stock volume using hybrid inference. Forest Ecology and Management 400, 48‑57. https://doi.org/10.1016/j.foreco.2017.04.046

Cortes, C., Vapnik, V., 1995. Support-vector networks. Machine Learning 20 (3), 273–297.

Dalponte, M., & Coomes, D. A. (2016). Tree-centric mapping of forest carbon density from airborne laser scanning and hyperspectral data. Methods in ecology and evolution, 7(10), 1236-1245. https://doi.org/10.1111/2041-210X.12575

D'Amico G., Vangi E., Francini S., Giannetti F., Nicolaci A., Travaglini D., Massai L., Giambastiani Y., Terranova C., Chirici G. 2021. Are we ready for a National Forest Information System? State of the art of forest maps and airborne laser scanning data availability in Italy. iForest 14: 144-154. – doi: 10.3832/ifor3648-014

Di Cosmo L., Gasparini P., Tabacchi G. 2016. A national-scale, stand-level model to predict total above-ground tree biomass from growing stock volume. Forest Ecology and Management, Volume 361, Pages 269-276, ISSN 0378-1127, https://doi.org/10.1016/j.foreco.2015.11.008.

Dixon, B., Candade, N., 2008. Multispectral landuse classification using neural networks and support vector machines: one or the other, or both? International Journal of Remote Sensing 29 (4), 1185–1206. https://doi.org/10.1080/01431160701294661

Foga, S., Scaramuzza, P.L., Guo, S., Zhu, Z., Dilley, R.D., Beckmann, T., Schmidt, G.L., Dwyer, J.L., Hughes, M.J., Laue, B. 2017. Cloud detection algorithm comparison and validation for operational Landsat data products. Remote Sensing of Environment, 194, 379–390. https://doi.org/10.1016/j.rse.2017.03.026

FAO; UNCCD.2015. Sustainable Financing for Forest and Landscape Restoration: The Role of Public Policy Makers; FAO: Rome, Italy; p.12.

Federici, S., Quaratino, R., Papale, D., Tulipano, S., Valentini, R. (2001). Sistema informatico delle Tavole Alsometriche d'Italia, DiSAFRi – Università degli Studi della Tuscia. [online] URL: http://gaia.agraria.unitus.it

Federici S, Vitullo M, Tulipano S, De Lauretis R, Seufert G, 2008. An approach to estimate carbon stocks changes in forest carbon pools under the UNFCCC: the Italian case. iForest 1: 86-95 [online: 2008-05-19] URL: http://www.sisef.it/iforest/

Francini S., Ronald E. McRoberts, Giannetti F., Marchetti M, Mugnozza G. S. & G. Chirici. 2021. The Three Indices Three Dimensions (3I3D) algorithm: a new method for forest disturbance mapping and area estimation based on optical remotely sensed imagery, International Journal of Remote Sensing, 42:12, 4693-4711, DOI: 10.1080/01431161.2021.1899334

Francini, S., McRoberts, R. E., D'Amico, G., Coops, N. C., Hermosilla, T., White, J. C., Wulder, M. A. et al. 2022,a. An open science and open data approach for the statistically robust estimation of forest disturbance areas. International Journal of Applied Earth Observation and Geoinformation, 106, 102663. https://doi.org/10.1016/j.jag.2021.102663

Francini, S.; D'Amico, G.; Vangi, E.; Borghi, C.; Chirici, G. 2022,b. Integrating GEDI and Landsat: Spaceborne Lidar and Four Decades of Optical Imagery for the Analysis of Forest Disturbances and Biomass Changes in Italy. Sensors 2022, 22, 2015. https://doi.org/ 10.3390/ s22052015

Frate L, Carranza M. L, Garfì V, Di Febbraro M., Tonti D, Marchetti M, Ottaviano M, Santopuoli G, Chirici G. 2015. Spatially explicit estimation of forest age by integrating remotely sensed data and inverse yield modeling techniques. iForest 9: 63-71. - doi: 10.3832/ifor1529-008

Garcia O, 1993. Stand growth models: Theory and practice. In: Advancement in Forest Inventory and Forest Management Sciences. Proceedings of the IUFRO Seoul Conference. Forestry Research Institute of the Republic of Korea, pp. 22-45.

Hansen, M. C., P. V. Potapov, R. Moore, M. Hancher, S. A. Turubanova, A. Tyukavina, D. Thau, et al. 2013. High-Resolution Global Maps of 21st-Century Forest Cover Change. Science 342 (6160): 850–853. American Association for the Advancement of Science. doi:10.1126/science.1244693.

Harris, N. L., Gibbs, D. A., Baccini, A., Birdsey, R. A., de Bruin, S., Farina, M., Fatoyinbo, L., et al. 2021. Global maps of twenty-first century forest carbon fluxes. Nature Climate Change 11, 234–240. https://doi.org/10.1038/s41558-020-00976-6

Hollaus, M., Dorigo, W., Wagner, W., Schadauer, K., Höfle, B., Maier, B., 2009. Operational wide-area stem volume estimation based on airborne laser scanning and national forest inventory data. Int. J. Remote Sens. 30, 5159‑5175. https://doi.org/ 10.1080/01431160903022894.

Houghton, R. A., & Nassikas, A. A. 2017. Global and regional fluxes of carbon from land use and land cover change 1850–2015. Global Biogeochemical Cycles, 31(3), 456-472.

Immitzer M., Stepper C., Böck S., Straub C., Atzberger C., 2016. Forest Ecology and Management Use of WorldView-2 stereo imagery and National Forest Inventory data for wall-to-wall mapping of growing stock. Forest Ecology and Management. 359, 232–246. https://doi.org/10.1016/j.foreco.2015.10.018.

INFC. 2007. Le stime di superficie 2005-seconda parte. In Inventario Nazionale delle Foreste e dei Serbatoi Forestali di Carbonio; Tabacchi,A.G., De Natale, F., Di Cosmo, L., Floris, A., Gagliano, C., Gasparini, P., Salvadori, I., Scrinzi, G., Tosi, V., Eds.; MiPAF–Corpo Forestale dello Stato-Ispettorato Generale, CRA-ISAFA: Trento, Italy, 2007

INFC. 2021. Italian forests. Selected results of the third National Forest Inventory. INFC 2015. Carabinieri Command of Forestry, Environmental and Agri-food units and CREA - Research Centre for Forestry and Wood. Tipografia Supernova (TN). Settembre 2021. ISBN: 978-88-338-5140-2

IPCC. 2006. IPCC Guidelines for greenhouse gases inventory. A primer, Prepared by the National Greenhouse Gas Inventories Programme, Eggleston H.S., Miwa K., Srivastava N. and Tanabe K. (eds). Published: IGES, Japan.

ISAFA. 2004. RiselvItalia Project. [online] URL: http://www.ricercaforestale.it/riselvitalia/index.htm. Kennedy, R. E., Yang, Z., Gorelick, N., Braaten, J., Cavalcante, L., Cohen, W. B., & Healey, S. (2018). Implementation of the LandTrendr algorithm on google earth engine. Remote Sensing, 10(5), 691.

ISPRA. 2021 (a). Moving to the 2006 IPCC Guidelines for UNFCCC reporting, ISPRA Rapporti 358/2021

ISPRA. 2021 (b). National Inventory Report 2021 - Italian Greenhouse Gas Inventory 1990-2019. ISPRA Rapporti 341/2021

Kangas A., Astrup R., Breidenbach J., Fridman, J., Gobakken T., Korhonen K.T., Maltamo M., Nilsson M., Nord-Larsen T., Næsset E.,et al. 2018. Remote sensing and forest inventories in Nordic countries–roadmap for the future. Scandinavian Journal of Forest Research. 2018, 33,397–412.

Kavzoglu, T., Colkesen, I., 2009. A kernel functions analysis for support vector machines for land cover classification. International Journal of Applied Earth Observation and Geoinformation 11 (5), 352–359. https://doi.org/10.1016/j.jag.2009.06.002

Kulbokas, G., Jurevičienė, V., Kuliešis, A., Augustaitis, A., Petrauskas, E., Mikalajūnas, M., Vitas, A., Mozgeris, G. 2019. Fluctuations in gross volume increment estimated by the Lithuanian National Forest Inventory compared with annual variations in single tree increment. Baltic Forestry, 25(2), 273-280.

Liaw, A., Wiener, M., 2002. Classification and regression by randomForest. Nucleic Acids Res. 5, 983‑999. https://doi.org/10.1023/A:1010933404324.

Matasci G., Hermosilla T., Wulder M.A., White J.C., Coops N.C., Hobart G.W., Zald H.S.J., 2018. Large-area mapping of Canadian boreal forest cover, height, biomass, and other structural attributes using Landsat composites and lidar plots. Remote Sensing of Environment 209, 90–106. https://doi.org/10.1016/j.rse.2017.12.020.

Italian Ministry for the Environment, Land and Sea (IMELS), 2019. National Forestry Accounting Plan, Dicember 2019 https://www.minambiente.it/sites/default/files/archivio/allegati/clima/nfap_final_re submission_2019_clean.pdf

McRoberts, R.E., Tomppo, E.O., 2007. Remote sensing support for national forest inventories. Remote Sens. Environ. 110, 412–419. https://doi.org/10.1016/j.rse.2006. 09.034.

McRoberts, R.E.; Naesset, E.; Gobakken, T. 2013. Accuracy and Precision for Remote Sensing Applications of Nonlinear Model-Based Inference. IEEE Journal of Selected Topics in Applied Earth Observations and Remote. 6, 27–34. DOI: 10.1109/JSTARS.2012.2227299

McRoberts, R.E., Chen, Q., Domke, G.M., Ståhl, G., Saarela, S., Westfall, J.A., 2016. Hybrid estimators for mean above-ground carbon per unit area. Forest Ecology and Management 378, 44‑56.

McRoberts R. E., E. Næsset, T. Gobakken, G. Chirici, S. Condes, Z. Hou, S. Saarela, Q. Chen, G. Stahl, B. F. Walters. 2018. Assessing components of the model-based mean square error estimator for remote sensing assisted forest applications. Canadian Journal of Forest Research, 48, 642–649. https://doi.org/10.1139/cjfr-2017-0396

Mountrakis, G., Im, J., Ogole, C., 2011. Support vector machines in remote sensing: A review. ISPRS Journal of Photogrammetry and Remote Sensing 66 (2011) 247–259. doi:10.1016/j.isprsjprs.2010.11.001

Nabuurs G.J., P.J. Verkerk, M. Schelhaas, J. González-Olabarria, A. Trasobares, E. Cienciala. 2018. Climate-Smart Forestry: Mitigation Implact in Three European Regions. From Science to Policy 6. European Forest Institute.

Næsset, E., Gobakken, T., Holmgren, J., Hyyppä, H., Hyyppä, J., Maltamo, M., Nilsson,M., Olsson, H., Persson, Å., Söderman, U., 2004. Laser scanning of forest resources:the nordic experience. Scand. J. For. Res. 19, 482‑499. https://doi.org/10.1080/02827580410019553.

Nonini, L., & Fiala, M. (2021). Estimation of carbon storage of forest biomass for voluntary carbon markets: preliminary results. Journal of Forestry Research, 32(1), 329-338. DOI: 10.1007/s11676-019-01074-w

Nord-Larsen, T., Schumacher, J., 2012. Estimation of forest resources from a country wide laser scanning survey and national forest inventory data. Remote Sens. Environ. 119,148‑157. https://doi.org/10.1016/j.rse.2011.12.022.

Nyamari, N., & Cabral, P. 2021. Impact of land cover changes on carbon stock trends in Kenya for spatial implementation of REDD+ policy. Applied Geography, 133, 102479. https://doi.org/10.1016/j.apgeog.2021.102479

Pal, M., Mather, P.M., 2005. Support vector machines for classification in remote sensing. International Journal of Remote Sensing 26 (5), 1007–1011. https://doi.org/10.1080/01431160512331314083

Paul, T., Kimberley, M. O., & Beets, P. N. (2021). Natural forests in New Zealand–a large terrestrial carbon pool in a national state of equilibrium. Forest Ecosystems, 8(1), 1-21. https://doi.org/10.1186/s40663-021-00312-0

Pinna, M. (1970). Contributo alla classificazione del clima d'Italia. Rivista Geografica Italiana, 77(2), 129-152.

Saatchi, S. S., Harris, N. L., Brown, S., Lefsky, M., Mitchard, E. T., Salas, W., Zutta, B. R. et al. 2011. Benchmark map of forest carbon stocks in tropical regions across three continents. Proceedings of the national academy of sciences, 108(24), 9899-9904.

Sellers P. J., Schimel D. S., Moore B., Liu J., Eldering A. 2018. Observing carbon cycle–climate feedbacks from space. Proceedings of the National Academy of Sciences, U.S.A. 115, 7860–7868. https://doi.org/10.1073/pnas.1716613115

Schepaschenko, D., Moltchanova, E., Fedorov, S., Karminov, V., Ontikov, P., Santoro, M., See, L. et al. 2021. Russian forest sequesters substantially more carbon than previously reported. Scientific reports, 11(1), 1-7. doi: 10.1038/s41598-021-92152-9

Smola, A.J., Schölkopf, B., 2004. A tutorial on support vector regression. Statistics and Computing 14 (3), 199–222. https://doi.org/10.1023/B:STCO.0000035301.49549.88

Tabacchi, G., Di Cosmo, L., Gasparini, P., Morelli, S., 2011. Stima Del Volume E Della Fitomassa Delle Principali Specie Forestali Italiene, Equazioni Di Previsione, Tavole Del Volume E Tavole Della Fitomassa Arborea Epigea.

Tomppo, E., Olsson, H., Ståhl, G., Nilsson, M., Hagner, O., Katila, M., 2008. Combining national forest inventory field plots and remote sensing data for forest databases. Remote Sens. Environ. 112, 1982‑1999. https://doi.org/10.1016/j.rse.2007.03.032.

Tomppo, E., Gschwantner, T., Lawrence, M., McRoberts, R. E., Gabler, K., Schadauer, K., Cienciala, E. et al. 2010. National forest inventories. Pathways for Common Reporting. European Science Foundation, 1, 541-553.

UNFCCC, 2015. The Paris Agreement. Report of the Conference of the Parties on its twenty-first session, held in Paris from 30 November to 11 December 2015. http://unfccc.int/files/meetings/paris_nov_2015/application/pdf/paris_agreement_english_.pdf

Van Der Werf, G. R., Randerson, J. T., Giglio, L., Van Leeuwen, T. T., Chen, Y., Rogers, B. M., Kasibhatla, P. S. et al. 2017. Global fire emissions estimates during 1997–2016. Earth System Science Data, 9(2), 697-720. https://doi.org/10.5194/essd-9-697-2017

Vangi E., D'Amico G., Francini S., Giannetti F., Lasserre B.; Marchetti M., McRoberts R.E., Chirici G., 2021. The Effect of Forest Mask Quality in the Wall-to-Wall Estimation of Growing Stock Volume. Remote Sensing, 13, 1038. https://doi.org/10.3390/rs13051038

Waser, L.T., Ginzler, C., Rehush, N., 2017. Wall-to-Wall tree type mapping from countrywide airborne remote sensing surveys. Remote Sens. 9. https://doi.org/10.3390/rs9080766.

White, J. C., Coops N. C., Wulder M. A., Vastaranta M., Hilker T., Tompalski P., 2016. Remote Sensing Technologies for Enhancing Forest Inventories: A Review. Canadian Journal of Remote Sensing, 42(5), 619-641. https://doi.org/10.1080/07038992.2016.1207484

Williams, P. A., Allen, C., Macalady, A., Griffin, D., Woodhouse, C. A., Meko, D. M., Swetnam, T. W. et al. 2012. Temperature as a potent driver of regional forest drought stress and tree mortality. Nature Climate Change 3, 292–297 . https://doi.org/10.1038/nclimate1693

Wolfe, R., Masek, J., Saleous, N., & Hall, F. 2004. LEDAPS: mapping North American disturbance from the Landsat record. In IGARSS 2004. 2004 IEEE International Geoscience and Remote Sensing Symposium (Vol. 1). IEEE.

Xu, L., Saatchi, S. S., Yang, Y., Yu, Y., Pongratz, J., Bloom, A. A., Bowman, C. et al. 2021. Changes in global terrestrial live biomass over the 21st century. Science Advances, 7(27), eabe9829. DOI: https://doi.org/10.1126/sciadv.abe9829

# 4. Conclusions

Innovation in technologies and techniques is rapidly shaping forest monitoring and simultaneously leading to new information needs. The plethora of data from new sensors, continuously updated and increasingly rich in the information they carry, and the ease of acquisition and processing have enabled unprecedented development in forestry research and operations. This scenario of emerging new data was the basis of my Ph.D., in which, the main objective was to explore the capability and possibility offered by these new RS data. Each paper is focused on a specific questions, attempting to answer and to contribute to the increase of scientific community knowledge. In this thesis some of the first applications of these new RS technologies in the forestry field were presented. New software and methods have been developed in an effort to reducing the gap between technology development and end users, and to meet compelling reporting needs.

The new PRISMA mission is expected to deliver imagery with a new level of quality in the hyperspectral filed with the finest spectral resolution, making it potentially suitable for application in all areas of EO. Its capacity in discriminating the main species groups in a Mediterranean environment bodes well for its future application in plant phenology, forest species classification, forest disturbances and change detection studies.

The new GEDI level 4A data, recently released, is expected to change biomass estimation studies, providing new knowledge in regions of the earth where it is challenging to obtain ground-based data for model calibration and validation. The new above-ground biomass data will be crucial for studying forest ecology and forest ecosystem evolution over time and space. Sharing knowledge and experience on lidar data acquired from space should allow a complete understanding of its strengths and limitations. To do this, as many people as possible should have easy access to every piece of information provided by the GEDI mission and the GEDI4R package provides a ready-to-use tool to get started.

The first comparative analysis of the FMs available in Italy was carried out, finding a negative relationship between FM accuracy and the standard error of the GSV estimate. This highlights the need to consider the quality of the FM in the estimation of forest

variables through the model-assisted estimator. An inadequate FM could bias the results of the estimates leading to errors in international reports.

Finally, an innovative spatial framework to track GSV and carbon stock changes between NFI surveys at local to national scales was set up, providing a reliable monitoring approach to meet the international reporting requirements and the climate mitigation goals.

This new method incorporates forest disturbance, such as forest fires and harvesting, the natural mortality rate and the current GSV increment, as well as the starting GSV, to estimate the above-ground carbon stock time series between two NFI. The reliability of the approach was assessed by comparing the results with the official estimates of GHG inventories and the last Italian NFI 2015, obtaining a promising performance.

In this thesis, the main objective has been to increase the knowledge of new space missions and the possibilities they offer to the forest monitoring sector by increasing the availability of consistent and reliable spatial data potentially useful in supporting the understanding of CC dynamics and its solutions. The data that RS provides is so unique that has the potential to not only augment traditional ground-based methods, but to open up wholly new research avenues in EO science.

Finally, I feel compelled at this stage to clarify a critical point: As should be clear from reading the papers, I do not mean by any means de-emphasizing the importance of *in situ* measurements and inventory-based approaches, rather these are essential datasets that should be used in synergy with remote sensing observations to improve what can be accomplished with one or the other alone.

# Other publications and contributions

## 1. Scientific papers

1.  Giannetti, F.; Chirici, G.; Vangi, E.; Corona, P.; Maselli, F.; Chiesi, M.; D'Amico, G.; Puletti, N. Wall-to-Wall Mapping of Forest Biomass and Wood Volume Increment in Italy. Forests 2022, 13, 1989. https://doi.org/10.3390/f13121989

2.  Bonannella, C., Chirici, G., Travaglini, D., Pecchi, M., **Vangi, E.**, D'amico, G., Giannetti, F. Characterization of Wildfires and Harvesting Forest Disturbances and Recovery Using Landsat Time Series: A Case Study in Mediterranean Forests in Central Italy. (2022) Fire, 5 (3), art. no. 68, https://doi.org/10.3390/fire5030068

3.  Francini, S., D'Amico, G., **Vangi, E.,** Borghi, C., Chirici, G. Integrating GEDI and Landsat: Spaceborne Lidar and Four Decades of Optical Imagery for the Analysis of Forest Disturbances and Biomass Changes in Italy. (2022) Sensors, 22 https://doi.org/10.3390/s22052015

4.  Parisi, F., **Vangi, E.,** Francini, S., Chirici, G., Travaglini, D., Marchetti, M., Tognetti, R. Monitoring the abundance of saproxylic red-listed species in a managed beech forest by landsat temporal metrics (2022) Forest Ecosystems, 9, art. no. 100050, https://doi.org/10.1016/j.fecs.2022.100050

5.  D'Amico, G., McRoberts, R.E., Giannetti, F., **Vangi, E**., Francini, S., Chirici, G. Effects of lidar coverage and field plot data numerosity on forest growing stock volume estimation
    (2022) European Journal of Remote Sensing, 55 (1), pp. 199-212. https://doi.org/10.1080/22797254.2022.2042397

6.  Giannetti, F., Pecchi, M., Travaglini, D., Francini, S., D'amico, G., **Vangi, E.,** Cocozza, C., Chirici, G. Estimating vaia windstorm damaged forest area in italy

using time series sentinel-2 imagery and continuous change detection algorithms. (2021) Forests, 12 (6), art. no. 680, https://doi.org/10.3390/f12060680

7.  D'Amico, G., Francini, S., Giannetti, F., **Vangi, E.**, Travaglini, D., Chianucci, F., Mattioli, W., Grotti, M., Puletti, N., Corona, P., Chirici, G. A deep learning approach for automatic mapping of poplar plantations using Sentinel-2 imagery (2021) GIScience and Remote Sensing, 58 (8), pp. 1352-1368. https://doi.org/10.1080/15481603.2021.1988427

8.  D'amico, G., **Vangi, E.,** Francini, S., Giannetti, F., Nicolaci, A., Travaglini, D., Massai, L., Giambastiani, Y., Terranova, C., Chirici, G. Are we ready for a national forest information system? State of the art of forest maps and airborne laser scanning data availability in Italy (2021) IForest, 14 (2), pp. 144-154. https://doi.org/10.3832/ifor3648-014

## 2. Conference talks and seminars

1.  Jevsenak J., **Vangi** E., Arnic D., Krajnic L., D'Amico G., Ferlan M., Chirici G., Skudnik M. Machine Learning Forest Simulator (MLFS): New tool for assessing the state of future forests. 26 APR 2022 – 28 APR 2022. Napoli DOI: 10.13140/RG.2.2.17923.78883 Conference: Landsupport final conference

2.  Elia **Vangi**, Francesco Parisi, Saverio Francini, Giovanni D'Amico, Francesca Giannetti, Marco Marchetti, Fabio Lombardi, Davide Travaglini, Sonia Ravera, Costanza Borghi, Elena De Santis, Roberto Tognetti, Gherardo Chirici. Is it possible to monitor multi-taxon biodiversity through Sentinel-2 time series analysis? 22 SEP 2022 – 23 SEP 2022. Bologna. ISBN edizione digitale: 978-88-8286-436-1 III Workshop tematico di Telerilevamento. ENEA-AIT 2022

3.  Giovanni D'Amico, Saverio Francini, Francesco Parisi, Elia **Vangi**, Costanza Borghi, Francesca Giannetti, Elena De Santis, Davide Travaglini, Rafael Da Silveira Bueno, Giovanna Sala, Tommaso La Mantia, Gherardo Chirici. Remote sensing to support health monitoring of vulnerable forest

environments: preliminary results on Norway spruce and Mediterranean pines in Italy 22 SEP 2022 – 23 SEP 2022. Bologna ISBN edizione digitale: 978-88-8286-436-1. XIII workshop di telerilevamento. ENEA-AIT 2022

4. Saverio Francini, Giovanni D'Amico, Elia **Vangi**, Costanza Borghi, Francesca Giannetti, Davide Travaglini, Gherardo Chirici. Verso un sistema integrato di monitoraggio delle foreste europee basato sul telerilevamento: i primi risultati del progetto European Forest Information Network (EFINET) 22 SEP 2022 – 23 SEP 2022. Bologna ISBN edizione digitale: 978-88-8286-436-1. XIII workshop di telerilevamento. ENEA-AIT 2022

5. **Vangi** E, D'Amico G, Francini S, Borghi C, Giannetti F, Corona P, Marchetti M, Travaglini D, Pellis G, Vitullo M, Chirici G. National high resolution yearly mapping of forest growing stock volume and above-ground carbon pool in Italy. 29 AUG 2022 – 2 SEP 2022. Berlin. ForestSAT2022.

6. Francini, S., D'Amico, G., **Vangi**, E., Borghi, C., Chirici, G. Integrating GEDI and Landsat: Spaceborne Lidar and Four Decades of Optical Imagery for the Analysis of Forest Disturbances and Biomass Changes in Italy 29 AUG 2022 – 2 SEP 2022 Berlin. ForestSAT2022.

7. Giannetti, F. Pecchi, M. Travaglini, D. Francini, S. D'Amico, G. **Vangi**, E. Cocozza, C. Chirici, G. Estimating Vaia windstorm damaged forest area in Italy using time series sentinel-2 imagery and continuous change detection algorithms 29 AUG 2022 – 2 SEP 2022. Berlin. ForestSAT2022.

8. D'Amico G*, Francini S, Giannetti F, **Vangi** E, Travaglini D, Chianucci F, Puletti N, Corona P, Chirici G. A deep learning approach for automatic mapping of poplar plantations using Sentinel-2 imagery 29 AUG 2022 – 2 SEP 2022. Berlin. ForestSAT2022.

9. **Vangi** E, D'Amico G, Francini S, Borghi C, Giannetti F, Corona P, Marchetti M, Travaglini D, Pellis G, Vitullo M, Chirici G. National high resolution yearly mapping of forest growing stock volume and above-ground carbon pool in Italy. 30 MAY 2022 – 2 JUN 2022. Orvieto. XIII congresso nazionale SISEF 2022.

10. D'Amico G, Francini S, Giannetti F, **Vangi** E, Travaglini D, Chianucci F, Puletti N, Corona P, Chirici G. A deep learning approach for automatic mapping of poplar plantations using Sentinel-2 imagery 30 MAY 2022 – 2 JUN 2022. Orvieto.. XIII congresso nazionale SISEF 2022.

11. Giannetti F, Giambastiani Y, Fiorentini S, Travaglini D, Francini S, D'Amico G, **Vangi** E, Marta C, Maselli F, Mattioli W, Lombardo E, Chirici G. The key role of multiscale remote sensing data to develop Forest Decision Support Systems 30 MAY 2022 – 2 JUN 2022. Orvieto. XIII congresso nazionale SISEF 2022

12. Zorzi I, Francini S, D'Amico G, **Vangi** E, Giannetti F, Travaglini D, Chirici G, Cocozza C. Analisi e confronto della stagione vegetativa di Abies alba e di Fagus sylvatica con tecnologia TreeTalker. 30 MAY 2022 – 2 JUN 2022. Orvieto.. XIII congresso nazionale SISEF 2022

13. Borghi C, Francini S, Parisi F, **Vangi** E, D'Amico G, Giannetti F, Travaglini D, Chirici G. Is it possible to use National Forest Inventory data to assess forest biodiversity? The Italian case 30 MAY 2022 – 2 JUN 2022 > – Orvieto XIII congresso nazionale SISEF 2022

14. Francini S, D'Amico G, **Vangi** E, Borghi C, Marchetti M, Chirici G. A Google Earth Engine application for forest disturbance mapping and area estimation 30 MAY 2022 – 2 JUN 2022. Orvieto. XIII congresso nazionale SISEF 2022

15. **Vangi** E., D'Amico G., Francini S., Giannetti F.,Chirici G., Lasserre B., Marchetti M. The New Hyperspectral Satellite PRISMA: Imagery for Forest Types Discrimination 13 SEP 2021 – 15 SEP 2021. Cagliari. X International Conference AIT

16. D'Amico G., Giannetti F., **Vangi** E., Borghi C., Francini S., Travaglini D., Chirici G. Multitemporal LiDAR data for forest carbon monitoring in Mediterranean Forest 13 SEP 2021 – 15 SEP 2021. Cagliari. X International Conference AIT.

17. Borghi C., Francini S., Pollastrini M., Bussotti F., Travaglini D., Marchetti M., Munafò M., Scarascia-Mugnozza G., Tonti G., Ottaviano M., Giuliani C., Cavalli A., **Vangi** E., D'Amico G., Giannetti F., Chirici G. Monitoring thirty-five years of Italian forest disturbance using Landsat time series. 13 SEP 2021 – 15 SEP 2021. Cagliari. X International Conference AIT

18. Giannetti F., Tattoni C., D'Amico G., Francini S., Chirici G., Romano E., Brambilla M., Travaglini D., **Vangi** E., Chianucci F. Multiscale monitoring of poplar plantations using proximal and remotely-sensed imagery 13 SEP 2021 – 15 SEP 2021. Cagliari. X International Conference AIT

19. Giannetti F., Giambastiani Y., Fiorentini S., Travaglini D., Francini S., **Vangi** E., D'Amico G., Chiesi M., Maselli F., Chirici G. The Key Role of Multiscale Remote Sensing Data to Develop Forest Decision Support Systems. 13 SEP 2021 – 15 SEP 2021. Cagliari. X International Conference AIT

20. **Vangi** E., D'Amico G., Francini S., Borghi C., Giannetti F., Travaglini D., Chirici G. A Spatial approach for multi-temporal spatial estimation of forest GSV and aboveground carbon pool. A case of study in Tuscany (Italy). 13 SEP 2021 – 15 SEP 2021. Cagliari. X International Conference AIT

21. Fanara V., Chirici G., Cocozza C., D'Amico G., Giannetti F., Francini S., Salbitano F., Speak A., **Vangi** E., Travaglini D. Estimation of Multitemporal Dry Deposition of Air Pollution by Urban Forests at City Scale. 13 SEP 2021 – 15 SEP 2021. Cagliari. X International Conference AIT

# Acknowledgements

Firenze, January 2023

*Elia Vangi*